RESEARCH AND DEVELOPMENT TECHNICAL REPORT
CECOM 82-CS029-F

AD A113698

WIDEBAND PROPAGATION

MEASUREMENTS IN THE

PRESENCE OF FORESTS

G.A. HUFFORD, R.W. HUBBARD,
L.E. PRATT, J.E. ADAMS,
AND S.J. PAULSON

U.S. DEPT. OF COMMERCE, NTIA/ITS
BOULDER, COLORADO

P.F. SASS
CENTER FOR COMMUNICATION SYSTEMS

JANUARY 1982

DISTRIBUTION STATEMENT:
APPROVED FOR PUBLIC RELEASE: DISTRIBUTION UNLIMITED

DTIC FILE COPY

DTIC
SELECTED
APR 27 1982
H

CECOM

U S ARMY COMMUNICATIONS-ELECTRONICS COMMAND
FORT MONMOUTH, NEW JERSEY 07703

82   04   26   097

REPORT DOCUMENTATION PAGE		READ INSTRUCTIONS BEFORE COMPLETING FORM
1. REPORT NUMBER CECOM-82-CS029-F	2. GOVT ACCESSION NO. AD-A113698	3. RECIPIENT'S CATALOG NUMBER
4. TITLE (and Subtitle) Wideband Propagation Measurements in the Presence of Forests		5. TYPE OF REPORT & PERIOD COVERED Final Report,Apr 79-Dec 81
		6. PERFORMING ORG. REPORT NUMBER
7. AUTHOR(s) G.A. Hufford, R.W. Hubbard, L.E. Pratt, J.E. Adams, S.J. Paulson, and P.F. Sass (U.S. Army CECOM)		8. CONTRACT OR GRANT NUMBER(s) CS-1-CS029-CS-WA
9. PERFORMING ORGANIZATION NAME AND ADDRESS US Dept of Commerce, NTIA Institute for Telecomm Sciences Boulder, CO 80303		10. PROGRAM ELEMENT, PROJECT, TASK AREA & WORK UNIT NUMBERS 1L162701.AH92.FA.02
11. CONTROLLING OFFICE NAME AND ADDRESS US Army Communications Electronics Command ATTN: DRSEL-COM-RF-2 Ft Monmouth, NJ 07703		12. REPORT DATE January 82
		13. NUMBER OF PAGES 162
14. MONITORING AGENCY NAME & ADDRESS(if different from Controlling Office)		15. SECURITY CLASS. (of this report) Unclassified
		15a. DECLASSIFICATION/DOWNGRADING SCHEDULE

16. DISTRIBUTION STATEMENT (of this Report)

Approved for public release: Distribution Unlimited

17. DISTRIBUTION STATEMENT (of the abstract entered in Block 20, if different from Report)

18. SUPPLEMENTARY NOTES

19. KEY WORDS (Continue on reverse side if necessary and identify by block number)

Channel impulse response; multipath delay spread; forest attenuation; UHF radio propagation; spread spectrum; wideband systems

20. ABSTRACT (Continue on reverse side if necessary and identify by block number)

This report describes the conduct and provides representative analysis of the results of an experimental program designed to measure the transmission characteristics of UHF radio channels in a forested environment. The program described is the initial phase of what may become a much larger effort, and the emphasis here is to test the experimental procedures, equipment, and analysis technique for their appropriateness to the long-range objectives, and to gain some preliminary insight to the propagation parameters important

DD FORM 1473 EDITION OF 1 NOV 65 IS OBSOLETE

for wideband and spread-spectrum systems. The test instrumentation used was a pseudo-noise channel probe with 300-MHz bandwidth. It provided a direct representation of the channel impulse response which then was recorded in both analog and digital formats. The analyses of these recordings now provide measures of overall path loss, multipath delay spreads, and derived spectral responses.

Accession For

MTIS GRA&I
DTIC T'B
Unannounced
Justification

By
Distribution/
Availability Codes
Avail and/or
Dist   Special

TABLE OF CONTENTS

LIST OF FIGURES

vi

LIST OF TABLES

WIDEBAND PROPAGATION MEASUREMENTS IN THE PRESENCE OF FORESTS

G. A. Hufford, R. W. Hubbard, L. E. Pratt, J. E. Adams,
S. J. Paulson*, and P. F. Sass†

This report describes the conduct and provides representative analysis of the results of an experimental program designed to measure the transmission characteristics of UHF radio channels in a forested environment. The program described is the initial phase of what may become a much larger effort, and the emphasis here is to test the experimental procedures, equipment, and analysis technique for their appropriateness to the long-range objectives, and to gain some pre-liminary insight to the propagation parameters important for wideband and spread-spectrum systems. The test instrumentation used was a pseudo-noise channel probe with 300-MHz bandwidth. It provided a direct representation of the channel impulse response which then was recorded in both analog and digital formats. The analyses of these recordings now provide measures of overall path loss, multipath delay spreads, and derived spectral responses.

Key words: channel impulse response; multipath delay spread; forest attenuation; UHF radio propagation; spread spectrum; wide-band systems

1. INTRODUCTION AND OBJECTIVES

The U.S. Army Communications R&D Command (CORADCOM)[1] is currently planning a multiphase effort (spanning several years) to obtain empirical data and statistical analyses on which channel characterization estimates may be based for ground-to-ground mobile spread-spectrum communications in the UHF band. Potential deployments include varied terrain and foliage.

This report describes a program, jointly undertaken by the Institute of Tele-communication Sciences (ITS) and CORADCOM, to carry out the first phase of this effort. This first phase is directed towards the assembly of necessary prototype equipment, its deployment in an environment of forest and hills, the collection of representative data under restricted conditions, and the testing of techniques for the statistical description of those data. The test area chosen was a forested area

---

near Tullahoma, Tennessee, and the equipment used centered about a pseudo-random noise (PN) channel probe developed in the ITS laboratories. Data analysis was done off-line using a large computer.

It should be emphasized that the scope of the experiment and the data collection in this phase was very limited and is subject to significant change for later phases of the program. The goal was only to determine the feasibility of the approach and to establish the basis for more confident planning of longer term efforts. It was not expected that sufficient data would result from this initial phase to allow significant modeling or other estimation of performance of spread-spectrum systems.

To define the experiment more closely, several specific questions were posed, and test procedures were planned and conducted in the hope of obtaining at least partial answers. First, there are questions related to the PN probe equipment:

(1) Is the system sensitivity great enough to allow measurements within the forest?

(2) Can a digital data acquisition system be advantageously coupled to the PN probe, and will such records be sufficient to describe the measurement?

There are also questions concerning UHF radio propagation in the chosen environment that are of narrowband (or cw) nature:

(3) What is the attenuation rate (or bulk conductivity) in this forest?

(4) Do measured values, particularly height-gain results, fit a slab model of the forest?

(5) Is the received signal level (RSL) as measured by the total energy in the impulse response related to the local median of a cw signal?

There are questions specifically related to the multipath characteristics:

(6) How many multipath components are there likely to be, and can this number be related to the specific conditions of the propagation path?

(7) How do multipath characteristics change with frequency?

(8) Does the multipath structure over a fixed path change with time, either short-term or long-term?

And finally, there are questions related to the data analysis:

(9) What is the proper statistical summary to describe multipath characteristics in the chosen environment?

(10) What is the best way to present the original data for public dissemination?

Most of these questions can be given only preliminary answers here; more definitive results must await later phases of the program.

The measurement program described in this report also has an added responsibility to coordinate with a parallel test program of interest to CORADCOM and related to the development of the Joint Tactical Information Distribution Syst a (JTIDS). Many of the selected test areas and sites used in the present program were originally selected for JTIDS tests (Presnell, 1979) and were carefully marked so that the two programs could use nearly identical paths.

2. INSTRUMENTATION AND EQUIPMENT

2.1 PN Channel Probe

The primary instrumentation used in this propagation program was a pseudo-random noise (PN) probe, developed in the ITS Laboratories at Boulder, Colorado. The system measures the equivalent impulse response of a radio transmission channel using a correlation detector process in the receiver. This type of instrument has been defined as a multiplex correlation process. It is described in comparison with other techniques by Linfield et al. (1976), and some of the theory behind it is given in Appendix A. The system, as actually deployed, is briefly described in the following paragraphs.

The transmitter consists of a stable reference oscillator (5 MHz) (from which the clock stream for the PN code generator, the IF signal, and the rf transmission frequency are derived), a modulator, and a final power amplifier stage. The latter is either a solid-state device or a TWT amplifier, depending on the operating frequency. The PN code is generated in a nine-stage shift register, providing a 511 bit (2^9-1) pseudo-random binary sequence. This signal biphase modulates an IF frequency of 600 MHz. The latter is then either transmitted directly as one operating frequency or is mixed with a higher frequency for transmission. In the latter case, two sidebands are generated 600 MHz on each side of the rf. One sideband is filtered out in the transmission line to the final amplifier stage. For the propagation measurements discussed here, the following table of frequencies apply:

Table 1. Operating Frequencies

Fundamental	IF	Transmitted
600 MHz	600 MHz	600 MHz
1800 MHz	600 MHz	1200 MHz
2400 MHz	600 MHz	1800 MHz

The basic clock rate for the PN generator is 150 MHz which produces a main-lobe spectrum 300 MHz wide. This is the primary lobe of a $(\sin x/x)^2$ spectral function and is centered on the transmitted frequencies shown in Table 1. A block diagram of the transmitter is shown in Figure 1. The three transmitter frequencies were combined for simultaneous transmission as shown in the figure. The 600-MHz signal was raised to its final transmit level by a solid-state power amplifier. The two higher frequencies, 1200 MHz and 1800 MHz, were both fed into a travelling wave tube (TWT) amplifier with a nominal power rating of 20 W. The input levels of these signals were adjusted in accord with the TWT gain characteristics at the two frequencies, so that the output power of both signals was nearly equal. Actual power levels used in the experiment are presented later in this report. The 600-MHz signal and the two higher frequency outputs were combined in a diplexer unit and fed to a common antenna. The antennas used in the measurements and the probe terminal vehicles are described in the following sub-section.

The receiver for the channel probe is shown in simplified block diagram form in Figure 2. All three test frequencies are received simultaneously on the common antenna. The lower band frequency and the two upper band frequencies are separated in the diplexer unit and channeled to their appropriate preamplifier stages. The receiver used in this experiment was originally designed for two-channel operation. Only the rf portion of the receiver was modified to accommodate the three test frequencies, and consequently the IF and signal processing portions were capable of only two-channel operation. Any of the three frequencies were selectable in pairs by the operator. This function was accomplished in the Selector block shown in Figure 2. The frequency/channel configuration was limited in order to minimize the calibration requirements. Table 2 shows the configuration that was followed throughout the experiment.

Table 2. Frequency/Channel Assignment

Frequency	Channel Assignment
600 MHz	Channel 1 only
1200 MHz	Channel 1 or 2
1800 MHz	Channel 2 only

4
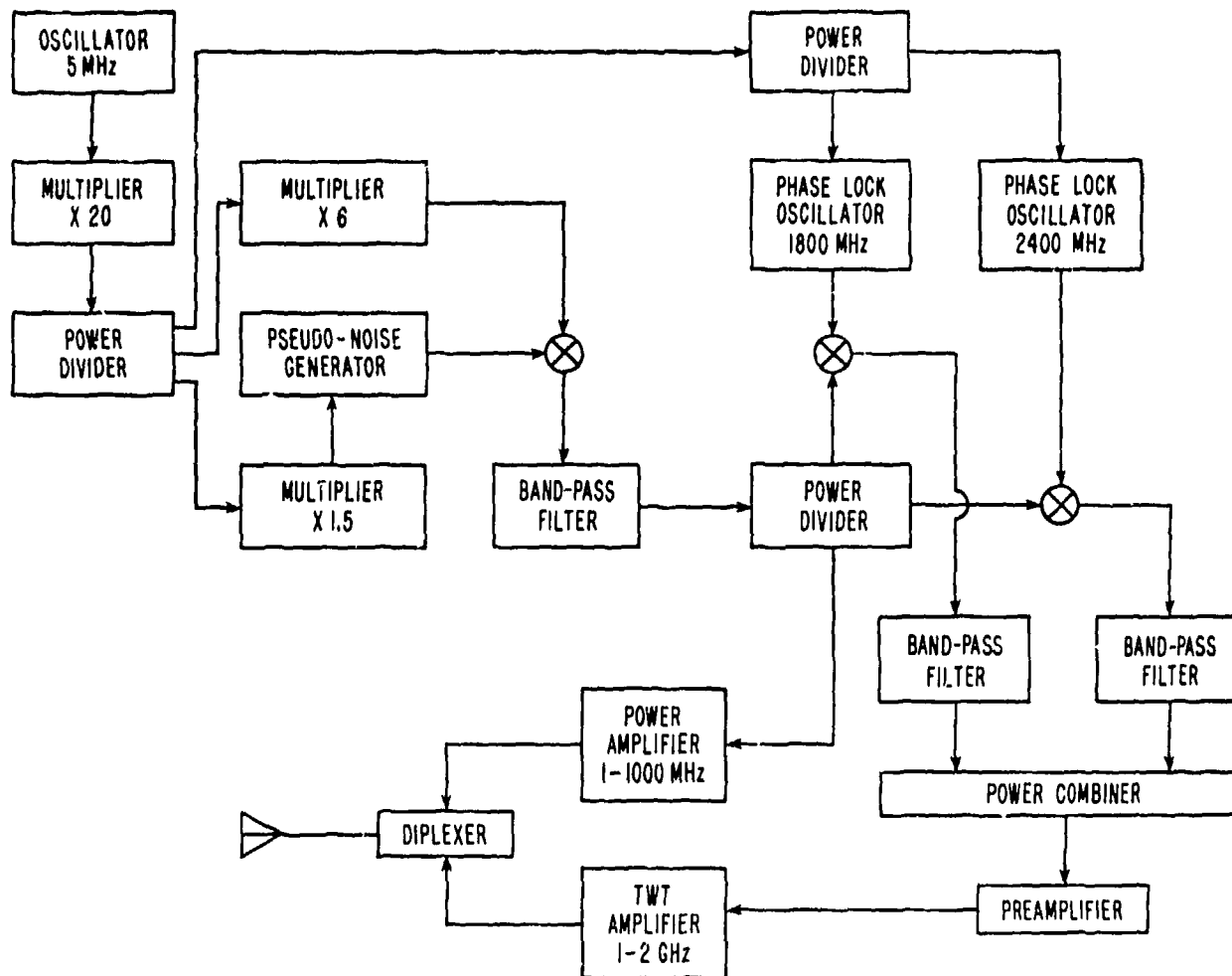
Figure 1. Simplified block diagram of the PN probe transmitter.
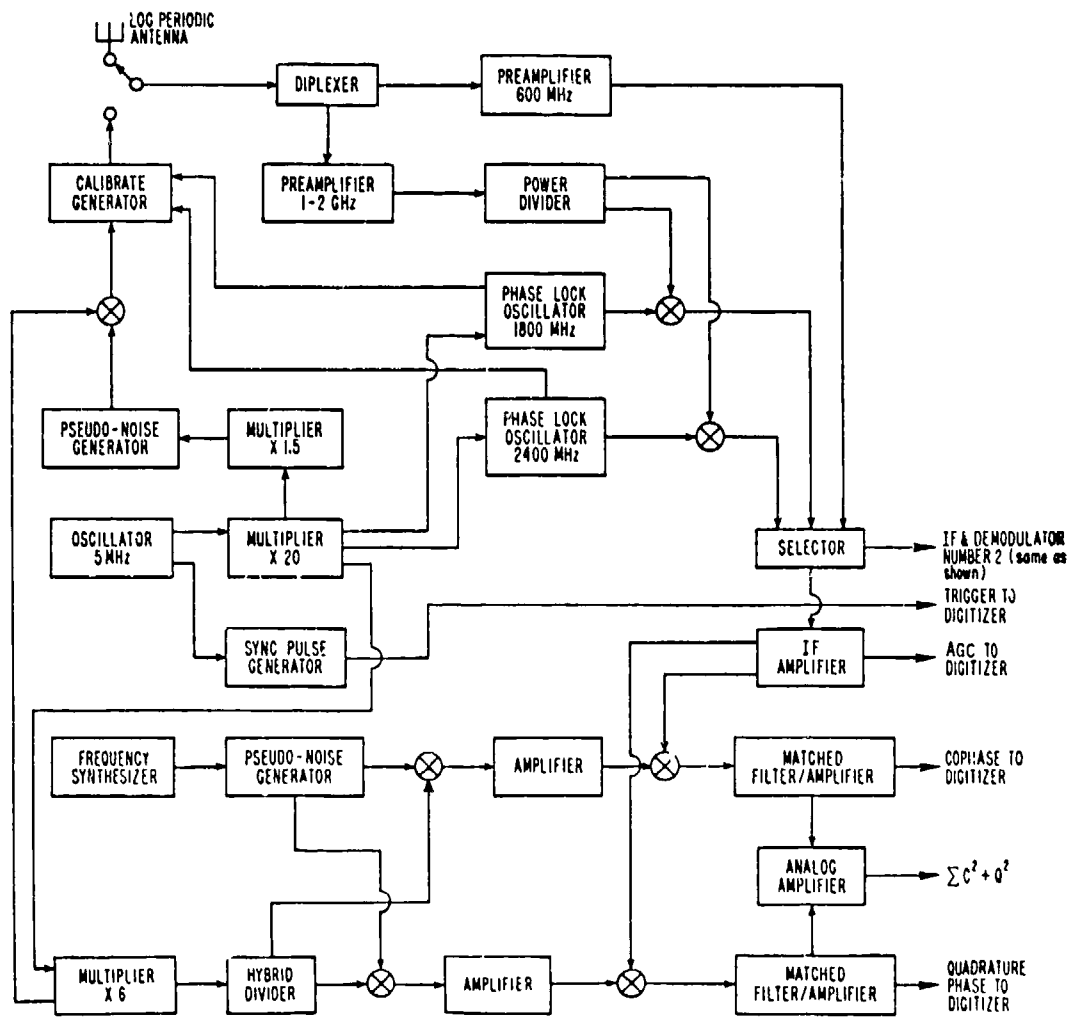
Figure 2. Simplified block diagram of the PN probe receiver. The receiver is a dual channel system; only one IF and signal processing section is shown.

In this manner, it was not necessary to calibrate both channels for all frequencies. However, as noted above, 1200 MHz could be assigned to either receiver channel. Thus, in the calibration procedures both receiver channels were always calibrated for the 1200-MHz signal. The calibration source is described below.

The diagram of Figure 2 illustrates only one channel of the IF and demodulator sections, which are both driven by the common pseudo-noise generator clocked from the frequency synthesizer. This portion of the receiver is briefly discussed below.

The receiver channels were calibrated with a self-contained calibrator source, which is shown in Figure 2. An independent PN generator is used in this section, clocked at the 150 MHz rate as is the transmitter PN generator. The 600-MHz IF signal is modulated identically to that of the transmitter and is mixed to the operating frequencies in the Calibrate Generator block. The output signals from the calibrate generator were at a fixed and known power level. In the calibrate mode, they are fed into the receiver through a set of manually adjusted precision attenuators in order to measure a complete calibration curve for each operating frequency. The nominal dynamic range of the receiver was 60 dB.

The detection process in the receiver is known as a multiplex type correlator (Bello et al., 1973). On each channel the output audio signal represents the equivalent low-pass impulse response of the transmission path, which is developed as a real and an imaginary component in a co-phase and quadrature-phase detector, respectively. The signal processing section of the receiver also has an analog circuit that develops the sum of the squares of these components, which yields the power impulse function. The distributed power in the impulse function is the total power in the output signal and thus is proportional to the received signal level (RSL). Furthermore, the constant of proportionality is determined by the AGC voltage at the IF amplifier, a quantity that is monitored in a log-linear fashion and is also available for recording at the receiver output as a continuous signal.

The correlation delay parameter is derived in the receiver from a PN data stream that is clocked at a slightly slower rate than that used in the transmit signal. The slow clock rate is developed by the Frequency Synthesizer shown in Figure 2. Thus, in the correlation process the reference bitstream in the receiver is in effect allowed to "drift" very slowly with respect to the received bit-stream.

In this manner the correlation function is developed dynamically as an analog signal from the Matched Filter/Amplifier units in the signal processing section of the receiver. Details of this correlation technique in comparison with other discrete delay methods can be found in the above reference and in Linfield et al. (1976).

7

The Frequency Synthesizer has been designed to provide several precise clock frequencies, each derived from the 5 MHz reference oscillator, so that impulse response data may be obtained at rates of 1/s, 2/s, 5/s, 10/s, 20/s, and 50/s. These are referred to as data frame rates or as window rates. The PN system was designed for many applications to propagation and communication problems and consequently has other operational features that are selectable by the operator. For example, the clocking rate for the PN generators can be selected for almost any desired rate, and the length of the PN bit stream may be changed. However, for the experiment reported here, these options were fixed at a clock rate of 150 MHz and a PN code length of 511 bits (2^9-1). The data frame rate was normally 1 Hz, but was occasionally changed to higher rates for selected experiments.

Other characteristics and specifications of the PN probe system (as applied in this experiment) are given in Table 3. The basic pulse resolution of the system is determined by selection of the PN clock rate for the measurements, and the maximum measurable delay spread also depends on this clock rate. As noted previously, this experiment was conducted exclusively at the 150-MHz clock rate, which provides a pulse resolution of 6.7 ns and a maximum delay spread of 3.4 μs. It should be noted here that multipath components with delays less than the 6.7-ns resolution time can be detected with this system. They will be observed as distortions of the pulse-- particularly of the phase relations as exhibited in the co-phase and quadrature- phase output. Examples of this feature are presented in a later section of this report.

2.2 Test Antenna and Probe Terminal Vehicles

For most of the experimental measurements reported below, the transmit antenna was a conical monopole, designed and fabricated in the ITS Laboratories for operation over the band of frequencies from 400 MHz to 2 GHz. The pattern measurements for this antenna are given in Appendix F to this report. The antenna was mounted on a 1.2-m (4-ft) square aluminum ground plane and fed by coaxial cable to the center of this plane. The feed pin for the antenna was that of a type N coaxial connector, physically attached to the point of the cone. When mounted to the ground plane, the center pin fed directly into a type N bulkhead fitting, mounted at the center of the ground plane. The antenna connection is made directly with a coaxial cable using a mating type N fitting. A photograph of the antenna removed from the ground plane is shown in Figure 3.

Table 3. Characteristics and Specifications for the Pseudo-Noise Probe as
Normally Configured for the Experimental Propagation
Measurements for Wideband Radio Systems

Band frequencies	600, 1200, 1800 MHz
Clock rate (bit rate)	150 MHz
Bandwidth	300 MHz
Pulse resolution	6.7 ns
Modulation	Bi-phase shift key (BPSK)
Code length	511 bits
Max delay spread	3.4 μs (about 1 km path length difference)
Transmitter:	
Power	4 to 10 W (36 to 40 dBm)
Diplexer losses	1 dB
Antenna	Conical monopole (omnidirectional, vertically polarized)
Gain	0 dBi
Height	Usually about 1.8 m
Receiver:	
Data signals	Co-, quad-, and power impulse responses; dual channel
Sync signal	1 per data frame
Frame rate	1 to 50 per second
Sensitivity	-85 dBm for AGC action -105 dBm for response measurements and phase lock
Antenna	Log-periodic (unidirectional, with crossed-planar polarizations)
Gain	7 dBi
Line losses	5 dB
Height	From 1 m to about 25 m
Max measureable path loss	146 dB
(Free space loss at 1200 MHz, 10 km, is 114 dB.)	

Figure 3. Photograph of the conical monopole antenna used at the transmitter terminal.

The vehicle used for the transmitter terminal was a Chevrolet Suburban[2]. The passenger seating in the rear of the van was removed to provide space for the PN probe transmitter equipment. The conical monopole antenna was mounted on the top of this vehicle, using a modified set of luggage racks. The antenna ground plane was hinged at one side of the luggage racks and normally bolted to the other side. When the ground plane was in a horizontal position, the conical monopole provided a vertically polarized pattern. Raising the ground plane to a near vertical position then provided a horizontally polarized pattern from this antenna. The pattern may be thought of as having the shape of a doughnut. Thus, the vertical polarized pattern was essentially omnidirectional in the horizontal plane. For measurements performed with horizontal polarization, the "doughnut" pattern stands on end, which results in a degree of directivity to the pattern in the horizontal plane. This feature can be seen from the pattern measurements presented in Appendix F. A

---

[2] Certain commercial equipment, instruments, or materials are identified in this paper to specify adequately the experimental procedure. In no case does such identification imply recommendation or endorsement by the National Telecommunications and Information Administration or by the U.S. Army, nor does it imply that the material or equipment identified is necessarily the best available for the purpose.

photograph of the antenna mounted on the top of the transmitter vehicle is shown in
Figure 4. When the antenna was raised for horizontally polarized measurements, the
bolts were removed and a pair of supports were attached to the ground plane. The
other end of the support rods were then bolted to the luggage rack.

Occasionally, in order to obtain some operational gain at the transmitter end
of a particular test path, a different antenna was used at the transmit terminal.
It was the same as the receiving antenna, which is described below.

The receiving antenna was a crossed-planar log-periodic type that was obtained
commercially from American Electronics Laboratories. It was designed for operation
over a frequency range from 0.4 to 4.0 GHz. Figure 5 describes the physical shape
and size of the antenna. The actual antenna used had a foam-filled radome at the
tip which provided some environmental protection to the higher frequency dipole
elements. This feature can be seen in Figure 6, which is a photograph of the actual
antenna used. The manufacturer's characteristics for the antenna are listed in
Figure 5, and the pattern provided at least a 25 dB front-to-back ratio. Thre
identical antennas of this type were procured. One was generally mounted to an
aluminum mast on the receiver van and one was mounted on the portable tower that was

Figure 4. Photograph of the conical monopole antenna
mounted on top of the transmitter van.

11
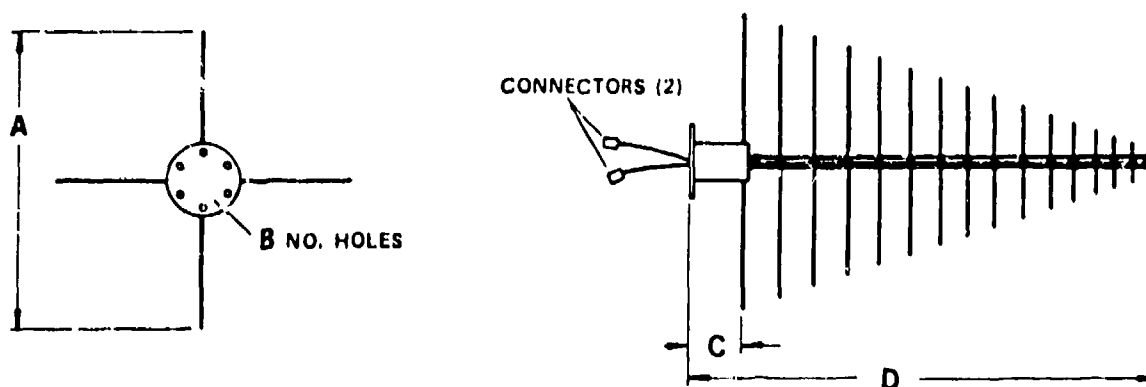
Dimensions:

A = 16.25 in.
B = 6
C = 3.50 in.
D = 26.50 in.

Characteristics:

VSWR   - 2:1
E plane   - 55°
H plane   - 85°
Gain   - 7 dBi
Isolation - 25 dB

Figure 5. Characteristics of the crossed-planar log-periodic receiving antenna.

Figure 6. Photograph of the crossed-planar log-periodic receiving
antenna. This antenna was also used as a transmitting
antenna for certain experiments.

12

used at the receiver locations. The third antenna was used as a spare and on occasion as a transmit antenna as mentioned previously. The power rating for this antenna was specified by the manufacturer at 20 W; it was therefore not used for extended periods of time as a transmit unit.

The receiver van used for the experiment was a 7-m (24-ft) travel-home, which was leased from a commercial outlet. The vehicle floor plan included a daybed with an overhead bunk that could be pulled down from the ceiling. The upholstered pads were removed from these two bunks, replaced with a sheet of plywood, and were then used to support the PN probe receiving equipment. The lower surface was used for the receiver and a digital data system including a digital tape deck. The upper surface was used to support an analog magnetic tape machine, the monitor oscilloscope, a spectrum analyzer, a paper stripchart recorder, and miscellaneous test equipment. Figure 7 presents three photographs of the equipment in the motorhome. The top photo shows the digital data system and terminal. The middle photo shows the upper bunk with the analog recording equipment and the spectrum analyzer. The lower photo shows the monitor oscilloscope used to display the impulse response functions. Two responses, one from each of the PN probe receiver channels, are seen on the screen.

As noted previously, the transmitter terminal equipment was installed in a suburban van. This vehicle also contained a small gasoline motor-generator set (1.5 kW) which was used to power the transmitter equipment. The unit was mounted toward the rear of the van, with an exhaust port provided through the floor. This generator set was also used occasionally to power the motor used in erecting the telescoping antenna tower. The latter equipment is described below.

Figure 8 shows two views of the transmitter van. The top photo shows a side view in which the transmitter antenna and ground plane can be seen on the top. The lower photo shows the rear of the van with one door open. The motor-generator power set is visible through the open door. The proximity of the generator to the PN transmitter did not cause any discernable EMC problem. Occasionally, when the transmitter van was engaged in mobile runs, a styrofoam bulkhead was placed between the test equipment and the motor-generator to reduce the noise level for the operating personnel.

Some of the measurements described in Section 3 of this report were made with the receiving antenna mounted on a tower. The tower that was used is the property of ITS. It is a telescoping unit, mounted on a tandem-wheeled trailer, and designed so that the nested sections pivot into a horizontal position for transit. Each tower section is nominally 6.1 m (20 ft) in length, and the fully extended height

13
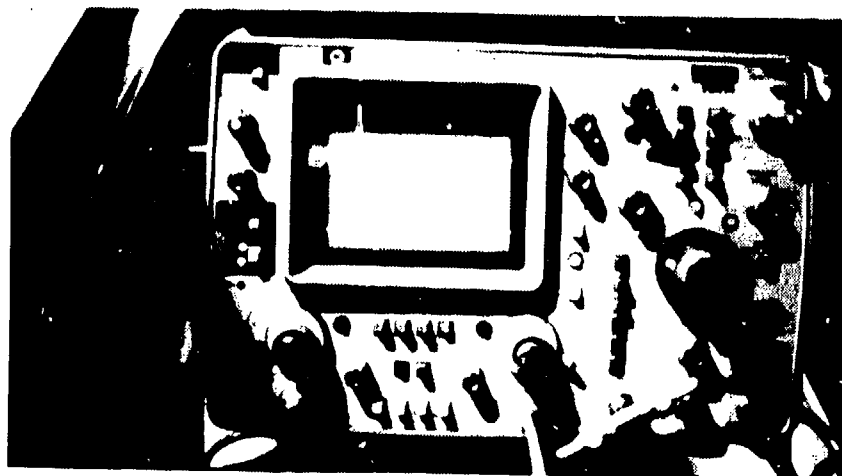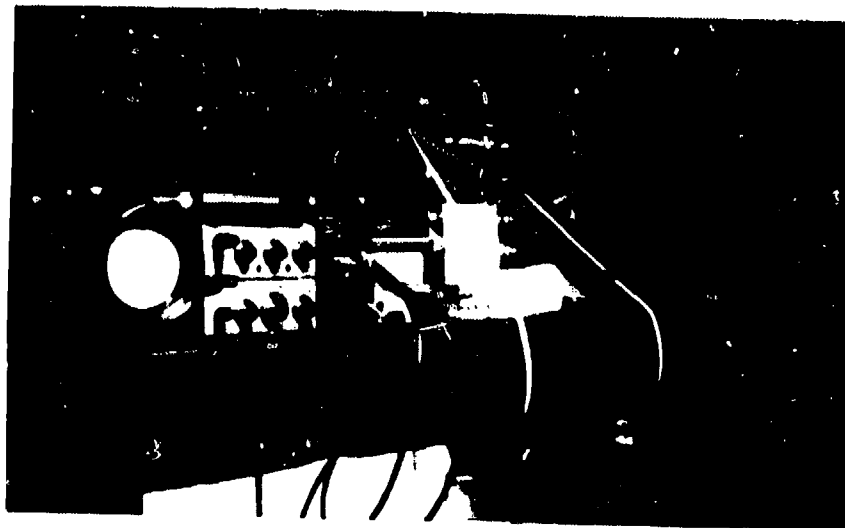
Figure 7.   Photographs of the receiving equipment in the motor-home receiving van.

14

Figure 8. Photographs of the transmitter van.

is approximately 45.7 m (150 ft). This full height was never used in the experiment, partly because of limitations imposed by the dense forest on the expanse of the required guying support. Figure 9 presents two photographs of the tower as used in the forest-grid (see Section 3) area of the experiment region. The top photo shows the tower fully guyed at a height of approximately 20 m (76 ft). The lower photo shows the tower extended by one section at the top to a height of approximately 25 m (91 ft). Note that at this height the top section was not guyed. This height was maintained for only short periods of time and in calm weather. It was used primarily for a height-gain data run described in Section 3.

The motor-home housing the receiver had a self-contained motor-generator unit capable of about 4 kW continuous load. All of the receiving equipment and the data acquisition systems were powered from this unit during mobile portions of the experiment. Some data runs were made in locations where commercial power was available. In these instances the entire motor-home system was switched to the commercial source using a heavy-duty drop cord. This arrangement was also used whenever the equipment was not in operation overnight and other off-duty hours. A secure parking area was provided by AEDC with access to commercial power. This arrangement made it possible to maintain all of the reference oscillators at their proper operating temperature, without relying on their standby battery power sources.

Figure 10 presents two photographs of the motor-home receiver. The top photo shows a full side view of the vehicle in one of the test locations near Normandy Lake (see Section 3). The receiving antenna is mounted on a 2-in. aluminum mast, which was clamped securely to the ladder at the rear of the vehicle. A close-up view of the mast and antenna is given in the lower photo of Figure 10. The cables feeding the antenna were run through an air-vent in the roof of the motor-home.

All of the vehicles described above were driven from the ITS Laboratories in Boulder, Colorado, to the test site at the USAF Arnold Engineering Development Center (AEDC), near Tullahoma, Tennessee. The suburban van was used to pull the tower/trailer, and both vehicles were driven by ITS personnel. All of the test instrumentation was transported to the test area via these vehicles.

2.3 Test Configuration Data

A number of different test configurations at both the transmitter and receiver terminals were used throughout the experiment, as described in Section 3. It is the purpose of this section to present some of the fixed system parameters and measurements that are applicable to the experiment configurations that will be described later.

16
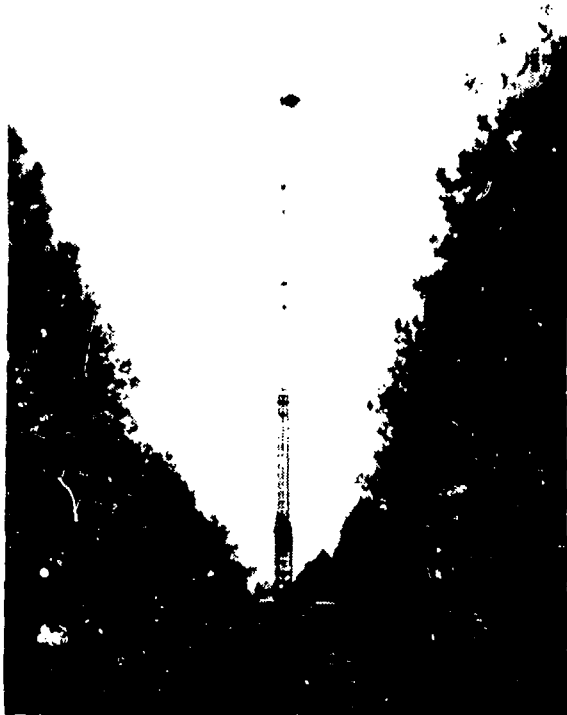
Figure 9. Photograph of the receiving antenna tower.

Figure 10.   Photographs of the motor-home receiver.

18

2.3.1 Transmitter Power Levels

The PN probe transmitter was equipped with a precision directional coupler and rf power meter for measuring the transmitted power at all three frequencies. The power levels were measured at the beginning of each day's run and checked at other times during the day to determine stability and to detect possible problems. The data presented in Table 4 may be used for all of the test configurations in this report, as the transmit power levels were maintained within a tolerance of ±0.5 dB to those tabulated.

Table 4. Transmitter Power Levels

Frequency	Power Into Antenna Cable	
600 MHz	2.7 W	34.3 dBm
1200 MHz	10.5 W	40.2 dBm
1800 MHz	7.3 W	38.6 dBm

2.3.2 Transmission Cable Losses

A number of cables were used in the various test configurations. Each cable used at the transmitter and receiver terminals was measured for its loss at each operating frequency. Table 5 presents a complete list of these cables, a note as to where each was used, and the measured loss at the appropriate frequency. It should be noted that all of the cable-loss measurements were made with the wideband PN probe signal as the source. This aspect is significant, as the loss for a cw source would be somewhat different from the values measured here. Thus, the measured loss applies directly to all test data presented. For simplicity, each cable has been assigned an arbitrary number in Table 5, and these numbers are used in Section 4 to ide... fy the cables used in any given configuration.

2.3.3 Calibration Levels

The calibration signal levels were measured using a precision power meter and are as follows for all of the calibration data:

600 MHz: -35 dBm

1200 MHz: -31 dBm

1800 MHz: -33 dBm.

2.4 Data Acquisition Systems

The data acquisition for this experiment was accomplished with two essentially independent systems. The first is an analog system that has been used previously

19

Table 5. Transmission Cable Loss

Cable No.	Cable Type	Approximate Length Ft	Approximate Length M	Test Configuration	Loss in dB 600 MHz	Loss in dB 1200 MHz	Loss in dB 1800 MHz
1	Andrew FH-J4-50 Heliax	10	3.05	Tx antenna cable; used on all mobile runs, where the conical monopole or log-periodic antennas were vehicle mounted	0.2	0.4	0.6
2	Andrew FH-J4-50 Heliax	50	15.24	Rx antenna cable; used on receiver configurations where the antenna was mounted on the test tower	1.0	1.6	2.3
3	Andrew FH-J4-50 Heliax	50	15.24	Same as note above for cable No. 2; used generally in tandem with cable No. 2 for antenna heights >45 ft	1.1	1.6	2.4
4	RG-9B	20	6.10	Rx antenna cable; used on the receiver van for the antenna mounted to the mast on rear of van (vertical polarization)	1.1	1.5	3.75
5	RG-9B	20	6.10	Rx antenna cable; same as configuration given for cable no. 4 (horizontal polarization)	1.2	1.6	3.8
6	RG-9B	6	1.83	Rx antenna cable; used on the receiver van between the receiver and side van port; connected generally to cables 2 and 3	0.5	0.7	1.0
7	Andrew FH-J4-50 Heliax	280	85.3	Tx antenna cable; used in tests where the transmit antenna was mounted on fire towers	6.0	9.1	12.2

with the PN probe. It is described in Section 2.4.1. The second system is digital (microcomputer based unit with digital recording capability and some inherent field processing). It is described in Section 2.4.2. The analog system was primarily used for on-site data monitoring, and the analog recordings retained as backup for the digital logging system.

2.4.1 Analog Data System

The analog data acquisition system was used to monitor directly the data signals from the PN receiver channels. A variable persistence oscilloscope was used to view either of the quadrature impulse responses, the linear power impulse response, or the log power impulse response at the discretion of the operator. A polaroid camera was used with the scope to record periodically any of these response functions for later review. The AGC voltages were recorded continuously on a strip-chart recorder for on-site observation. These signals were also recorded on analog magnetic tape as outlined below.

A time-code generator/reader was part of the analog system. A standard IRIG Code B timing signal was generated and recorded on one channel of the magnetic tape during all data runs. The recorded tapes may be played back from the same tape deck for review purposes. The recorded timing signal can in this case be read by the generator/reader to locate any specific section of recorded data. Other timing signals available from the generator/reader were used for controlling other operations or placing time marks on records such as the strip-chart recorder.

The analog tape recorder is equipped with an audio band edgetrack. It was used to provide voice annotation when required on the analog tapes.

The signals that were recorded on the analog tapes are as follows:

(1) IRIG Code B time-code signal,

(2) Rec. Chan. 1 power impulse function,

(3) Rec. Chan. 2 power impulse function,

(4) RSL, Rec. Channel 1,

(5) RSL, Rec. Channel 2,

(6) PN code sync signal,

(7) Spare track for either one quadrature function or the logarithm of the power impulse function, and

Edge - Voice annotation.

2.4.2 Digital Data Acquisition System

The digital data acquisition system was the primary system for recording the measured data. Called the Wide Band Propagation Measuring System (WBPMS), the

21

system is directed by a microcomputer, the iSBC 80/30 using the 8085 CPU. It accepts commands from a portable terminal wired directly into it and writes information records, calibration records, and data records on 9-track phase-encoded magnetic tapes. It receives input directly from the PN probe in the form of the analog traces of the two quadrature impulse responses from each of the two received channels. It samples these traces, converts the samples to digital numbers, and records the results. It can take up to 1000 samples per frame at a rate of up to 10,000 samples per second. (A "sample" here means four different values from the four received traces.) The A-D conversion provides a precision of 12 bits, thus allowing about a 1000 to 1 ratio between the strongest and weakest readable pulses in the response functions.

Recorded in each data record along with the four responses are the date, time (to within 1 s), and the AGC voltage on the two receiver channels (we assume this remains constant throughout each frame). In addition, accompanying the receiver van is an infrared distance meter with a digital readout. This was used on occasion to monitor the receiver antenna height. Its output value is part of the data record.

The tape is written in fixed length records of 4096 8-bit bytes with occasional end-of-file marks. The information may be in ASCII characters, Intel 1-byte or 2-byte integers, or Intel FORTRAN 4-byte real numbers. The records are divided into sections representing single measurement runs. Each section begins with a header record which describes various parameters of the run. Following that is an optional calibration record for the AGC values. On the first section of a tape, the calibration record is mandatory. Then comes a sequence of data records, each frame requiring two physical records. Finally, following the data records is a "trailer" record in which is described the success or failure of the complete run. Further details may be found in Appendix D.

3. EXPERIMENT CONFIGURATIONS

The measurement program was conducted in October 1979 in areas in and around Tullahoma, Tennessee, and the USAF/AEDC. Three specific areas were used for measurements as follows:

(1) Camp Forrest area,

(2) AEDC Main Gate area, and

(3) Normandy Lake and Negro Hill.

The following paragraphs describe these areas in some detail. Section 4 presents specific details of the various measurement runs together with a brief narrative of on-site results. Later sections will discuss analyses of these data.

22

3.1 Camp Forrest Area

Camp Forrest is an abandoned Army camp on AEDC property. All structures have been torn down and removed, and the area has been planted with trees. What remains of the camp is the set of old asphalt roads and streets. As one sees in Figure 11, these form a fairly regular rectangular grid of access roads and produce a very excellent area for making forest penetration studies. The camp is bisected by a modern two-lane highway, and measurements were made only in the northern section where the forest is more homogeneous and the terrain flatter.

The forest in this northern section is now about 15 m (50 ft) high and consists of both deciduous and coniferous trees. Five specific sections or "blocks" were identified in preliminary site surveys as being particularly good for studies of the desired kind. Each has somewhat different characteristics of forestation. They are shown as shaded areas in Figure 11, and their properties are described in Table 6.

Table 6. Forest Characteristics in the Camp Forrest Area

(Densities given are area densities and indicate the amount of tree trunk wood per unit area. They were measured with a forester's densitometer. Note that a density of 1% is equivalent to 100 m^2/hectare or about 440 ft^2/acre.)

___

Section 1 between 3rd and 4th Streets:

Fairly homogeneous stand of pine with little underbrush. Only top half is foliated. Height, 16 m (52 ft); density, 0.28%.

Section 2 between 6th and 7th Streets:

Tall skinny pines with moderate underbrush. Height, 16 m (52 ft); density, 0.25%.

Section 3 between 17th and 18th Streets:

Very dense, mixed with heavy underbrush; 16 m (52 ft) pines mixed with 6 m deciduous trees. Density, 0.30%.

Section 4 between 25th and 26th Streets:

A stand of pines with light underbrush. The pines are 14 m (46 ft) high but have large diameters. Density is 0.28%. A concrete foundation is prominent near Avenue A and 25th Street.

Section 5 between 29th and 30th Streets:

A heavy mixture similar to Section 3. Pines are 11 m (36 ft) high with some higher. There are some very big deciduous trees, 0.6 m (2 ft) in diameter and 16 m (52 ft) high. Density is 0.25%.
___

23

Figure 11. The Camp Forrest area on AEDC property. The map is taken from the northeast corner of the Tullahoma quadrangle (USGS).

For documentation purposes, the two long east-west roads were called Avenues A and B. The short crossroads (shown as dashed lines on Figure 11) were then numbered consecutively from west to east and called Streets. Thus, 1st Street may be found at the left of Figure 11.

The transportable tower was erected at site S1 on 30th Street between the two Avenues. In addition, just south of the highway opposite to 22nd Street, there is a lookout tower some 20 m (65.6 ft) high. It is called T1 in Figure 11 and was used to support one or other of the terminals in some of the measurements.

3.2 AEDC Main Gate Area

The AEDC main gate is located about 12 km east of Camp Forrest. It is in this area that secure parking space was available and that commercial power could sometimes be used. The area directly in front of the complex and bordering the highway is characterized by large evergreen trees that are widely separated (compared to the dense forest areas), and by no undergrowth. The grass under these trees is maintained, and most of the foliage on the trees is limited to the upper half. The area is outlined in Figure 12 and was used in the measurement program as an example of a quite different kind of forest.

About a kilometer west of the main gate is a second lookout tower very similar to the one in Camp Forrest. It was used to support the receiver antenna in a long, overnight run. It is indicated in Figure 12 as the point T2. The TX van was positioned at the point called S6, about 197 m away.

3.3 Normandy Lake and Negro Hill

This area is located to the northwest of Tullahoma. The general location was selected to establish several propagation paths which were either line of sight or which went across isolated and fairly well-defined simple contoured hills. Negro Hill is virtually an island in a small TVA reservoir, and, as illustrated in Figure 13, many of the paths used cross it. The emphasis for tests in this area was based on terrain features and on the possibility of scatter from the tree-covered hills surrounding the lake.

For these measurements, the receiver antenna was mounted on a mast at the rear of the RX van. The two test vehicles were located at off-road points predicated on road conditions, available parking space, and minimum vehicle movement. Since the TX van was the more mobile, it was moved more frequently and into the more remote locations. The antenna mast on the RX van was mounted so that the azimuth adjustments could be made by rotating the mast, thus minimizing the required motion of the van.

25
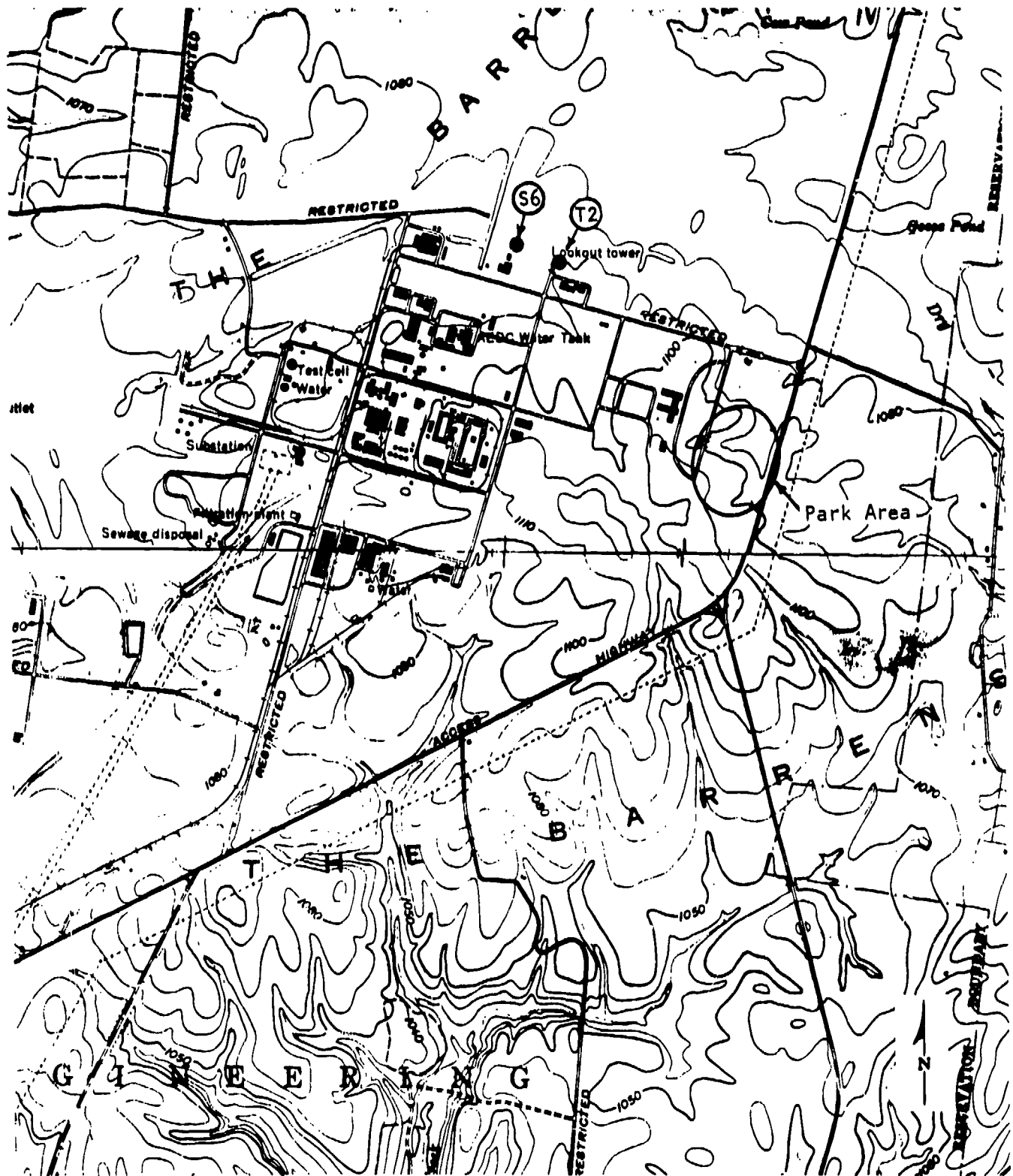
Figure 12.   The AEDC Main Gate area.   The map is taken from the Capitol Hill
and Manchester quadrangles (USGS).
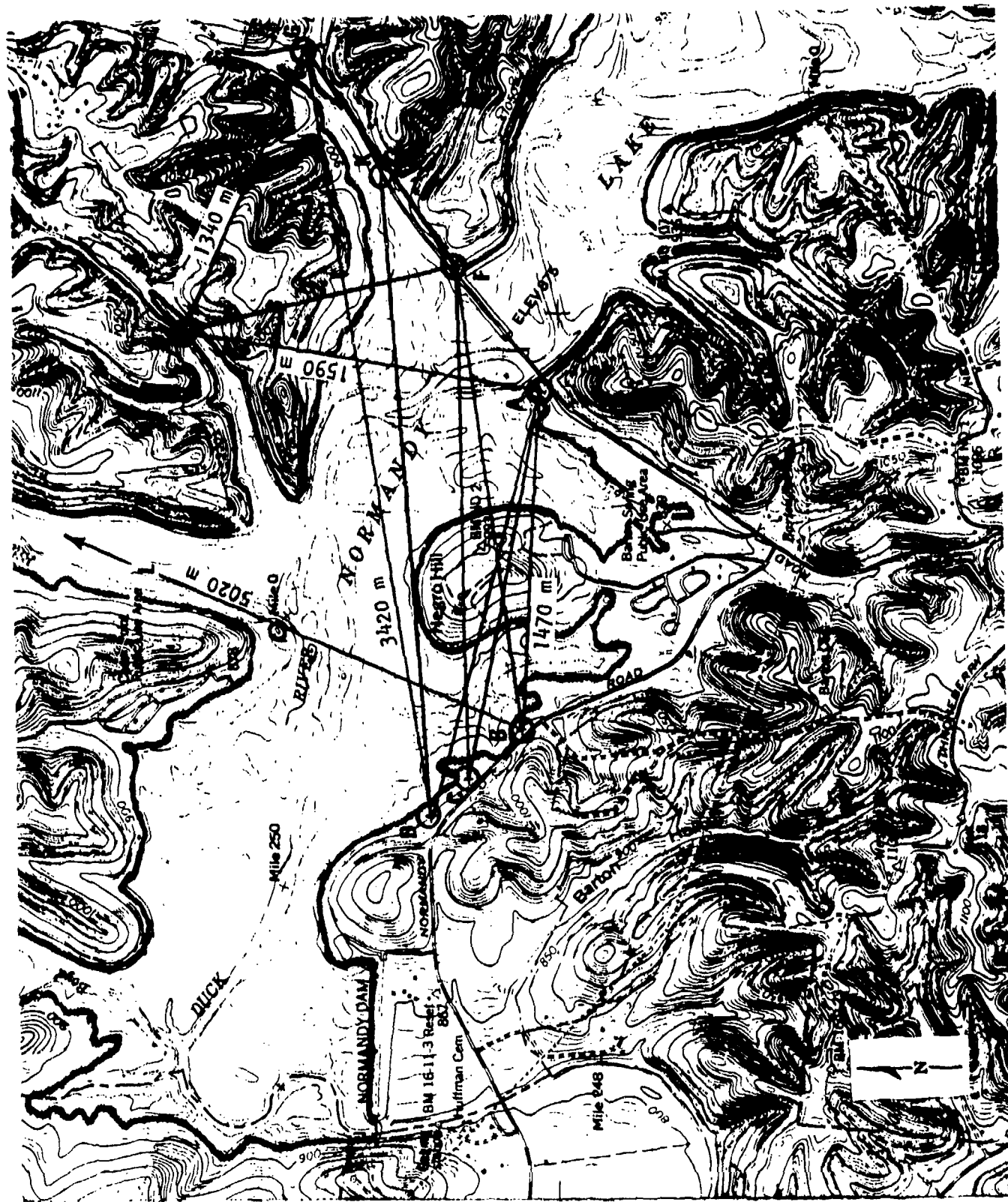
Figure 13. The Normandy Lake and Negro Hill area. The map is taken from the
western edge of the Normandy Lake quadrangle (USGS).

4. MEASUREMENT PROCEDURES AND PRELIMINARY RESULTS

The purpose of this section is to describe the conduct of the experiment and to present important on-site observations and some preliminary results derived from the analog records. Some analog data were processed to determine answers to particular questions that arose in the digital analyses. Some of these results are presented later in this report.

The elements of the total experiment described below are presented in the order in which they were conducted. Most of the originally planned variety of path types were used in the conduct of the experiment.

4.1 Test Period and Setup

The measurements were performed during the period of 10-26 October 1979. After driving the test equipment to AEDC in Tullahoma, Tennessee, the first day was spent in arranging for secure vehicle parking space and access passes to AEDC for both personnel and vehicles. The test tower for the receiver antenna was erected at the site S1 on 11 October to an initial antenna height of 21.0 m (69 ft). This was the maximum height that could be reached with full guying, due to lack of a larger grid base for guy anchors in the heavy forest. The tower was raised one additional section on occasions (noted below) without permanent guyed support. This provided a maximum antenna height of 27.8 m (91 ft).

The experimental period was divided between the three configurations/areas cited in Section 3 as follows (all dates are in 1979):

Date	Configuration or Area
10/11 thru 10/18	AEDC North Grid area
10/18-19	Special all-night run performed in AEDC base area
10/20 thru 10/23	Normandy Lake/Negro Hill area
10/24	AEDC Main Gate area
10/24-25	AEDC North Grid area

4.2 AEDC Grid Area Measurements (10/11-18)

The test tower was erected on crossroad No. 30, approximately 1/4 of the distance from Avenue B toward Avenue A. The distance from the intersection of 30th and B to the tower was approximately 70 m (230 ft), as determined from a USGS map of the region. The first objective of the measurements was to obtain data relative to the attenuation of the forest, beginning in Section 5 as shown in Figure 11.

28

A run was made beginning with the TX located on crossroad 29, directly across Section 5. Data were recorded at 600 and 1200 MHz in two configurations: one with the receiver antenna on the tower and one with the receiver antenna mounted to a mast on the rear of the receiver van. The configuration parameters for this and subsequent data runs in this series were as follows:

RX Antenna Location	RX Antenna Height (ft/m)	RX Ant. Cable Nos.	RX Cable Loss		TX Ant. Cable No.	TX Cable Loss	
			600 MHz	1200 MHz		600 MHz	1200 MHz
Tower	76.5/20.2	2, 3, 6	2.6 dB	3.9 dB	1	0.2 dB	0.4 dB
Van	16/4.9	4	1.1 dB	1.5 dB	1	0.2 dB	0.4 dB

The initial plan was to continue the above runs, moving the TX progressively away from the receiver block by block. Measurements were continuously recorded on the strip chart and analog tape recorders as the TX van was moved. During the movement, an enhanced signal level was observed at times that appeared to correlate with intersection positions of the TX van on Avenue B. Thus, the run sequence was altered to include short data runs at TX locations both within the forest on the crossroads, and at intersections with Avenue B. The sequence was continued until the TX van had moved to crossroad 27.

In order to provide some LOS reference data for the attenuation due to the forest, two additional runs were performed. The first of these was with the TX van located at the intersection of 30th and B. In this configuration, the propagation path was along crossroad 30. The distance between TX and RX was approximately 70 m (230 ft), and the signal was received off the side of the RX antenna at the 270° point on the pattern. In other words, the RX antenna was still oriented toward the west, since it could not be changed without lowering the tower.

The second series of LOS measurements were made with the RX van moved to the intersection of 30th and B. The TX van was moved progressively away from the RX van toward the west along Avenue B. Analog data were recorded continuously, and digital data were recorded with the TX van stopped for short periods at each intersection (about every 140 m). One of the objectives of this particular run was to evaluate the terrain effects on the propagation with respect to the forest attenuation measurements. It was noted at the outset of this series that the terrain rose gradually in elevation toward the west. At some point in the series along Avenue B, the TX van moved over the horizon and the path became one of diffraction for the low RX van

29

antenna. This will be seen in the results presented later in this section. This series was continued with the TX van moving out to crossroad 17, 1680 m away, and returning. A few data points were repeated as the TX van returned toward crossroad 30.

During the above runs, it was observed that the 600-MHz data were subject to a considerable amount of interference. An investigation was made using a spectrum analyzer, and, as is shown in Figure 14, several interfering sources could be seen. Indeed, there are four UHF television stations in Huntsville, Alabama, about 75 km (46.6 mi) away. They operate on channels 19, 25, 31, and 48 with picture carriers at 501.25, 537.26, 573.26, and 675.24 MHz, respectively. These probably correspond to the four strong signals in Figure 14; the split lines for each probably represent the picture carrier and the audio signal with 4.5 MHz separating them.

A second series of measurements almost identical to those described above was conducted on 15 October 1979. The interference was not so severe on this date, and most of the results could be used and compared with the earlier data. The analog data for these runs were analyzed, and results were very similar to the digital data analysis described in Section 9.
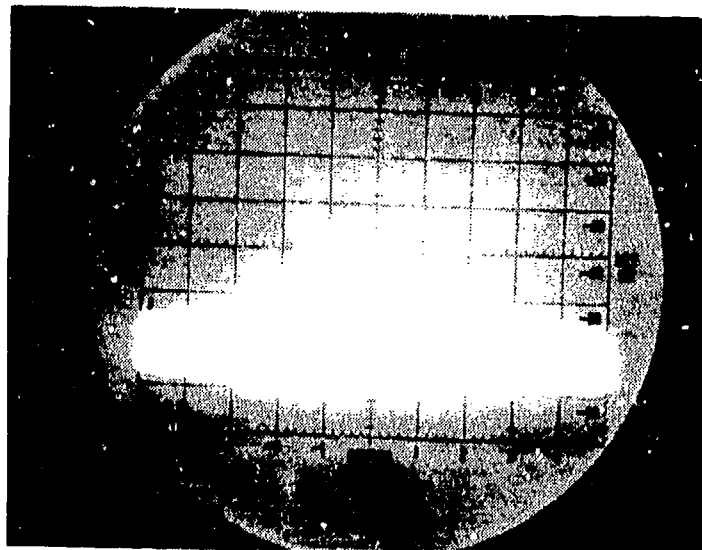
Figure 14. A spectrum analyzer display of the interference signals
            observed near the 600 MHz test signal. The center fre-
            quency is 600 MHz and the scale is 50 MHz/division.

Figure 15 presents the data for the measurements along Avenue B on 12 October 1979, which were performed to evaluate the effects of the terrain irregularities with respect to the forest attenuation data. In other words, the question was to delineate between forest attenuation and possible diffraction effects in the data runs. An exaggerated plot of the terrain profile along Avenue B is included in the figure for reference. It can be seen from the horizon lines plotted between the RX and TX locations that at a point somewhere near the intersection of crossroad 25, the propagation path becomes diffractive. The general shape of the curve for the 1200-MHz data confirms this fact. The ordinate for this curve is the "attenuation relative to free space." Also called the "excess path loss" or simply the "attenuation," it is the amount (in decibels) by which the measured RSL is less than what should have been observed at the same distance in free space.

Note that the companion 600-MHz curve, as indicated by the dashed portion, shows the effects of the strong interfering signals we have previously noted. The possibility of interfering signals is also observed in the 1200-MHz data towards the far end of the curve between crossroads 19 and 17.

We cannot explain at this time the variation in signal level measured at 1200 MHz between crossroads 24 and 23. The rise in the terrain at crossroad 25 obviously has an effect. The impulse response throughout these runs was quite dispersed, indicating a number of propagation paths. In addition, Avenue B is heavily forested on both sides. Just as a consideration of what the off-path contributions might be in this environment, we can consider the size of the Fresnel zones. For example the radii of the first Fresnel zones at mid-path for a path between crossroad 30 and crossroad 27 are on the order of 7 and 5 m (23 and 16 ft) for the 600-MHz and 1200-MHz signals, respectively. Thus, we would speculate that the forest on both sides of Avenue B can make a difference in the total path loss. No doubt it is this effect that is measured as the excess path loss between these two crossroads.

It was stated previously that during the conduct of these measurements a signal enhancement was observed when the TX van moved from a position on a crossroad within the forest out to the corresponding intersection with Avenue B. A brief comparison of the data points for the observations of 12 October and 15 October confirms this position gain in most cases for the runs that extended out to crossroad 25. The one exception was observed for the data points on crossroad 29. Here the loss at the intersection was greater than that observed when the TX van was deep in the forest on that crossroad. We currently have no explanation for this result. All of the other data points with the RX antenna above the treetops indicate a "position gain" between 3 and 7 dB when the TX antenna moved out to an intersection.

31

Figure 15. Path loss measurements performed along Avenue B, with the RX stationed at the Intersection of Crossroad 30 and Avenue B.
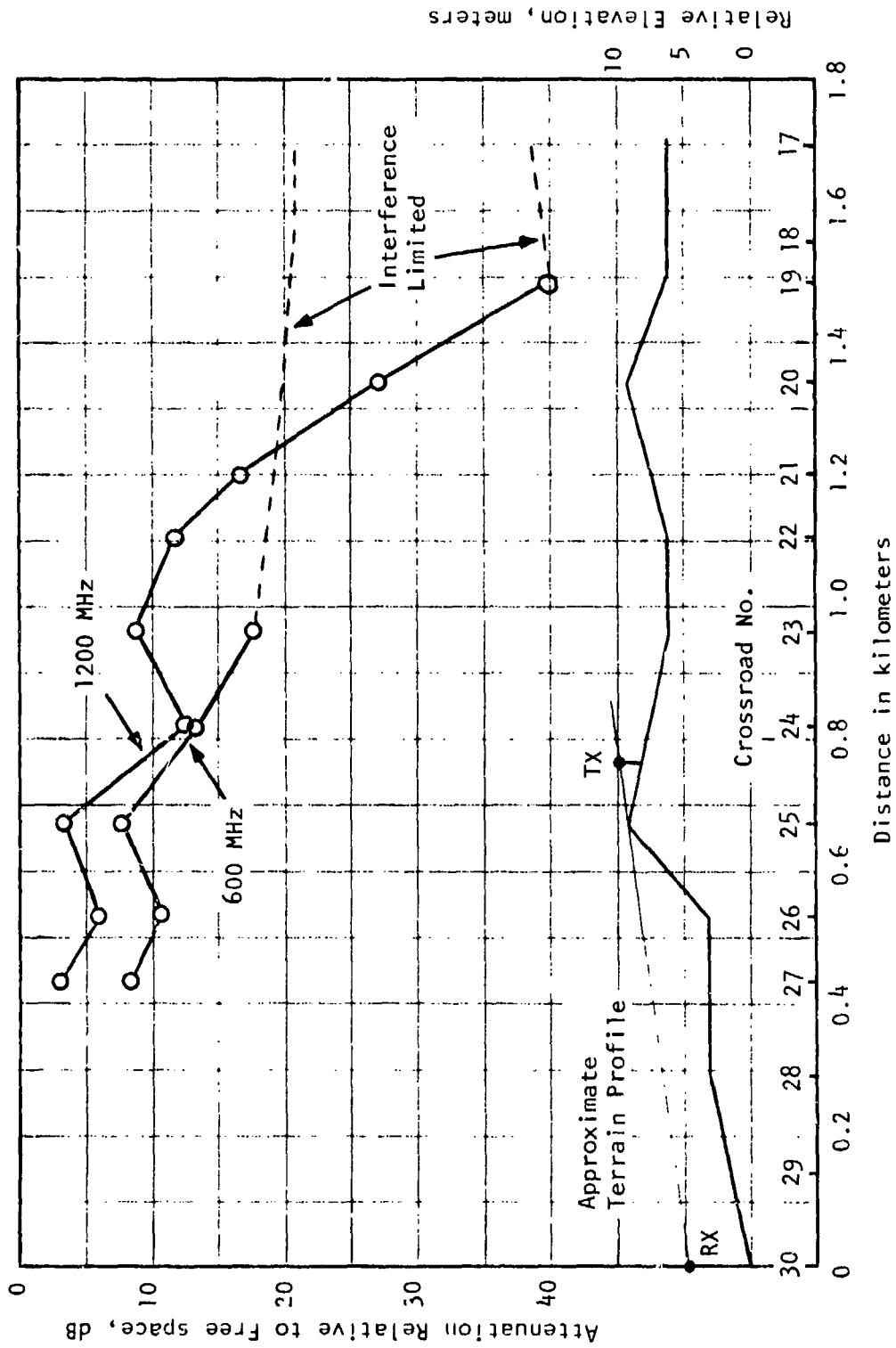
RX Antenna Height = 4.9 m, TX Antenna Height = 1.8 m

32

Similar data with the RX antenna well below the treetops indicate position gain values of 1 to 3 dB. This result suggests the possibility of some form of waveguide effect created by the trees which lined the roadways. However, we have no means of confirming such a speculative answer. The data points are very limited, and the result could be due only to differences in the forest density over the different paths. Further analyses would be required before this conclusion could be verified.

An important aspect of the measurements should be mentioned at this point with regard to the runs made on 12 October and 15 October. Many of the runs were repeated on these two dates, and a comparison of the AGC results indicated an agreement within 3 dB or less at both operating frequencies for 13 out of 15 possible comparisons. The two measurements that did not agree were a result of interfering signals seen in the 600-MHz data on 12 October.

Two additional types of measurement were performed in the AEDC North Grid area that we will discuss briefly here. The first was a run performed as a height gain measurement through the forest. The RX van was positioned in its original location at S1 on the test tower at 30th Street. The transmitter was located at the lookout tower T1 south of the highway that divides the North Grid area from a similar area to the south. The location of this path is shown by the line in Figure 11. The path distance was 1.2 km between the towers. The lookout tower is located in a fairly open area with only a few trees in the immediate vicinity. The forested area did not begin until the path crossed the highway. For this run, the TX antenna was a log-periodic type identical to that used at the RX tower. The height of the lookout tower was approximately 20.6 m (68 ft) at the top platform. The tower was a rectangular walk-up type, with full platforms at a spacing approximately 4.1 m (13 ft). A long foamflex cable (cable No. 7 in Table 5) was used to feed the transmitter antenna. The procedure for the run was as follows:

(1) Both antennas were at their maximum height well above the tree tops at the beginning of the run. The RX antenna tower was raised one section above its guyed height to 27.8 m (91 ft), and the TX antenna was mounted at the top platform level of 20.6 m (68 ft).

(2) Each antenna was lowered independently, beginning with the TX antenna. The TX antenna was lowered in steps (one platform level at a time) of 4.1 m (13 ft) each.

(3) The RX tower was lowered one section at a time—approximately 4.6 m (15 ft). Each section was lowered in a continuous manner, driven by the motor/cable mechanism.

(4) Digital data were recorded at each of the fixed antenna heights. Analog data were recorded continuously as the RX antenna was lowered.

The results of the height-gain run, as analyzed from the analog AGC records, are shown in Figure 16. These measurements were made using 600 and 1800 MHz. Both frequencies demonstrated a slight increase in signal level (∿1 dB) after the TX antenna was lowered from the top to the first landing below. Perhaps the result is a function of the penetration of Fresnel zones into the forest. The average tree height is nearly 16 m (52 ft), and the high point in the terrain profile coincides with the edge of the forest nearest the TX terminal along the highway. A cursory plot of the path profile and the initial height of the TX antenna reveals that the first Fresnel zone was very close to a grazing state at the treetop level near the lookout tower. After the TX antenna is lowered to the 16.4 m (54 ft) height, the first Fresnel zone would penetrate into the trees, again near the TX terminal. In this case, the signal level would indeed be expected to rise slightly as it did in the measurements.

The two sets of curves in Figure 16 (one set for each frequency) reflect the height dependence at the receiver terminal. In other words, two measurements for different RX antenna heights were made at each height of the TX antenna. We note that the measurements at both frequencies display a significant height-gain advantage at the receiver terminal at all levels, even when the antennas are near and below the tops of the trees. Each set of curves appear to be convergent, but the 1800-MHz data indicate a greater height gain for the same configuration as do the 600-MHz data. However, the rate of attenuation at 1800 MHz is also considerably greater.

The second type of measurement performed in the Camp Forrest area involved a change in polarization under a variety of conditions. Several blocks in the area were selected for these measurements, and the impulse response function was measured for various antenna polarization configurations and orientation with respect to the forested blocks. In free space a received response function will be simply a delayed copy of the transmitted pulse. But as the environment becomes increasingly cluttered with such objects as terrain, trees, and undergrowth, the receiver will respond not only to energy from the direct wave but also to energy reflected or scattered from these objects. Since the distance from transmitter to object to receiver is longer than the direct distance from transmitter to receiver, these scattered waves arrive at later times than does the direct wave. Thus the response function takes on the appearance of a sequence of "multipath components" which come at successively later times and produce a "multipath delay spread" where the

34
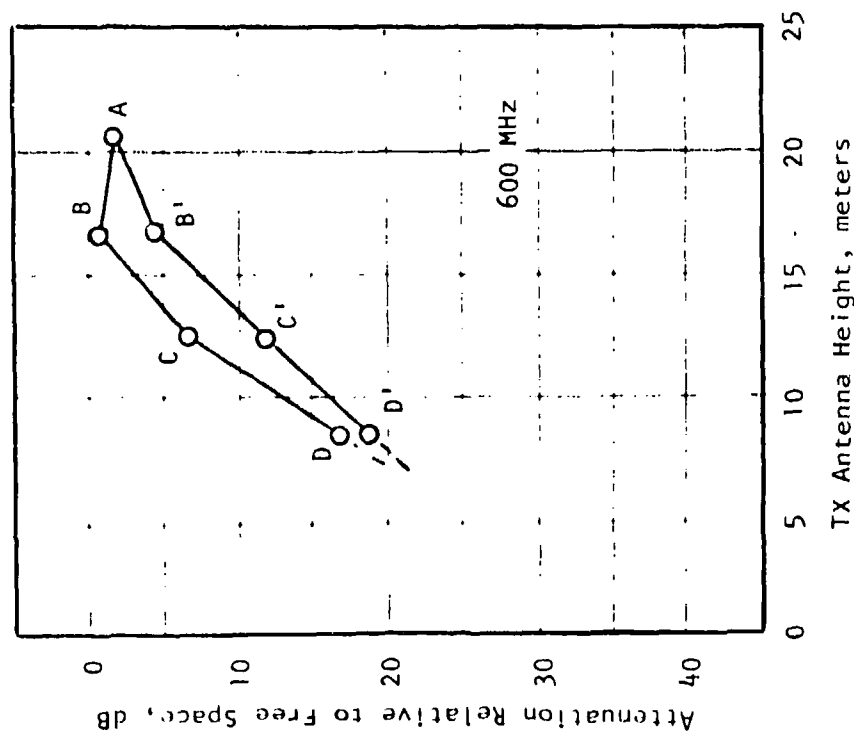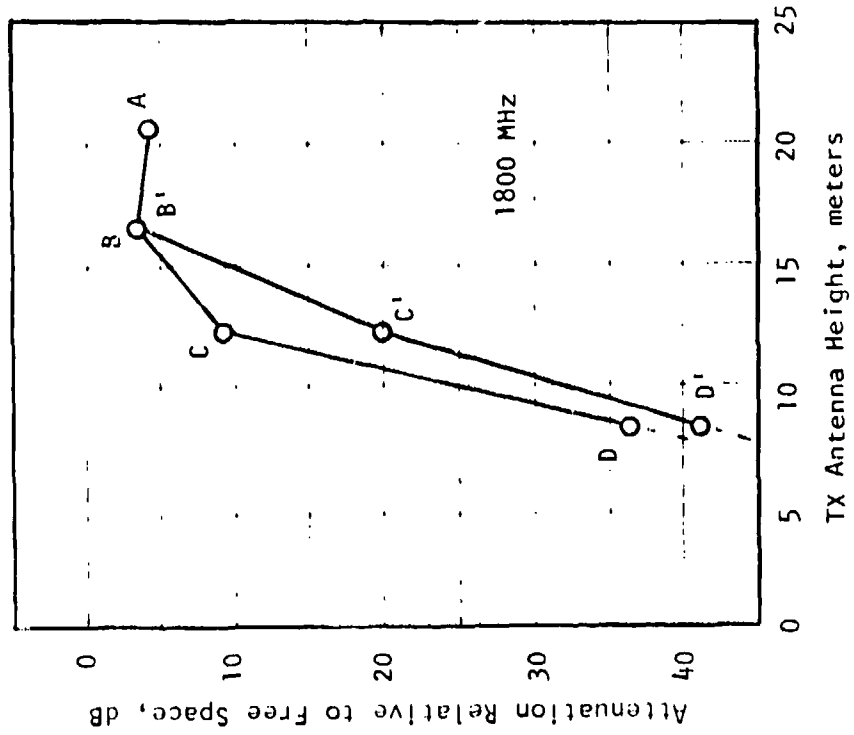
Figure 16. Height gain run performed between the fire lookout tower and the test tower in the AEDC North Grid area; path length was 1.2 km.

35

originally clean pulse is spread out over a considerable period. The magnitude of these multipath components will be determined by the scattering efficiency of the objects and by the attenuation the waves suffer as they pass through the medium. The direct wave, too, will suffer this latter attenuation and, indeed, may be completely blocked by the clutter.

Since most of the larger parts of a tree are directed vertically, it is reasonable to suppose that scattering efficiency is greater for vertical polarization than it is for horizontal polarization, and that therefore when the waves are vertically polarized there should be more observable multipath components appearing at greater delay times. On the other hand, one would also suppose that the attenuation rate is greater at vertical polarization, a fact which should counteract the above tendency. Nevertheless, it has been generally observed (see, e.g., CCIR, 1978) that the features usually attributed to multipath are more pronounced for vertical than for horizontal polarization.

The measurements we made tend to confirm these ideas. In most of the runs of this set it was observed that changing to horizontal polarization had a rather dramatic effect on the multipath signal structure. Two significant changes took place in both the low and high frequency tests as follows:

(1)   The delay spread in the response function was generally less with horizontal polarization.

(2)   The impulse response when horizontal polarization was used generally revealed a dominant initial response (path) that was frequently not seen in the corresponding response for vertical polarization data.

The changes were usually more pronounced in the higher test frequencies than they were in the 600-MHz data. As one example of the results, a series of polaroid photographs taken during one of the runs on 16 October are shown in Figures 17 and 18. Figure 17 displays the two characteristics noted above quite well. The top photo is the response for vertical polarization across the forest block between crossroads 17 and 18 (a 146-m path). The lower photo is the response for the same path, where the two antennas were changed to horizontal polarization. Figure 18 presents two photographs of the response function over the same path using a cross-polarized configuration. The top photo is the response for vertical polarization at the TX and horizontal polarization at the RX. The bottom photo is the reverse of this configuration. These results seem to imply that the polarization of the receiving antenna has the greater influence. This has not been confirmed however.

600 MHz

1800 MHz

(a)   Vertical polarization

600 MHz

1800 MHz
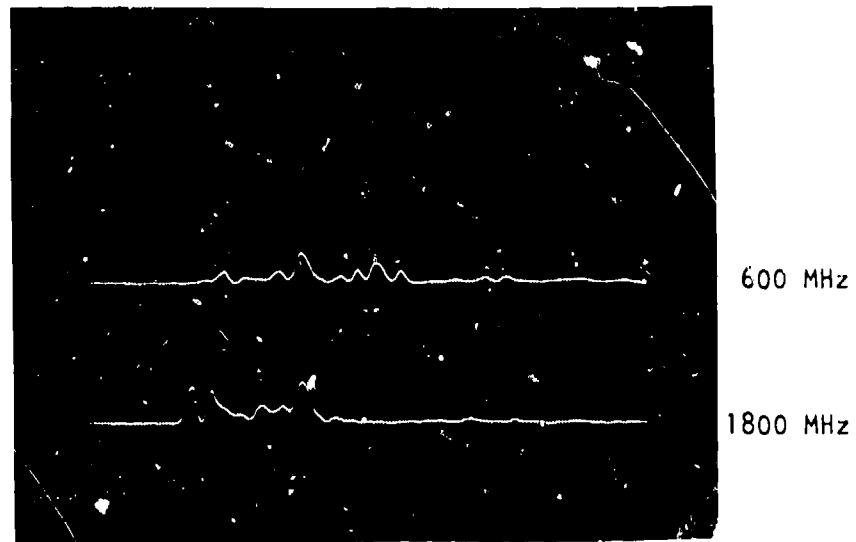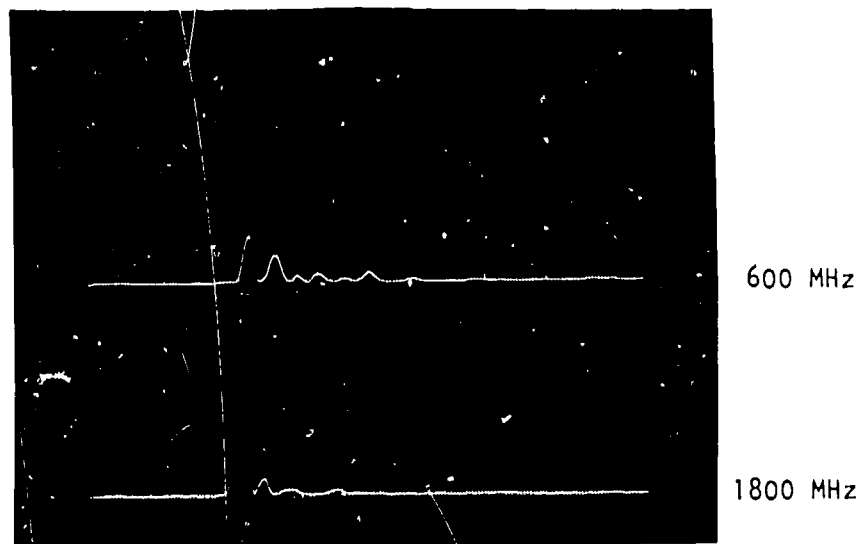
(b)   Horizontal polarization

Figure 17.   An example of the change in the power impulse with a change in
antenna polarization.   The measurement was made through the
forest between Crossroads 17 and 18.   Each trace covers a total
time span of 250 ns.

37
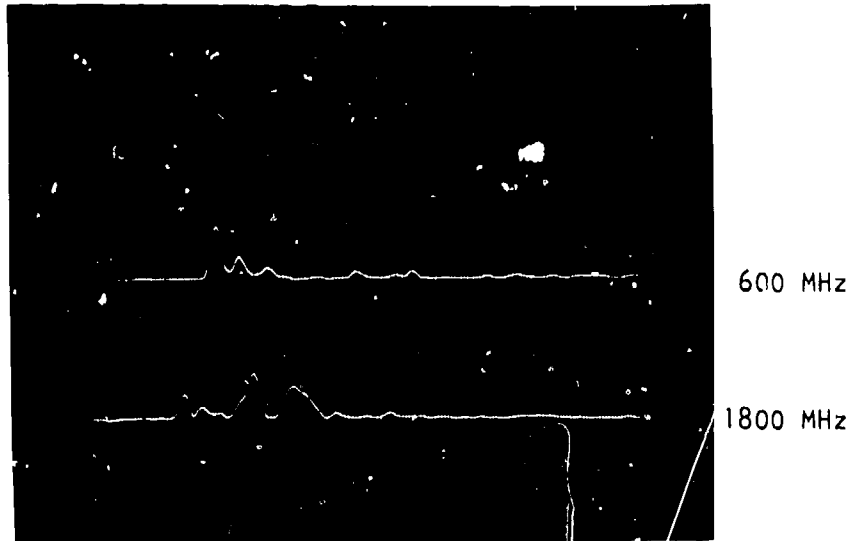
(a) TX - Vertical polarization
     RX - Horizontal polarization
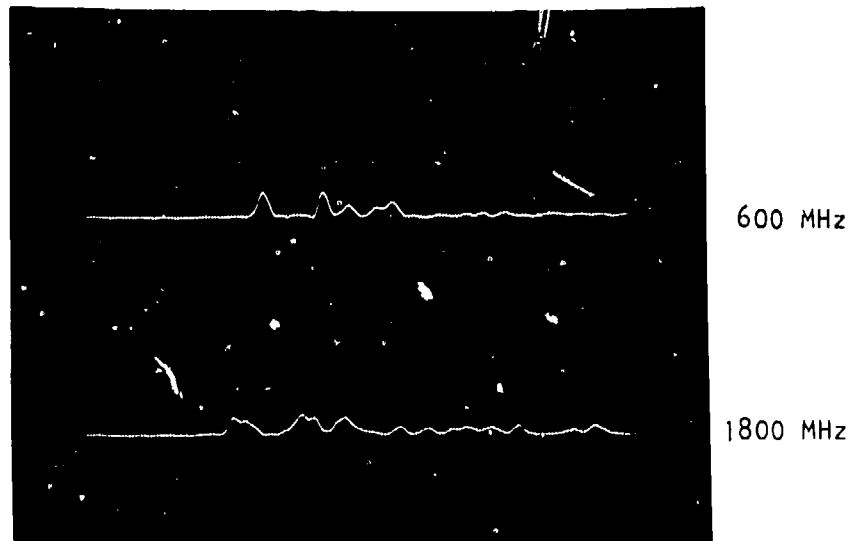
(b) TX - Horizontal polarization
     RX - Vertical polarization

Figure 18. An example of the power impulse function measured through the forest
            in cross-polarized antenna configurations. The test location was the
            same as that given in Figure 17. Each trace covers a total time span
            of 250 ns.

In all of the photos in Figures 17 and 18, the top trace is the 600-MHz response, and the bottom trace shows the 1800-MHz data.

4.3 AEDC Base Area

A special long-term run was performed in the AEDC base area on 18-19 October 1979. The weather forecast for the nighttime hours called for rain in the vicinity, and the run was originally planned to obtain comparative data under dry and wet conditions in the forest. Rather than operate the run on motor-generator power for a long period of time, a site was chosen within the main AEDC base area where commercial power was available for both the TX and RX terminals. The site chosen was near the building which housed the security offices and a fire station, approximately 1 km west of the AEDC main gate. A lookout tower identical to the one used for the height gain run (above) was located behind this building. A block of forest, containing almost exclusively deciduous trees, stood between the tower and the next building to the west. The RX van was positioned on a roadway near the latter building, and a service cable was run into the building for ac power. The distance between TX and RX was 152.4 m (500 ft). The TX antenna was mounted on the top platform of the lookout tower (20.6 m or 68 ft), and the RX antenna was on the van mast at 4.9 m (16 ft). Thus, the elevation angle of the path from the RX antenna was approximately 6°. Both antennas were the log-periodic type for this run.

The run was started at 1600 local time on 18 October and completed at 1200 local time on 19 October. The test frequencies were 600 MHz and 1200 MHz until 1030 local time on 19 October. The on-site observations indicated that there was more variation to the impulse response at 1800 MHz than the other test frequencies at that time. Thus the operating frequencies were changed to 1200 and 1800 MHz for the balance of the run. The polarization of the antennas was changed approximately every 2 hours during the run; and some data were obtained in a cross-polarized configuration. An example of the impulse response data is shown in the photographs of Figure 19. The top photo shows the power impulse responses measured under vertically polarized conditions around 0600 on 19 October. The bottom photo shows the horizontal polarized responses observed earlier around 0130 on the same date. Note here that the same general observations made previously for the difference in the two polarizations apply. The change is more pronounced at the higher test frequency as before. In addition, it should be noted that the multipath in the 600 MHz response has made a significant change between the two polarizations. The strong component nearest the more direct response in the top photo appears to become even stronger and move to a shorter delay time in the bottom photo. It is seen as a

39
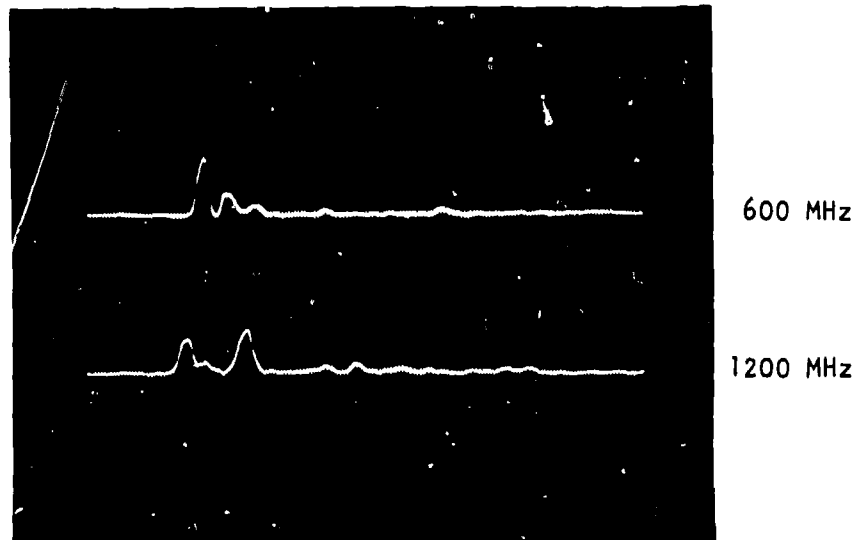
(a)   Vertical polarization
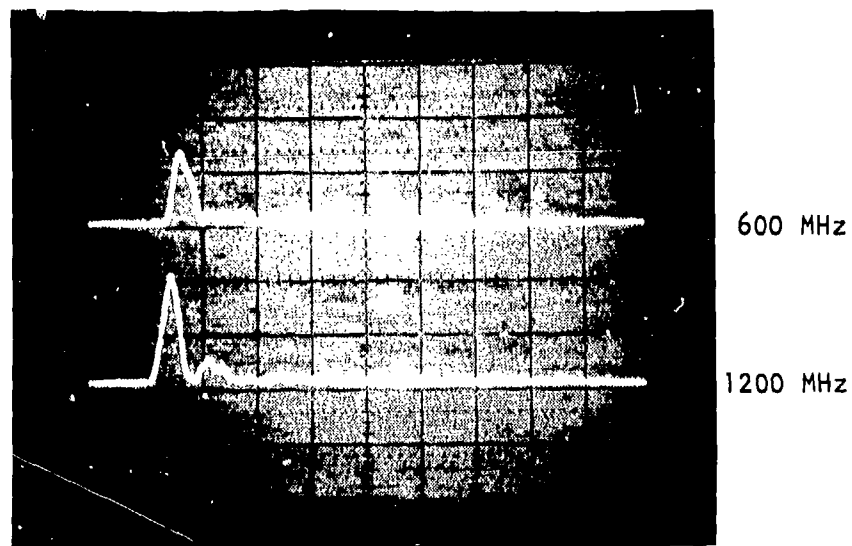
(b)   Horizontal polarization

Figure 19.   An example of the power impulse functions measured during the
long overnight run on 18-19 October 1979.   The time scale in
the photographs is 25 ns/division.

distortion on the trailing edge of the initial response rather than at a discrete response. In other words, the delay has become short compared to the absolute resolution of the probe.

Unfortunately the weather front that had been predicted did not develop, and no rain fell during this run. However, the run did fulfill one of the functions proposed in the test plan, i.e., to determine the long-term variations in the response data. The variations were minor for the most part, as can be seen from Figure 20. The responses in the top photo were measured at 0055 on 19 October. Those in the lower photo were observed at 0920 on the same date, some 9 hours later. Note the nearly identical character to the responses at both frequencies.

Some additional measurements were made near the main gate of AEDC and the administration building on 24 October. As illustrated in the lower photograph of Figure 10, the area is characterized by large evergreen trees that are widely separated (compared to the dense forest areas) and by no undergrowth. The grass under these trees is maintained, and most of the foliage on the trees is limited to the upper half. Thus, the trunks are quite visible, and it is possible to see for some distance through the area. It was anticipated that the effects of this type of forested area would be somewhat different from those observed in the Camp Forrest area. However, in general, the impulse response measured over paths in this region appeared as dispersive as those in the dense forest. Analyses of these data have not been completed however. An example of one frame of response is shown in Figure 21 for 1200 and 1800 MHz.

4.4 Normandy Lake/Negro Hill Area

The period from 20 October through 23 October was spent in performing the measurements in the Normandy Lake area. The majority of the paths tested involved Negro Hill as outlined in Section 3.3. All of the paths indicated in Figure 13 were tested during this period. Some useful data were obtained on most of the paths, but we experienced a considerable amount of interference during the period. An example of the interference seen on all three test frequencies is shown in Figure 22, which consists of photographs taken from the spectrum analyzer in the early afternoon of 20 October. The RX van was positioned at Point A in Figure 13, and the antenna was vertically polarized at a height of 4.9 m. The scale for all photographs in Figure 22 is 50 MHz/division, with the test frequency centered in each display. Other interference patterns were observed using a horizontally polarized RX antenna. Insignificant differences in both magnitude and spectral location of the interference was observed, suggesting that most of the sources were circularly polarized signals or that their signals were greatly depolarized.

41
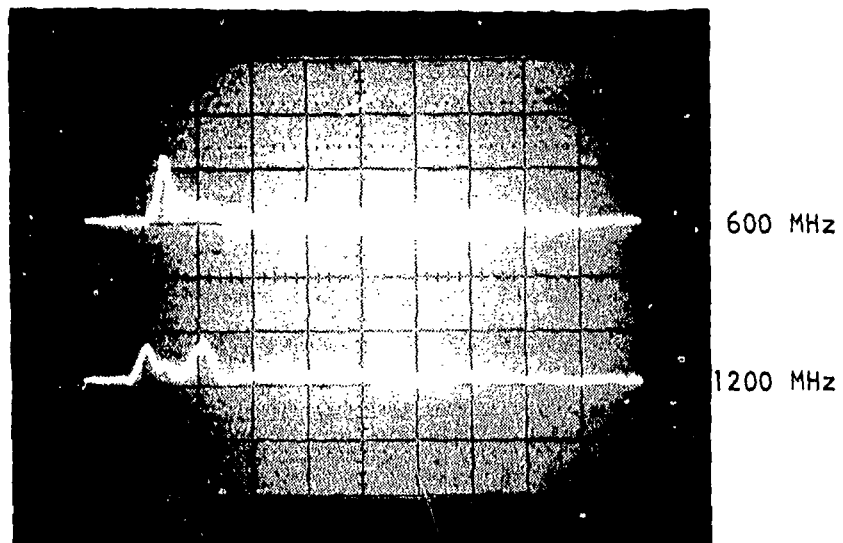
(a) Vertical polarization
Local time: 0055, 19 October 1979
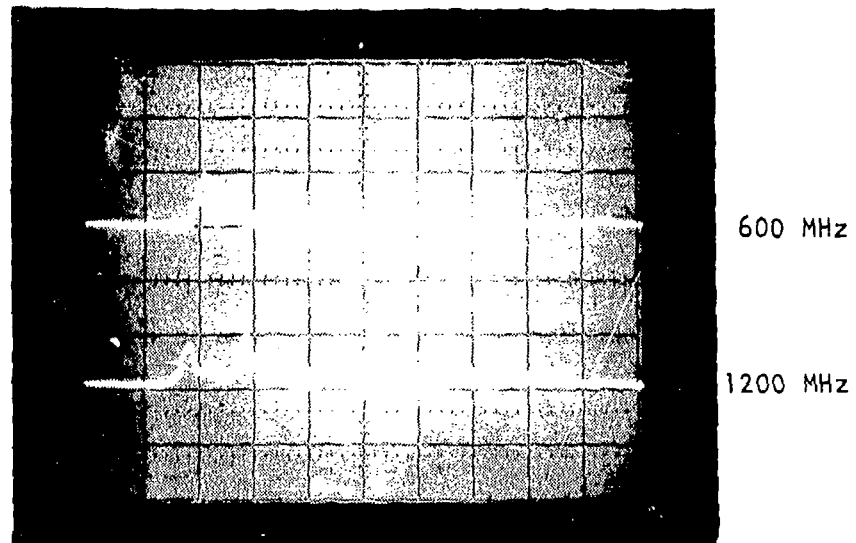
(b) Vertical polarization
Local time: 0920, 19 October 1979

Figure 20. An example of the long-term stability of the power impulse functions during the overnight run on 18-19 October 1979. The time scale is 25 ns/division.

42

1200 MHz

1800 MHz
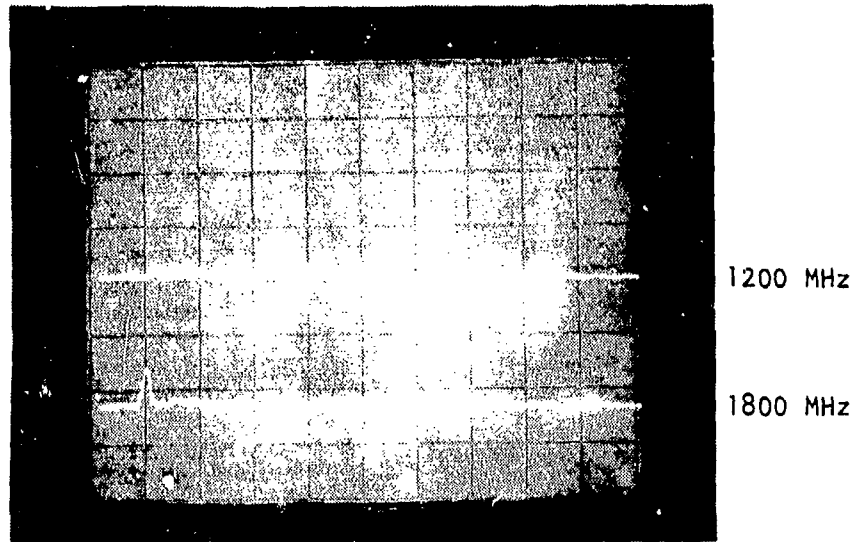
Figure 21. The power impulse functions measured in the area near the main
            gate of AEDC and the Administration Building. The antenna
            polarizations were vertical, and the time scale is 50 ns/division.

The value of the AGC data from the runs containing interference depends upon
the overall success of evaluating an adjusted RSL from the impulse data, assuming
the interfering signals are decorrelated by the RX detector. The impulse response
from most of these runs displayed the same type of dispersiveness as seen in the
North Grid measurements, whenever the path crossed a forested area such as the top
of Negro Hill. They became less dispersive for LOS paths such as from D to K in
Figure 13. An example of the response for a nearly LOS path from D to G is shown in
Figure 23 for the 600-MHz and 1200-MHz measurement. Note that both responses indi-
cate a fairly clear LOS condition. The only possible obstruction on this path would
be the hill east of the path toward point E in Figure 13. The 600-MHz response is
attenuated due to the effect of interference on the receiver AGC. It shows, however,
a distinct multipath component at a delay of around 30 ns. This delay is much too
long for any form of surface reflection from the lake. It must therefore be from an
off-path point such as the hill between points E and G in Figure 13. The responses
in Figure 23 were measured with vertical polarization. Horizontal polarization
produced a cleaner response in both records.

43
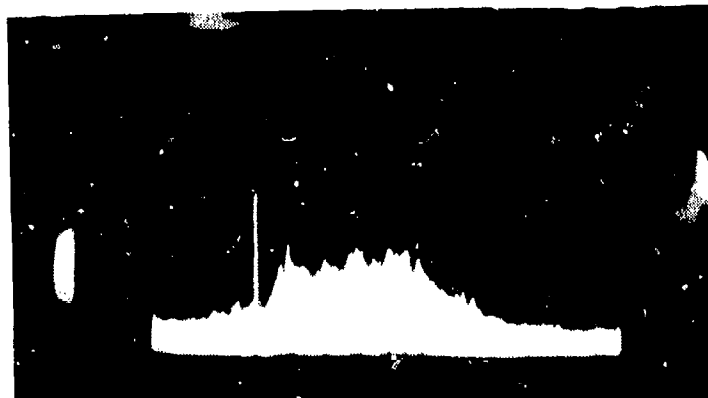
600 MHz

1200 MHz
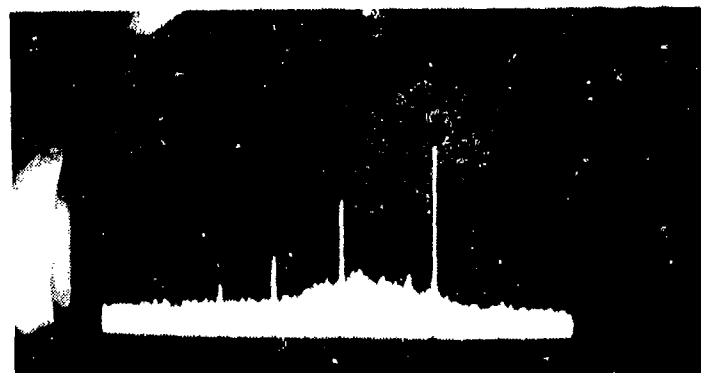
1800 MHz

Figure 22. Spectrum analyzer displays of interference signals observed at point A in the Normandy Lake region on 20 October 1979. Local time was 1420.

600 MHz

1200 MHz
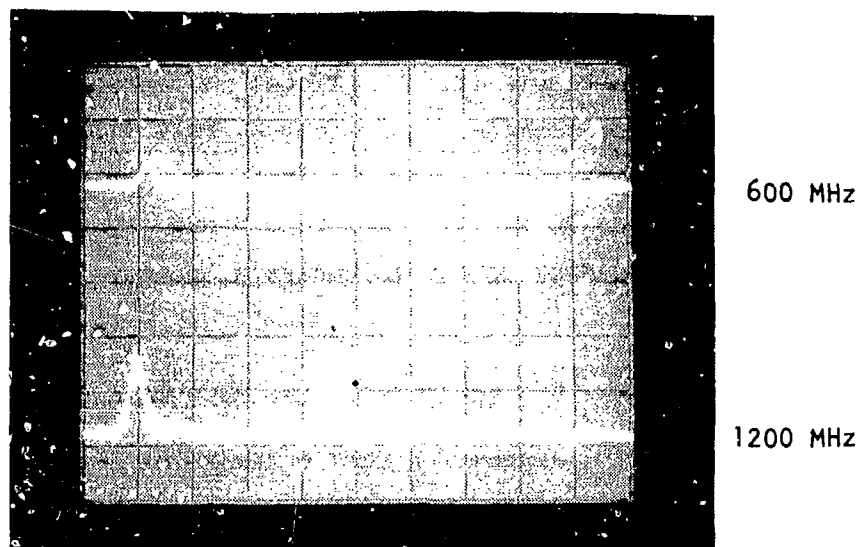
Figure 23.   The power impulse functions measured over the path between
             points D and G in the Normandy Lake area.   The time scale
             is 20 ns/division.

The paths between points E and F and E and G in Figure 13 pushed the probe
system almost to the limits of its dynamic range.   The diffraction loss was so large
over these paths that measurements were difficult.   The last path E-G produced
an impulse response that was just barely discernable on the oscilloscope with
increased gain.   Digital recordings were made for an extended time so that the
analysis process could be tested for on-line signal averaging as a means of
enhancing the data.   Unfortunately, results were unreadable and so the test proved
negative.

The afternoon of 23 October was spent near Meadows Hill somewhat east of
Normandy Lake.   However, the diffraction loss over these paths was apparently
so high that test-signal reception was never established.   Thus, these measurements
could not be made as planned.

4.5   AEDC Grid Area Measurements (10/24-25)

The final two days of the experiment were devoted to some test paths selected
to determine what effect (if any) locating a terminal in clearings within the
forest might have.   These measurements were of interest because of on-site obser-
vations such as those already noted for the possible "waveguide" effect in the Grid
area.

45

The RX for these measurements was located at the fire lookout tower in the South Grid area shown in Figure 11. The TX was driven to several open areas within the AEDC recreation complex (golf course, ball field, etc.) to the west of the lookout tower. The TX was also driven into a number of clearings in the North Grid area near crossroads 20 and 21, crossroad 8 and Avenue A, and crossroad 20 and Avenue A. None of these data have been analyzed to date, so the results are not available.

5. EXAMPLES OF RECORDED DATA

The primary recording system for this measurement program was a Digital Data Acquisition System (DDAS) whose details are described in Section 2.4.2 and in Appendix D. In brief, it digitized the base-band receiver signals and recorded them on digital magnetic tape to allow off-line processing at a later time. Note that since there were two frequency channels, each having both a co-phase and a quadrature-phase channel, there were actually four of these base-band signals to treat. This was done by time division multiplexing in such a way that the four were obtained almost simultaneously. The fastest sampling rate used was a little over 10,000 samples per second, i.e., more than 40,000 data samples per second. Following a trigger signal, which worked the beginning of a frame, the first 1000 samples of each analog signal were recorded. In addition other pertinent facts were recorded such as the date and time of each recorded frame and the two AGC voltages.

In the 2 week period of the Tennessee measurements, such data were recorded on some 19 magnetic tapes, the contents of which are summarized in Appendix E. In this section we want to show some examples of how the actual recorded data appear and of some of the problems connected with them. In subsequent sections we shall use various processing techniques to examine particular questions in detail. In all cases we are using the digitized records reformatted for a large computer (a CDC Cyber 170/750), and we are using the power of that large computer and its associated graphical display device (an FR80 microfilm plotter).

Figure 24 summarizes a run made on 11 October, the first day of operations. It took place on a path in Camp Forrest with the receiving antenna on a tower 23 m above ground and hence about 8 m above the forest top. The transmitting antenna was, as usual, vehicle-mounted and vertically polarized, and was buried in the forest about 160 m from the receiver. The path may therefore be characterized as an up-and-over path: up through the forest and over the top. The figure shows the train of impulse responses for both the 600- and 1700-MHz channels. Note that time goes in both directions--from left to right to show each individual response curve

46

600 MHz

1200 MHz

3.19 μs
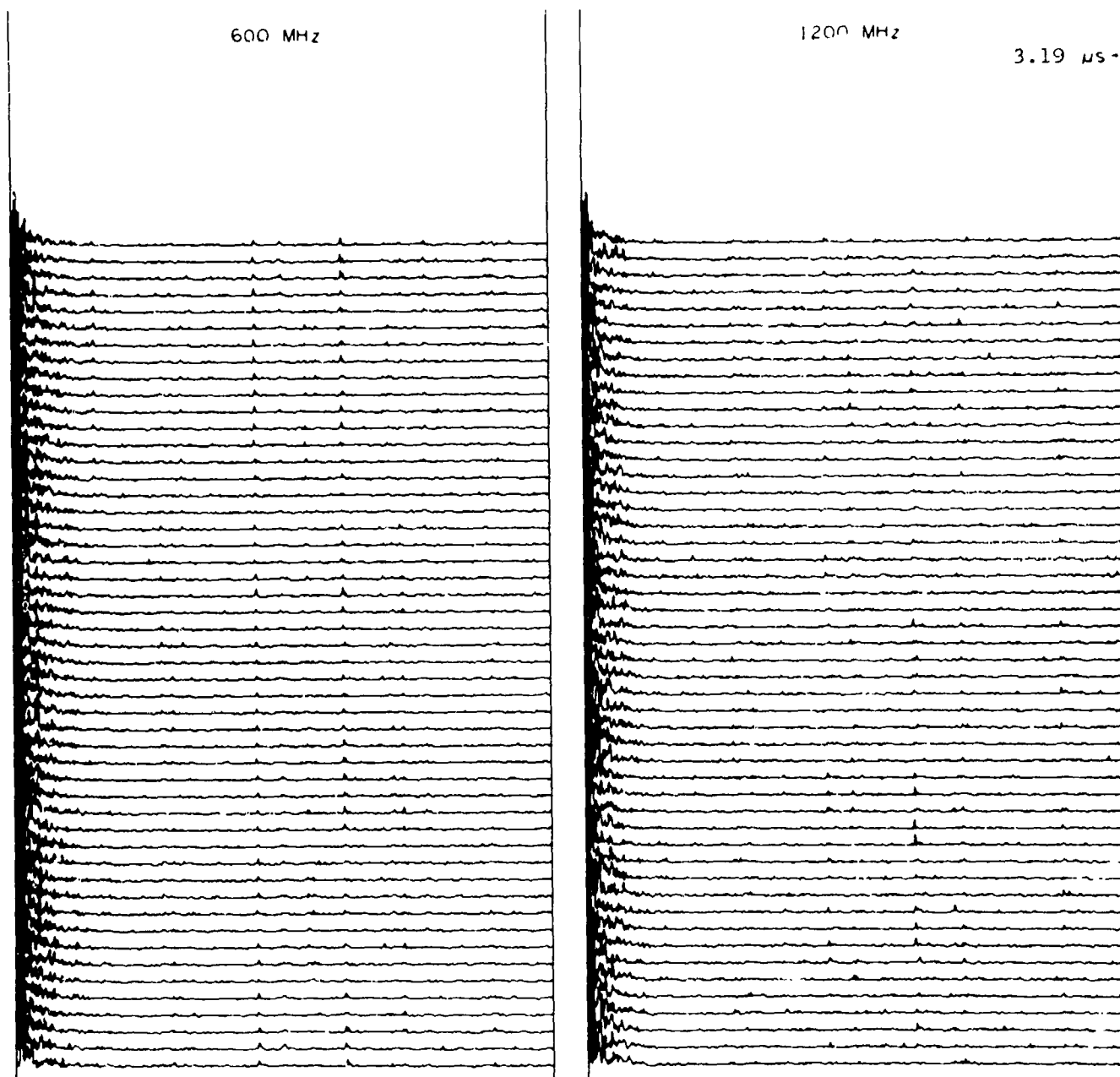
Figure 24. The train of impulse responses for a single run in Camp Forrest. The
receiving antenna was on a tower 23 m above ground and about 8 m above
the forest top. The transmitter was buried in the forest about 160 m
away. A total of 100 frames were recorded of which every other one is
pictured here. The total time span (vertically) is 60 s.

47

and from top to bottom to show how the responses change with time. As indicated near the upper left corner of the figure, the horizontal axis (on each channel) represents a time delay of 3.19 μs; the succeeding responses are at intervals of 1.2 s. (We have plotted only every other one of the recorded responses.) The entire figure covers a time span (vertically) of 60 s. What is plotted is the amplitude of the responses--the root-sum-square (rss) of the two quadrature components. This differs from the power impulse responses displayed in Section 4 since the latter give the square (the power instead of the amplitude) of the functions shown here. The present figure is designed to provide some idea of the delay spread involved and of how rapidly the response changes in time (i.e., the "doppler spread"). Admittedly, because of the too cramped condition, this figure is difficult to read. Still, it demonstrates the entire set of recorded data for this run. Note that one can clearly see that at least the tail ends of the responses are changing quite markedly so that there seem to be no consistent features. This is probably due to wind blowing in the treetops. One obvious feature in Figure 24 is the appearance of small but persistent blips that occur rather late in the record. Two of the stronger of these follow the beginning of the records by about 1.4 and 1.9 μs. These same blips appear in other records taken under other circumstances. Since they even appear in tightly controlled calibration runs, it seems very probable that they are somehow introduced by the receiver itself.

Figure 25 is a detailed look at just one of the responses of Figure 24. This particular response is from the 600 MHz channel and is the second of the pictured train. It is plotted three times in three different ways. At the top of the figure are plotted the co-phase and quadrature-phase components on the same axis. (Again, the cramped conditions make this difficult to see.) This represents the actual information generated and recorded in the field and thus provides the most complete picture of the response. (The response, being a 300-MHz wide "narrowband" version of the real response function, is a complex-valued function of delay time and must therefore be represented as such.) The lower two plots display this same function in polar form. The middle plot is the amplitude--simply an enlarged version of the corresponding plot in Figure 24. The bottom plot shows the phase relations between at least the larger multipath components. It is a kind of Lissajous figure in which the co-phase component is plotted along the x-axis, the quadrature phase component along the y-axis, and time serves as the independent parameter. In this case, for example, one sees the initial response starting off into the third quadrant, doubling back on itself, and then, as a second component enters, swerving into the second and first quadrants to emerge as a strong multipath component in the fourth quadrant.

3.19 µs·
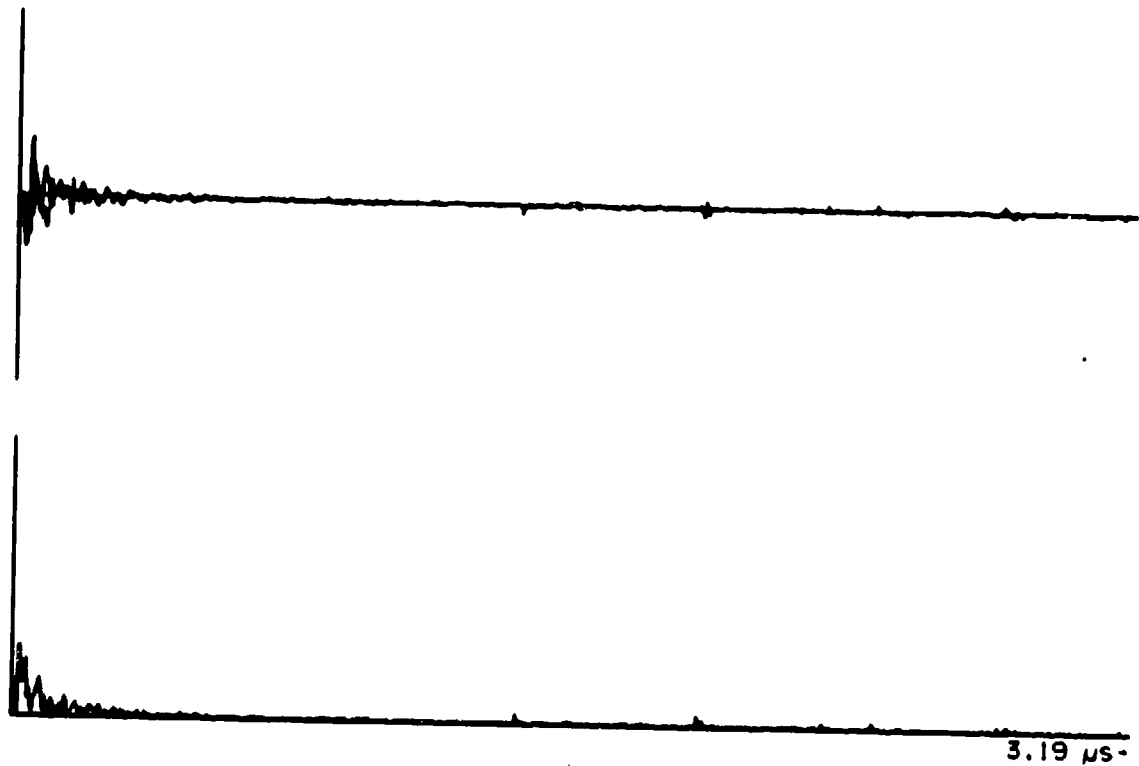
Figure 25.   A detailed look at one of the 600-MHz responses of Figure 24. The three graphs provide three different ways of viewing the responses and are described in the text.
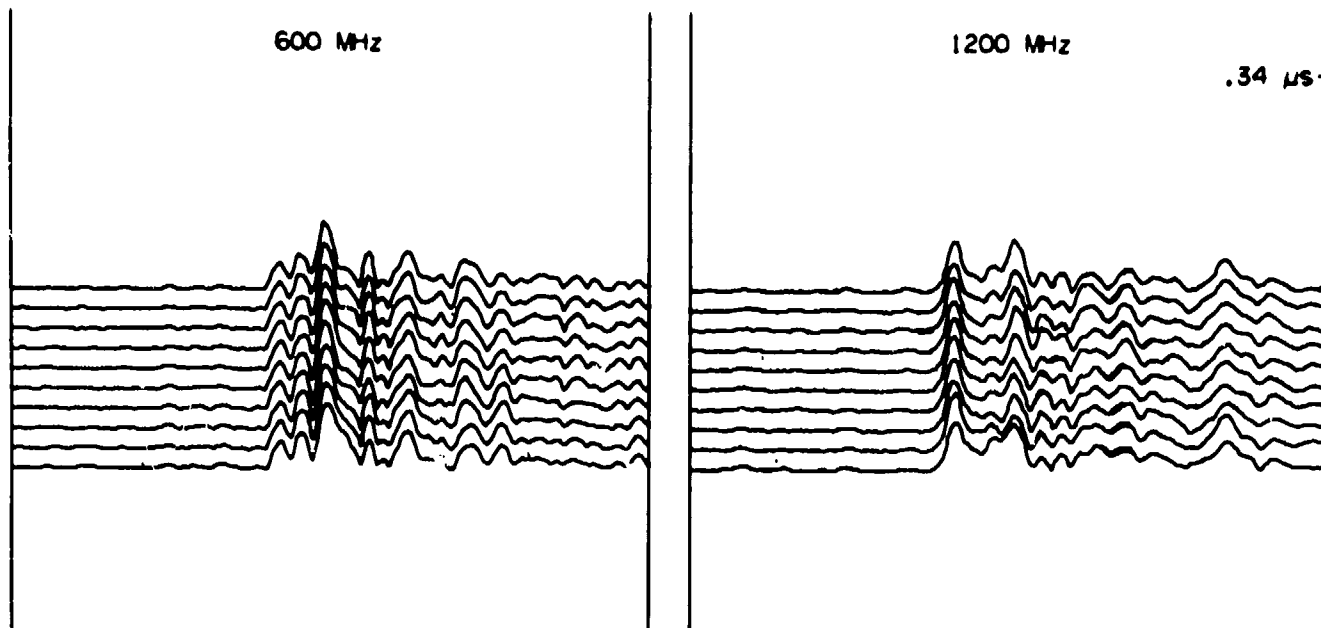
Figure 26.   The train of impulse responses for a single run in Camp Forrest.
Both antennas were low and buried in the forest; they were sep-
arated by about 160 m.   Ten frames were recorded at a rate of one
per second.

After that the plot becomes a confusing tangle about the origin.   From the first two
plots of the figure, one sees the initial response (probably the direct wave) fol-
lowed about 20 ns later by a second strong multipath component, followed by a
steadily decaying string of components which finally disappear from sight before
about 400 ns.

The "window" through which we look at an impulse response is determined by the
frame rate (from 1 to 10 per second), the digitizing rate (usually about 10,000 per
second), and the number of samples recorded (usually equal to 1000).   The placement
of the response within the window (which is done manually) is also important.   The
window of Figures 24 and 25 is almost a full frame of 3.41 μs.   It is certainly more
than is needed, and in Section 7 an expanded version of Figure 25 is shown in which
the long noise record in the response tail has been discarded.

In contrast to the cramped conditions of these figures are the plots of Figures
26 and 27.   Here the window is too small, equal, as it is, to something less than a
tenth of a frame.   In this run, the frame rate was 1 Hz and the digitizing rate
about 10,000 Hz; thus the 1000 samples recorded took up only one tenth of a full
frame.

50

RUN 002   79/10/12.   TEST SITE 001
FRAME 9   13.39.41.
Channel 1.   600 MHz

.32 µs-
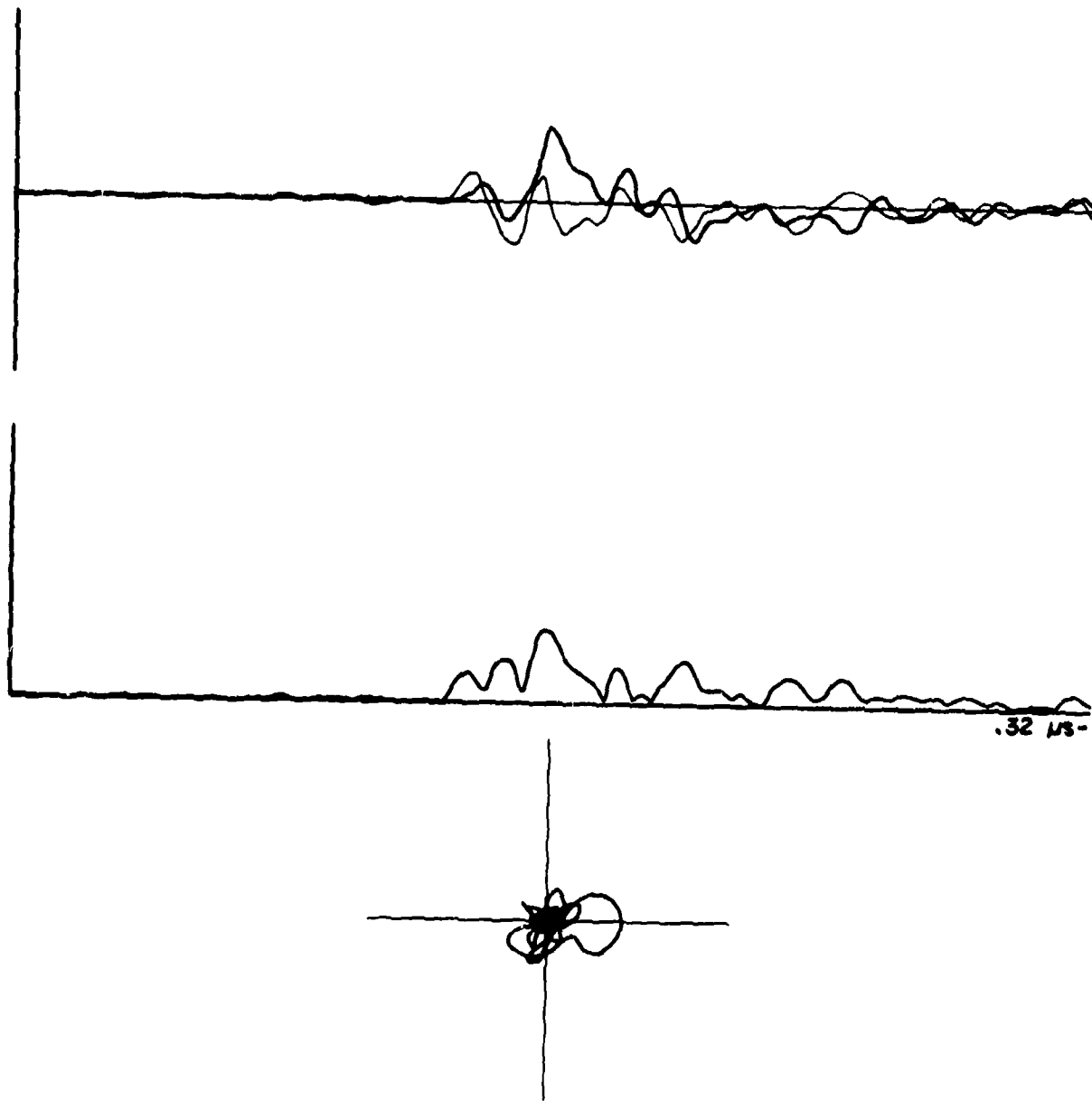
Figure 27.   A detailed look at one of the 600-MHz responses of Figure 26.

Figure 26 summarizes a short run made on 12 October. The antennas were in Camp Forrest about 160 m apart, and both were vehicle-mounted. Thus the path passes directly through the forest for one block of the Camp Forrest grid of streets. From the onset of these responses almost half way through the pictured window to the end of the window is only about 190 ns; the response tails have been lost and cannot now be recovered. Presumably, as we have also verified by examining the backup analog record, there followed only a continuing decay of the already small multipath components. We seem to have lost only a minimal amount of information, and certainly the strongest components in the beginning half of the impulse response are very advantageously represented here.

The succeeding responses in Figure 26 are separated by an interval of 1 s, and the total time of the run is 10 s. Note that there is very little change from one response to the next. In the 1200-MHz train there appear regularly timed short bursts of noise. The origin of these bursts is unknown.

Figure 27 gives a detailed look at one of the 600-MHz responses. We note from both the full record at the top and the response amplitude in the middle there are three principal multipath components separated by about 11 ns from each other and successively larger in magnitude. We would suppose that the first of these is the direct wave which has had much of its energy removed because of scattering by the forest. Perhaps this scattered energy is rescattered and added to other, off-path, components to combine at the receiver with a larger magnitude at a delayed time. Whatever the reason, this figure shows that the largest component of a response function is not necessarily the first.

We may also take advantage of the clear portrayal of the first few components to note here the appearance of considerable distortion. The response amplitude, for example, does not seem to consist of a series of smoothed, symmetric triangular pulses; the slopes on each side are asymmetric and the peaks are too blunt. Furthermore, consider the full record at the top. In the case of an ideal isolated multipath component (and an ideal channel probe), we should observe a (real) triangular pulse multiplied by some constant phase factor; the co-phase and quadrature phase components should rise and fall together. But we see this does not happen; in particular, the positions of the two maxima do not coincide.

One possible reason for such distortion is that each of these "components" is actually the sum of two or more closely spaced components. The first pulse, for example, probably consists of two fairly strong components. The third and largest pulse has a long, irregular trailing edge. Even from the response amplitude one suspects it involves at least two components; but from the full record, one sees clearly three separate components and the suspicion of a fourth.

52

The Lissajous figure at the bottom of Figure 27 also shows how the various components are distorted. For an ideal triangular pulse the corresponding Lissajous figure would simply show the signal going out from the origin along a radial and returning back upon itself. The wide, open circles and loops here mean that this ideal is far from reality. In particular, one can almost identify the three multipath components of the largest pulse; the first leads the co-phase direction by about 45°, the second lags by about 45°, and the third is much smaller and lags by about 90°.

In Figure 28 we change the scene to Normandy Lake. The path involved in this run is the path from C to A in Figure 13; it is a diffraction path about 1700 m long with a 50-m obstacle. The two channels were at 1200 and 1800 MHz. Both antennas were vehicle-mounted and out in the open. The path begins at the shore of the lake, crosses over a bay to the island of Negro Hill, whose crest forms the diffracting object, and then continues over water to the receiving terminal, again at lakeside. Negro Hill is covered with trees as are the hills surrounding the lake. Close to the lake the land is bare.

The responses for this run were recorded at intervals of 1 s; in Figure 28, however, we have plotted only every sixth response. The 1200-MHz train shows considerable variability, but also several definitely persistent features. The 1800-MHz train seems so contaminated with noise that little can be said about it.

Figure 29 is a detailed look at one of the 1200-MHz responses. Note that the tail is very long; even 500 ns after the first pulse, there seem still to remain small, but visible, multipath components. There is an initial cluster of four pulses separated by about 10 ns; perhaps they arise from scattering by trees on the hill crest. Most striking, of course, is the strong component, or group of components, appearing about 200 ns after the initial pulse. Perhaps this arises from a reflection, or scatter, by the hills near the omnidirectional antenna at the transmitter or perhaps from other parts of Negro Hill. The geometry would support either interpretation.

The curious excursions into the first and second quadrants of the Lissajous figure are those that arise from this second strong group of components. They imply that there are three distinct elements to the group, a conclusion that can also be reached by an examination of the full co-phase and quadrature phase record.

6. THE GENERATED PULSE

To study a recorded impulse response in detail, we need to know what the system-generated pulse looks like--the pulse unaltered by an intervening propagation

1200 MHz

1800 MHz

.77 µs
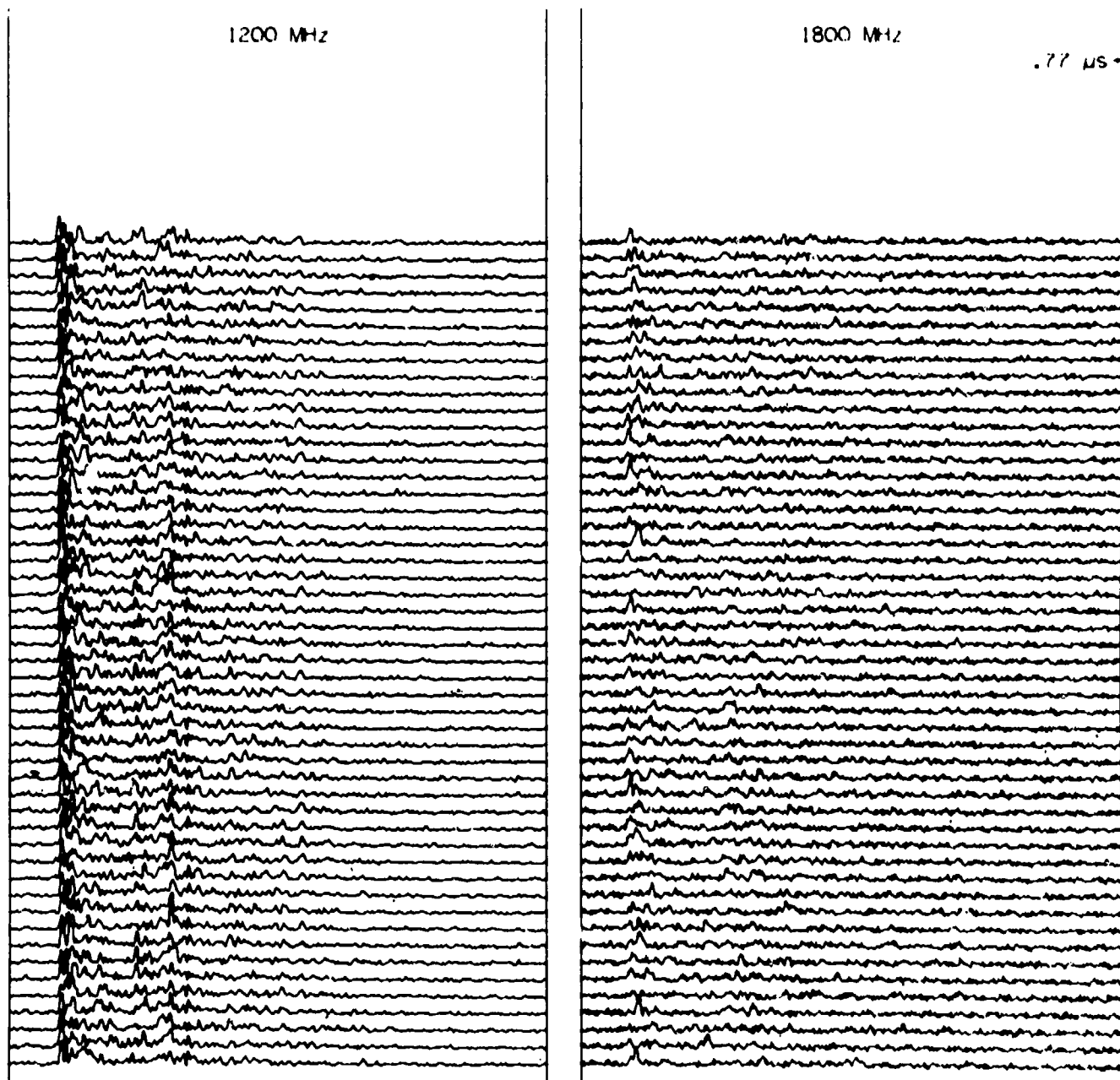
Figure 28.   The train of impulse responses for a single run at Normandy Lake.
The antennas are both vehicle-mounted and are separated by about
1700 m.   The path is a diffraction path surrounded by forested
hills.   A total of 300 frames were recorded at a rate of one per
second.   Every sixth frame is pictured here.

54

RUN 013   79/10/20.   AT POINT A, NORMANDY
FRAME 122   13.32.44.
Channel 1, 1200 MHz

.77 μs
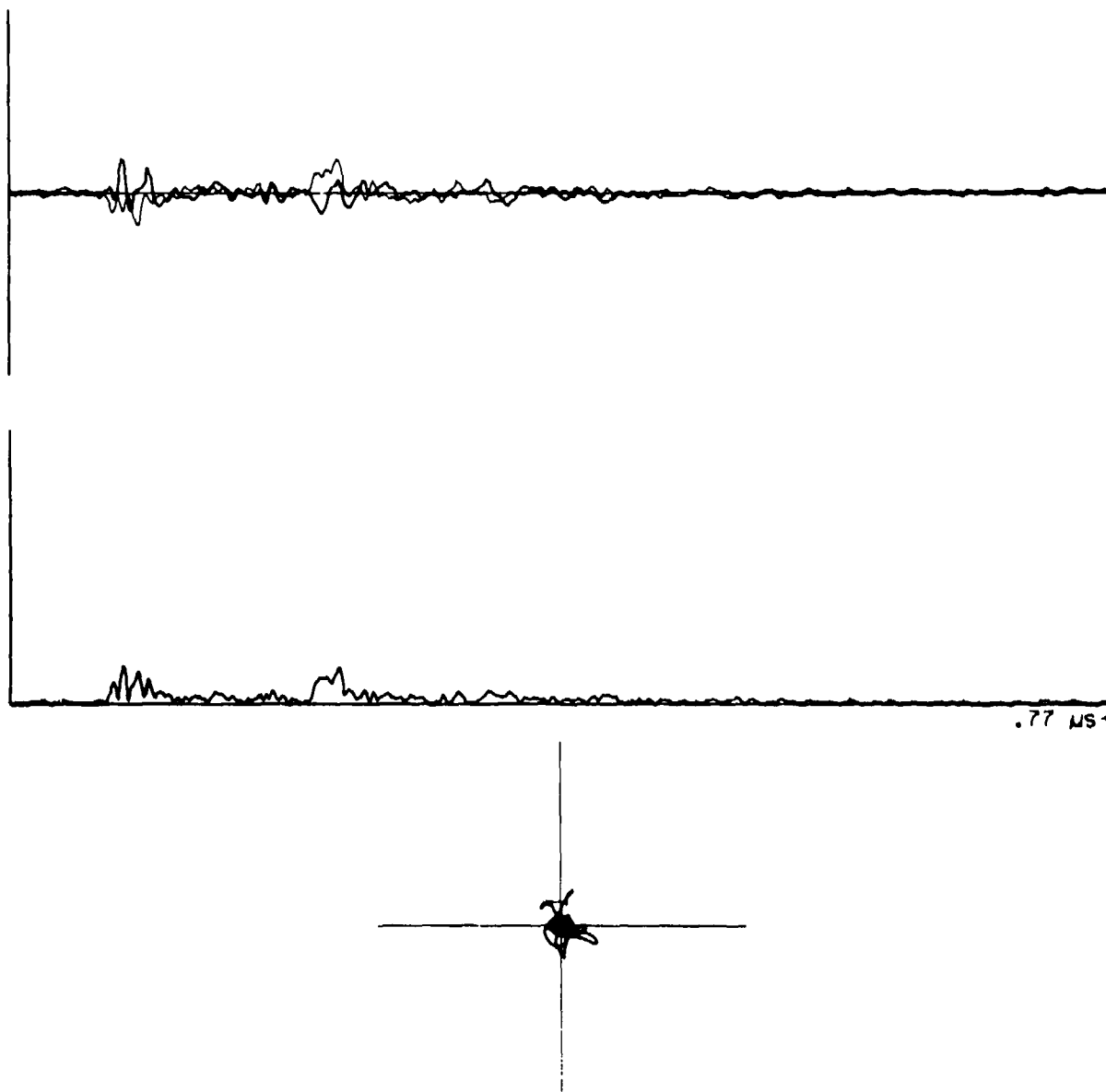
Figure 29.   A detailed look at one of the 1200-MHz responses of Figure 28.
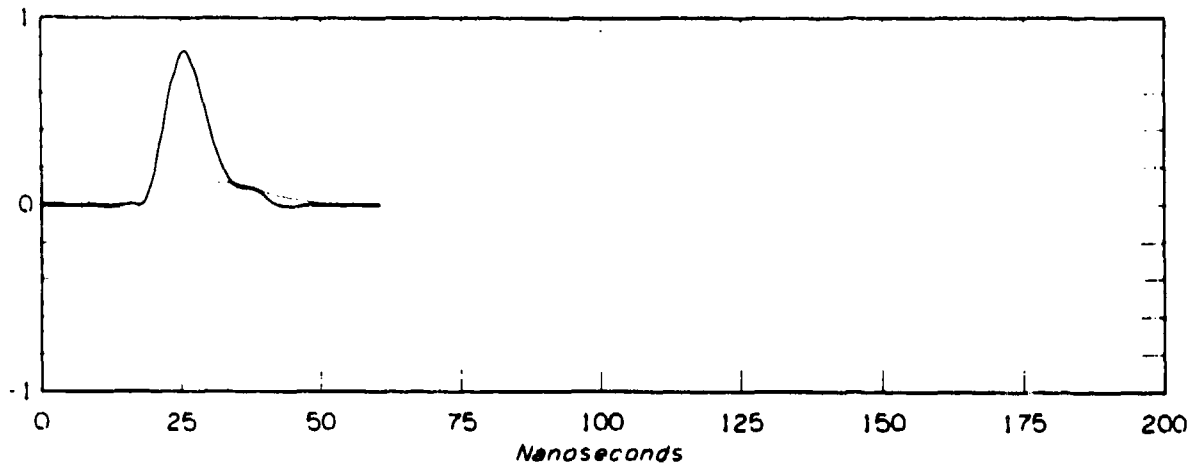
Figure 30.   The effective pulse generated by the channel probe system as
recorded during a calibration run.

channel. As described in Appendix A, the originally generated pulse is triangular
with a 13.3-ns base; it is, however, subjected to a series of equipment-dependent
filters whose effects cannot be computed a priori but can only be measured.

In Figure 30 we have plotted an example of the pulse. This is a composite,
being the average of ten very similar pulses recorded during a calibration run.
Note that the vertical scale is an arbitrary one having to do with base-band ampli-
fication and digitizer parameters. We have adjusted it so that the illustrated
pulse has the same energy as would a perfect triangular pulse of unit height. Both
co-phase and quadrature-phase components are shown in the figure; the co-phase
component being the darker. The low step appearing in the trailing edge of the co-
phase component and the fact that the quadrature phase component is not identically
zero are both evidence of unexpected distortion within the system. Fortunately,
this distortion is relatively small.

Let us consider the spectrum of this pulse. For comparison we show in Figure
31 the spectrum of a perfect triangular pulse. In Figure 32 is the spectrum of the
pulse of Figure 30 obtained as a discrete Fourier transform using the methods
described in Appendix C. The top graph is the amplitude of the Fourier transform
expressed in decibels; in the lower graph we have plotted the phase of the trans-
form. Note that the deep null of the triangular pulse spectrum has almost dis-
appeared. We can only suppose that noise components have filled in the null. The
assymmetry that appears--and the fact that the peak amplitude falls some 15 MHz
below the center frequency--is a consequence of the fact that the quadrature phase
component in Figure 30 is nonzero. On the other hand, note that the phase is

56
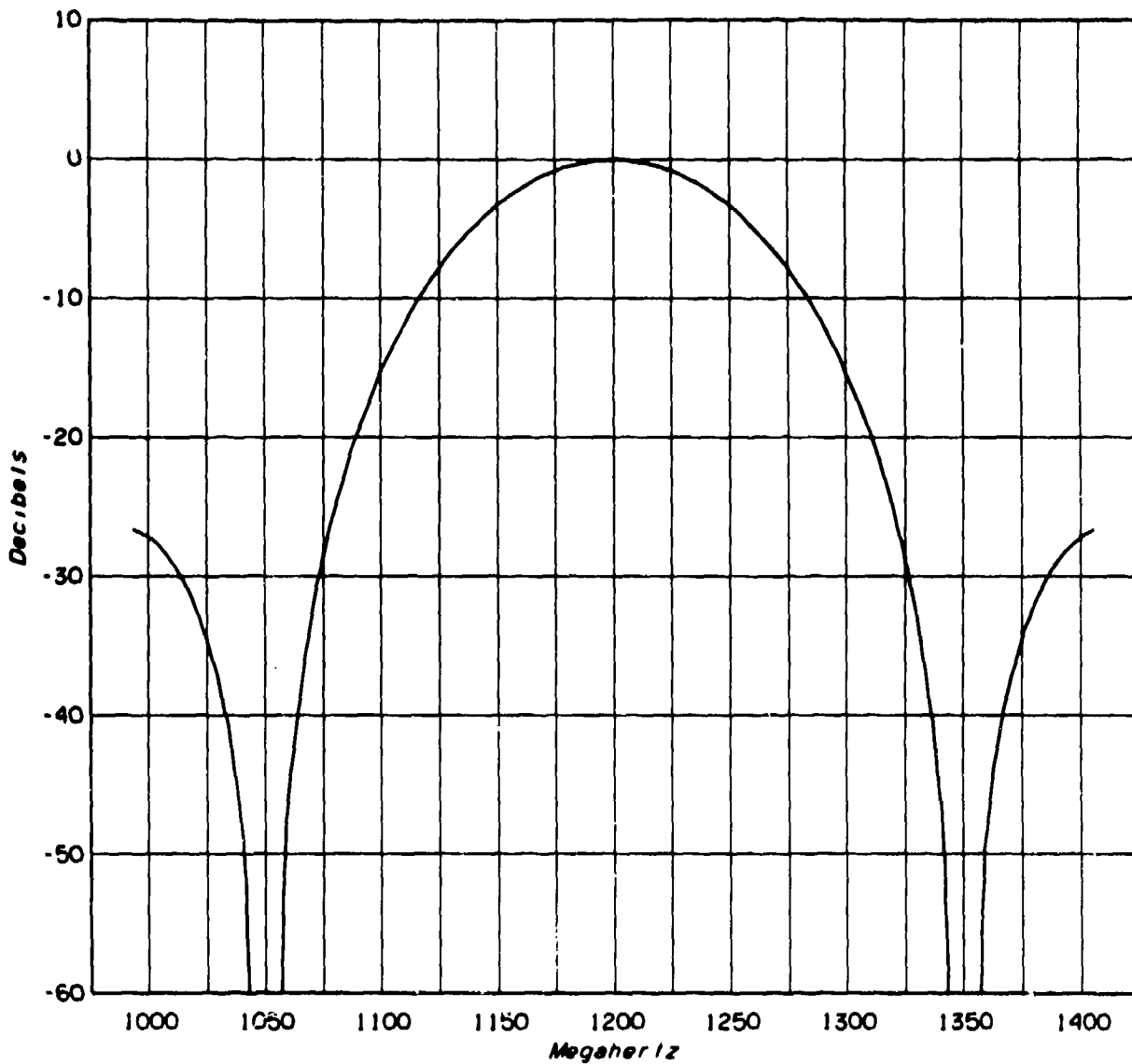
Figure 31. The spectrum of a perfect triangular pulse with 13.3-ns base.
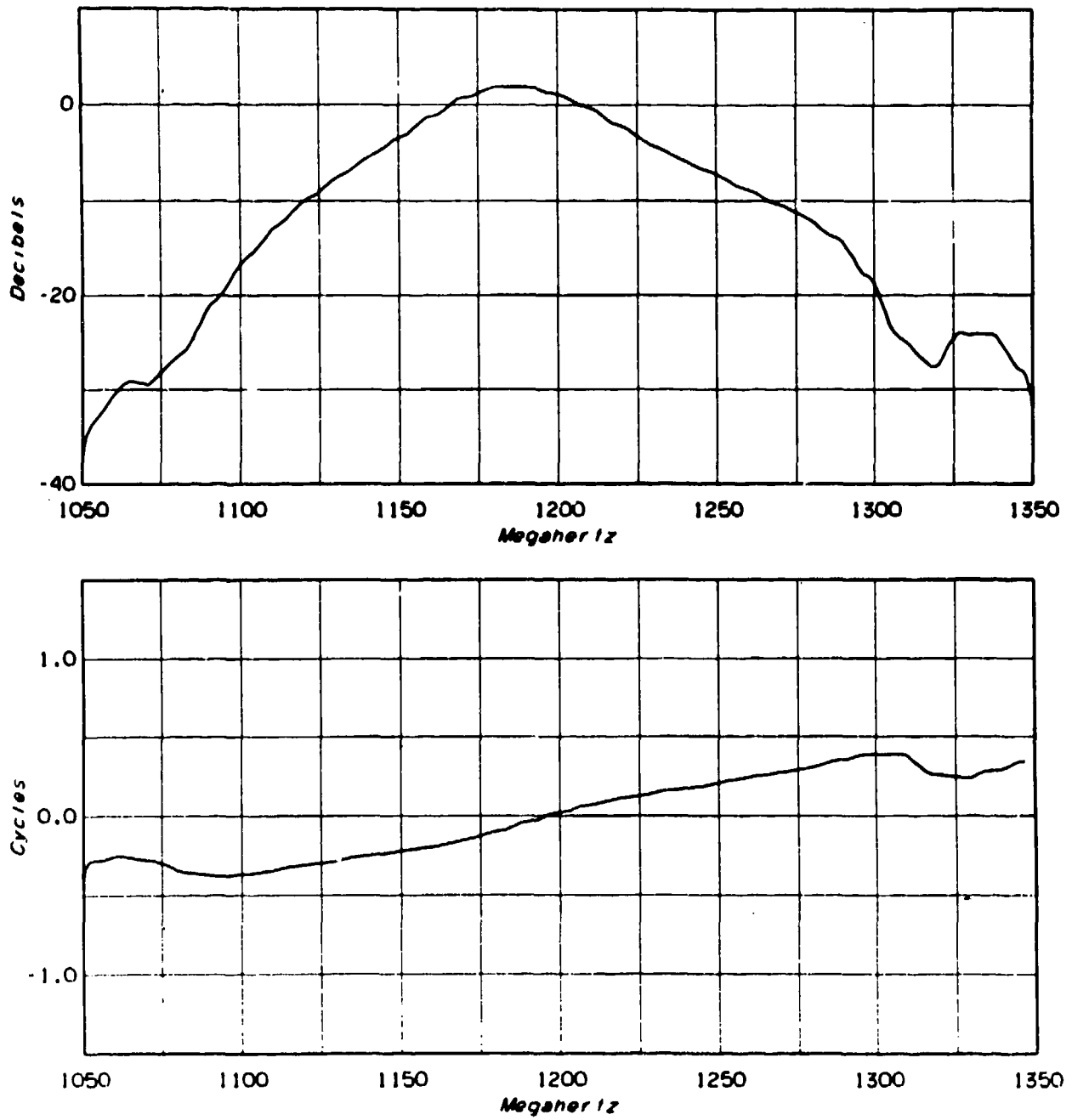
Figure 32.   The spectrum of the system-generated pulse shown in Figure 30.

satisfyingly linear over most of the pictured range; this implies that there is little phase distortion in the pulse.

A knowledge of the shape and size of the generated pulse is important to us; their measurement is a critical part of the calibration of the system. We need to know the size in order to make a determination of the absolute received signal level, particularly when extraneous signals are affecting the IF channel response. And we need to know the shape in order to estimate the multipath structure of impulse responses such as those exhibited in Section 5.

According to the results of Appendix A, we would suppose that the shape and size of the generated pulse is a function of the transmitter and receiver filters and hence of the center radio frequency, the receiver channel, and the frame rate. What Figure 32 shows is at 1200 MHz on the second channel with a frame rate of 10 Hz. Furthermore, since it is taken from a calibration run, it does not include the actual pseudo-noise signal emitted by the transmitter. At this time it is the only example of the generated pulse we can offer. We hope it represents closely enough the generated pulses obtained under all other circumstances.

7. ANALYSIS OF THE INDIVIDUAL IMPULSE RESPONSE

In this section we shall examine some techniques for the study of a single recorded impulse response. As representative response functions, we choose from among those illustrated in Figure 24. Recall that this run was made in Camp Forrest with the receiving antenna on a tower about 8 m above the trees and with the transmitt.. antenna down within the trees some 160 m away.

The first question is one of normalization. We must delimit (truncate or time-clip) the function along the time axis so that only the extent of the actual impulse response is to be treated--so that the onset is placed in a standard position and so that the noise components in the tail are deleted. Our technique for doing this is described in Appendix C. We must also adjust the vertical axis in some standard way.

In the top graph of Figure 33 we show a normalized version of the same response that was displayed in Figure 25. In the bottom graph is shown its companion at 1200 MHz. The vertical axis has been normalized so that the total energy in the response function equals the energy of a perfect triangular pulse with unit height. The RSL power is indicated in the upper right corner and should equal the actual power in the total wideband signal. It is obtained from the calibrated AGC voltage adjusted by the change in the multiplying factor needed in the normalization here over that required for the system pulse of Figure 30. In the figure we have chosen

59
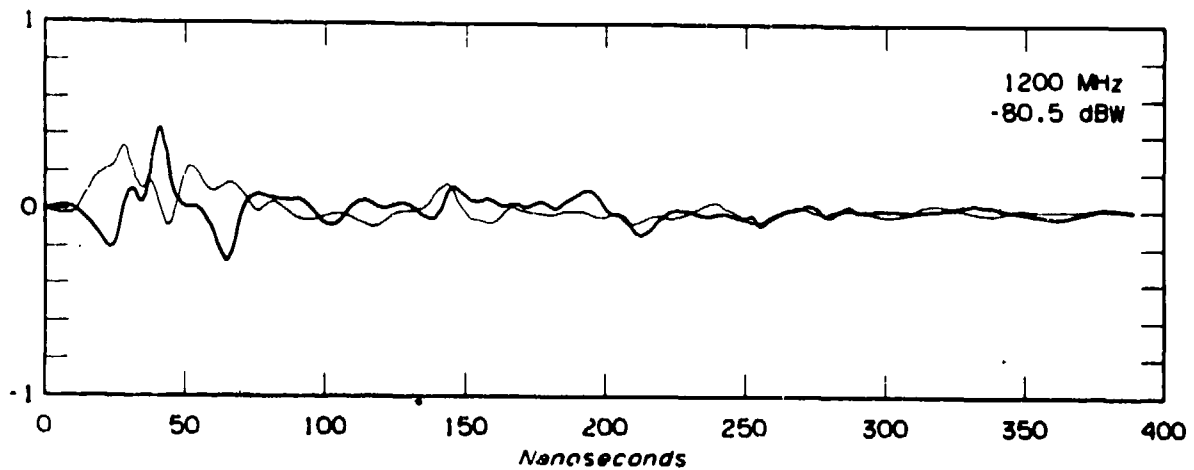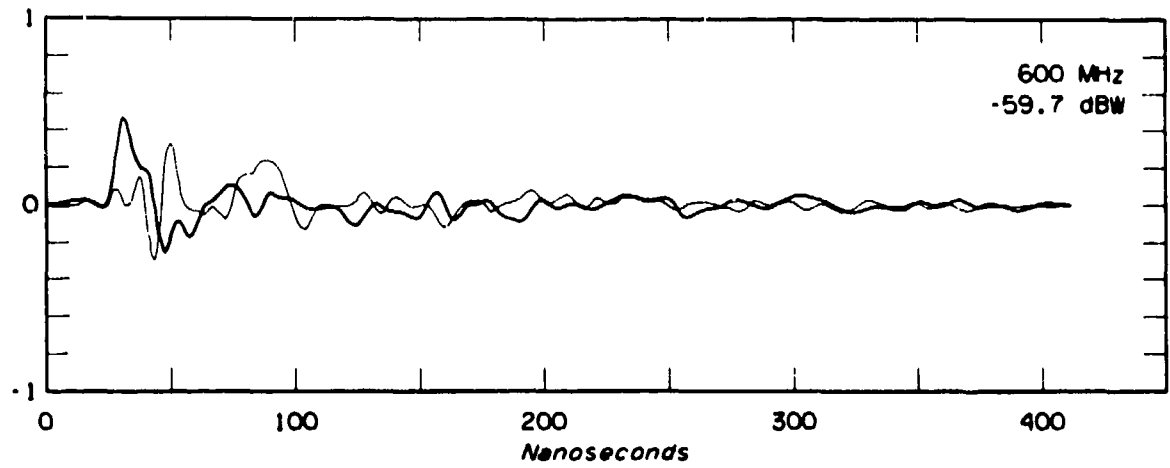
Figure 33. Normalized versions of response functions from Figures 24 and 25. Both co-phase and quadrature phase components are shown with the co-phase component being the darker.

to plot both co-phase and quadrature-phase components, thinking that this is the most complete representation of what we have actually measured. We have, however, multiplied the complex response function by a constant unit complex number--thus rotating the function in the complex plane--so that the peak value is real and positive. This provides a second standardization to aid viewing the results.

Incidentally, the noise level of the 600-MHz response as determined by the process of Appendix C is equal to -99 dBW. This is 39 dB below the signal but some 65 dB above the value given in Appendix B as that due to thermal noise. The discrepancy might be due to receiver noise (for example, the blips of Figure 24) or to interference (and, as we have indicated elsewhere, there was probably quite a lot). But it may also be due simply to an extension of the tail of the response--to a more or less continual electromagnetic "ringing" of the forest. It is our suspicion that this latter was the most prominent cause.

In the commonly accepted view of response functions such as those portrayed here, there is a direct wave followed by a series of multipath components which arise because of scatter from off-path objects such as tree trunks, branches, foliage, and ground. Each multipath component should be a recognizable, but distorted, copy of the transmitted pulse. (Distortion arises because the scattering process is from irregular objects, thus involving diffraction and similar wave phenomena.) But when one tries to identify such multipath components from a record as in Figure 33, one finds a difficult problem. There seems to be such a confusion of components as to defy analysis. Each "component", when examined closely, turns out to be the sum of several. This is particularly clear in the full co-phase, quadrature-phase record where the first two components of Figure 25 (at 600 MHz) now seem to be four. One suspects that if a finer resolution were available one might well discover many more. This is perhaps not very surprising when one recalls that the electromagnetic waves travel through a forest and that for any given delay time (which then defines an ellipsoid of revolution with the two terminals as foci) there will surely be an ample supply of scatterers. It would therefore seem best to abandon, or at least to amend considerably, the notion of discrete multipath components. In transmission through a forest, there is probably a continuous supply of such components, and the appearance of pulses in our displays is perhaps simply an accident arising mostly because of the necessarily finite resolution of the probe system.

When one wants to describe quantitatively a few of the more important characteristics of an impulse response, then certainly the first to be considered is the overall received power. The next most important is probably the duration or delay

spread; and to this, one might add the related characteristic of location (or central time delay) of the pulse. Unfortunately, because of the nature of an impulse response, there is no universally recognized measure of these characteristics. For example, the duration of the true response is probably infinite since there will be an endless tail as scattered energy scatters again from objects in the path. This tail, however, vanishes into the noise and becomes undetectable; it is only that portion of the response that is visible to us that we should consider.

In Figure 34 we have reproduced the responses of Figure 33, superimposing on them indications of four different definitions of location and five different definitions of delay spread. The definitions of location are these: (a) the point at which peak power is attained; (b) the center of gravity--i.e., a normalized version of $\int t|h(t)|^2 dt$ where $h(t)$ is the complex response function; (c) the average group delay as determined from the phase of the spectrum--this will be further discussed below; and (d) the 50% energy point--i.e., the point for which half of the total energy of the response comes before and half follows. For the spread we have used these definitions: (e) the total time from onset of the response to the point at which the tail of the response disappears into the noise; (f) the diameter of gyration--i.e., twice the radius of gyration which, in turn, is the square root of a normalized version of $\int (t-t_c)^2 |h(t)|^2 dt$ where t_c is the center of gravity defined above; (g) the 10% peak amplitude limits--i.e., the time between those moments when the amplitude first exceeds 10% of its peak value to when it last falls below that level; (h) the time between the 10% and 90% energy points; and (i) the time between the 5% and 95% energy points.

In Table 7 we list the computed values for these nine measures of location and spread of the two responses in Figure 34. One should note here that the location, by any of the four definitions, cannot be an absolute measure of time delay. We have no true way of making such a measure since the channel probe has no way of knowing when the pulse was first transmitted. The times indicated in Table 7 are all relative to an arbitrarily chosen origin which, following the approach of Appendix C, is approximately 20 ns ahead of what we have called the onset. Since the path length here was 160 m, to obtain an absolute delay time we would have to add on an additional time of the order of magnitude of 500 ns.

Note the wide range of values resulting from the different definitions, particularly for the delay spreads. It is even difficult to compare the two frequencies: For some measures the delay spread is smaller at 600 MHz than it is at 1200 MHz; for other measures the opposite is true.
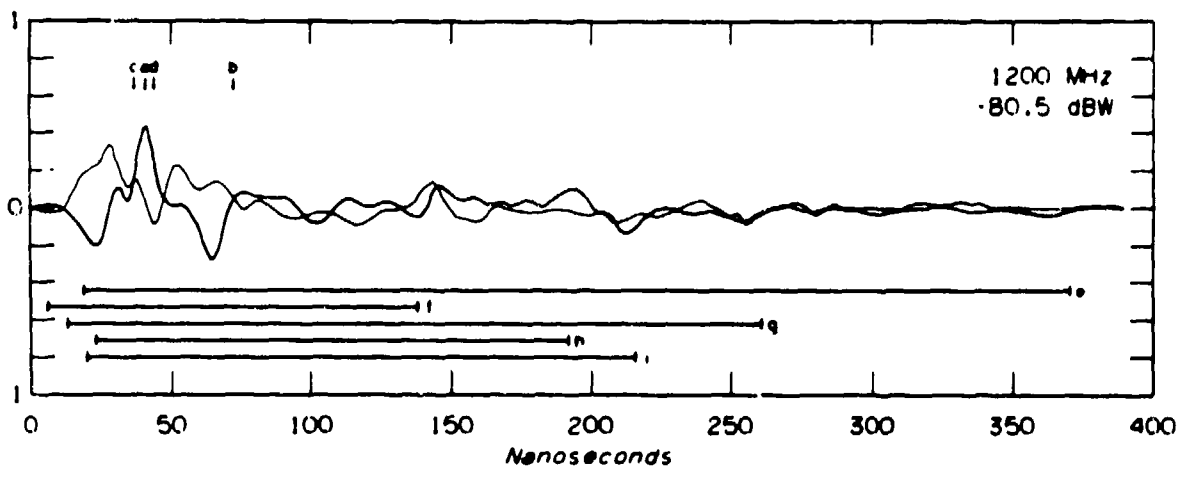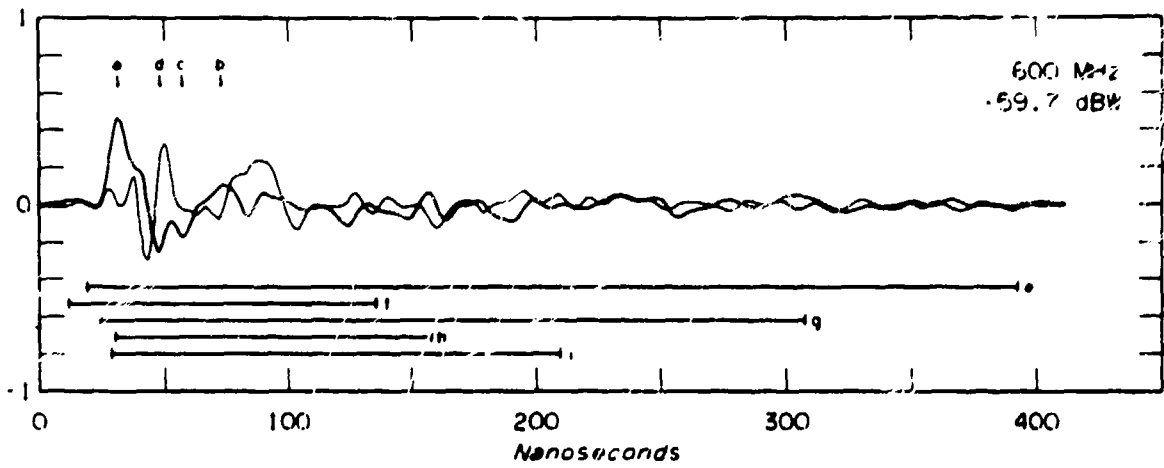
Figure 34.   Measures of pulse location and multipath delay spread superimposed
on the response functions of Figure 33.   The several measures pre-
sented here are explained in the text.

Table 7. Examples of Location and Delay Spread

(Values here are for the response functions in Figure 34.)

	Location	600 MHz	1200 MHz
a)	Peak amplitude	31.8 ns	42.2 ns
b)	Center of gravity	73.4	72.3
c)	Average group delay	57.3	37.2
d)	50% energy	48.7	43.9
	Delay Spread		
e)	Onset to noise	373.5 ns	351.1 ns
f)	Diameter of gyration	123.9	132.3
g)	10% peak amplitude	283.1	247.9
h)	10% to 90% energy	127.6	168.6
i)	5% to 95% energy	180.4	195.7

The next most interesting property of an impulse response is probably its spectrum. In Figure 35 we show the spectrum of the response pictured in Figure 25. What we have in this figure is the amplitude of the Fourier transform measured in decibels relative to the overall RSL. The transform here involved the entire frame of recorded data which, as we see in Figure 25, includes a long period (over 85% of the frame) of what should really be called noise. This is the reason for the noisy appearance of Figure 35. Since the fluctuation rate in the spectrum is directly proportional to the delay spread of the response, by allowing the long noise record to be included, we have introduced the small, rapid fluctuations one observes here. If we utilize instead the truncated response of Figure 33, we obtain the smoother spectrum of Figure 36. The spectrum of the companion 1200 MHz response (truncated) is pictured in Figure 37. These two spectra are, of course, still somewhat adulterated with additive noise, but we believe they give as faithful a representation as is possible.

In these figures we have examined only the amplitude of the Fourier transform. But we can also consider the phase. Figure 38 shows graphs of phase versus frequency for the two companion responses of Figure 33. Note that we have chosen to
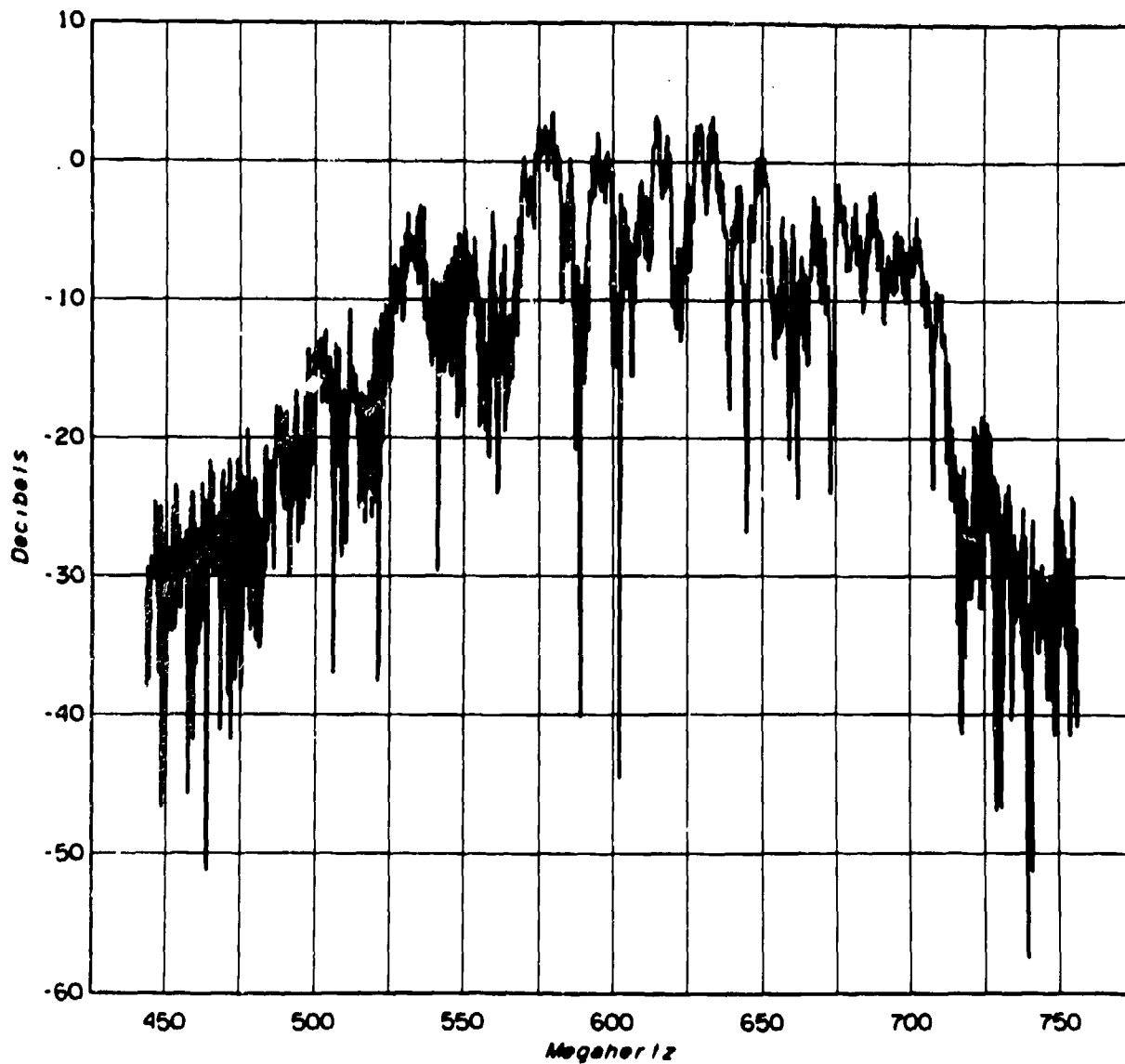
Figure 35.   The spectrum of the response function shown in Figure 25.
The rapid fluctuations are caused by the long noise tail
in the record.
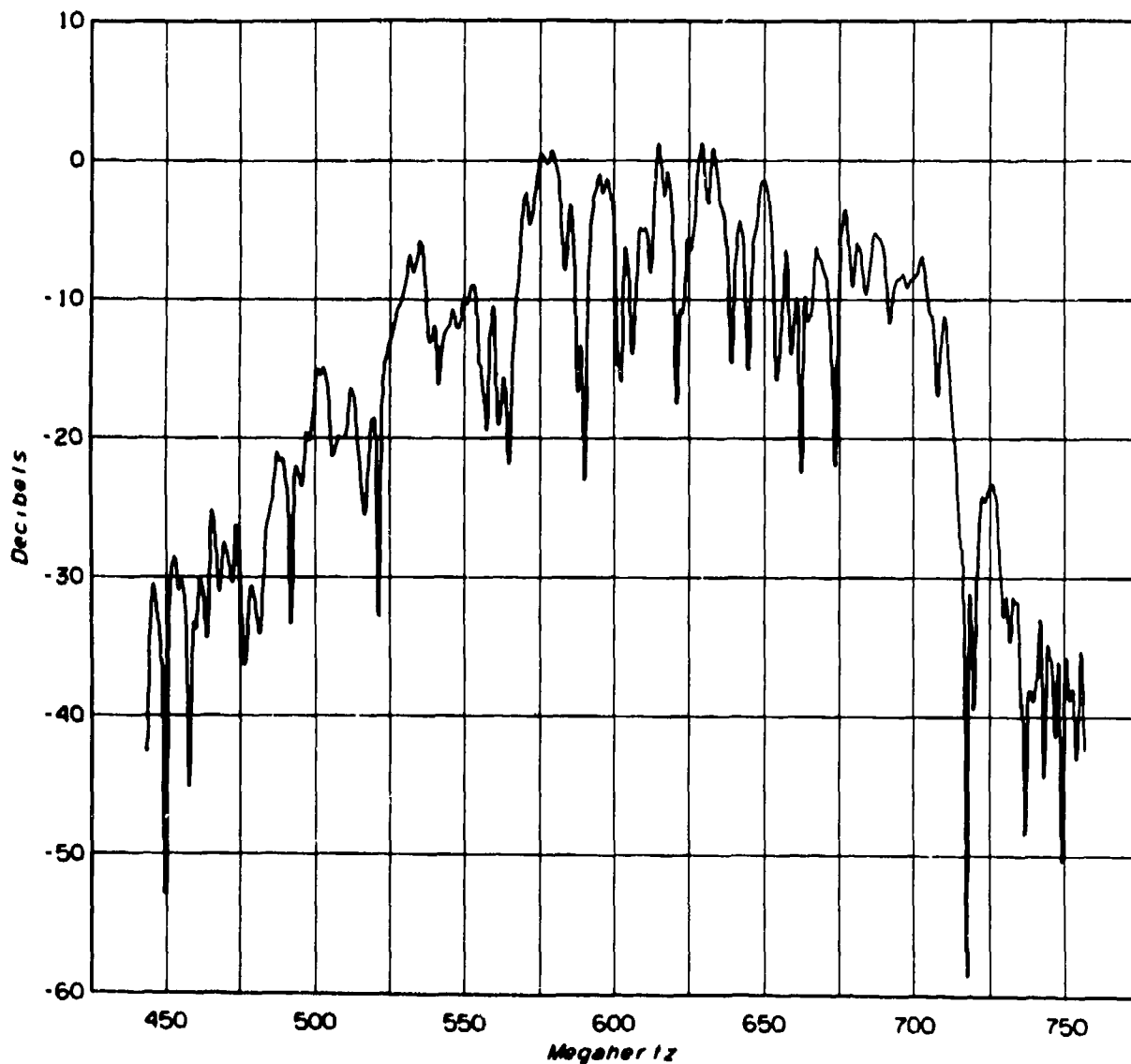
Figure 36. The spectrum of the truncated 600-MHz response function of
Figure 33.
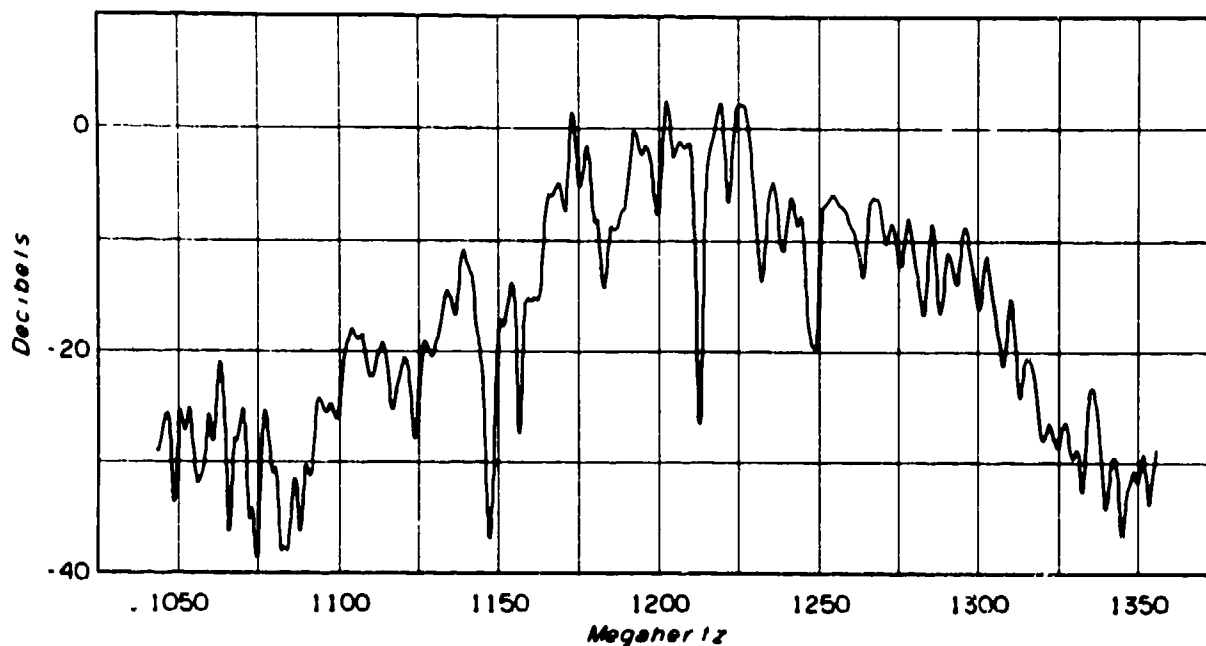
Figure 37.   The spectrum of the truncated 1200-MHz response function
of Figure 33.

measure the phase in cycles, i.e., in complete rotations of 360° or 2π radians. Of
course, in an ideal channel with no phase distortion, the phase will be a linear
function of frequency; it is the deviation of a spectral phase plot from a straight
line that indicates distortion. In Figure 38 the general appearance is one of con-
siderable phase distortion; but note that there do exist small bands--for example,
the band from 475 to 550 MHz--within which there is only a little distortion.

Phase is always a difficult quantity to compute, chiefly because of the several
associated ambiguities. In the first place, phase is only defined to within a
whole number of cycles, and the complex number 0 has no phase at all. But also, an
important part of the spectral phase has to do with the delay time of the response;
if t_d is this delay time and if no distortion is present, the phase is just νt_d
cycles, where ν is the frequency. Such a function is nearly impossible to follow
when t_d has any appreciable size; furthermore, the term "delay time" can itself be
subject to different interpretations: It could be the absolute delay time or a
purely arbitrary delay time such as we have used in our previous analyses. The
importance of the definition used can be seen when we realize that a change of only

67
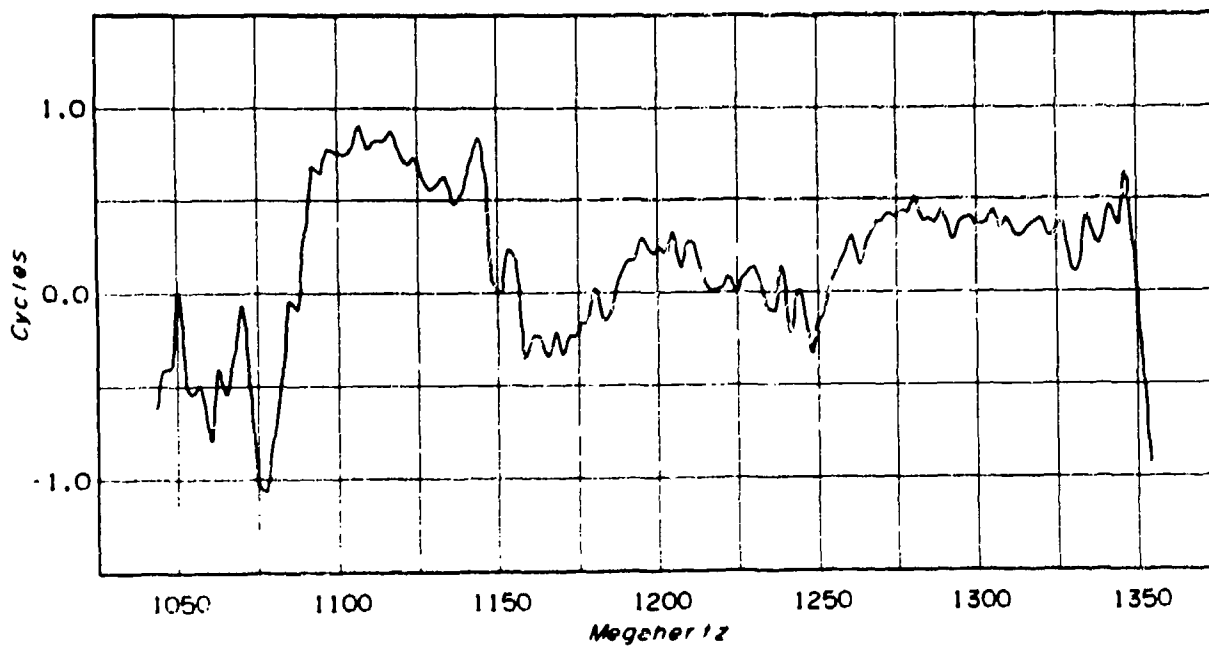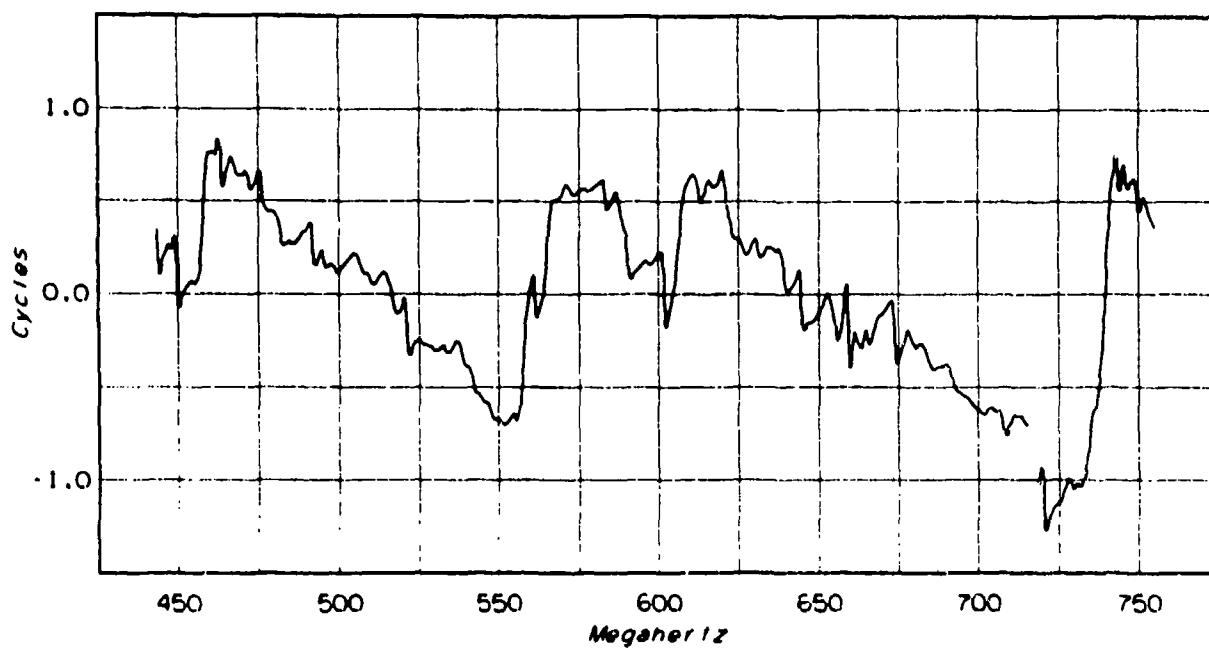
Figure 38.   The channel phase response--the phase of the Fourier transforms
of the response functions of Figure 33.

10 ns will add or subtract to the spectral phase a straight line which changes by one complete cycle every 100 MHz. To construct the curves of Figure 38, we have (1) been careful to define the integer part of the phase so as to make the curves continuous, (2) left gaps where the amplitude of the spectrum is too small to define satisfactorily a phase; and (3) subtracted from the curve a straight line whose slope is chosen to make the resulting curve appear horizontal on the average.

When the spectral phase ϕ is measured in cycles, the derivative $d\phi/d\nu$ may be directly interpreted as a "group delay time," i.e., as the time of delay of the group of spectral components with frequency near ν. Furthermore, this derivative is actually easier to compute than is the phase itself, for the multivalued arctangent function is not then involved. In Figure 39 we show plots of this derivative for the two responses of Figure 33. The points of these plots have been computed directly from the Fourier transforms and quite independently of the values used in Figure 38. The zero delay time--the origin of the vertical axes in these plots--corresponds to the zero delay time used in Figure 33, i.e., to a point approximately 20 ns before the onset of the response. The "average group delay" of Figure 34 and Table 7 is just the average of these curves taken over the central 200-MHz band. Furthermore, this average group delay is exactly the slope of the straight line that was subtracted from the phases in Figure 38.

Phase distortion can be as easily observed in these plots of group delay time as in plots of the phase itself. Here it is the deviations from a constant value that determine distortion. Admittedly, it takes a discerning eye to note from Figure 39 that there is only a little phase distortion in the band from 475 to 550 MHz. Nevertheless, we feel that there are many advantages to a consideration of the group delay time and that this function may turn out to be a very useful one.

The general shape of Figures 36 and 37, when the multipath-caused fluctuations have been ignored, is due, of course, to the spectrum of the input to the channel, i.e., to the spectrum of the generated pulse as portrayed in Figure 32. Another way to present the spectrum of an individual response function is then to remove the effects of the generated pulse by simply dividing the Fourier transform of the measured function by that of the generated pulse. Of course, some restraint must be exercised since towards the edges of the 300-MHz wide band we will be dividing one noise signal by another. In Figure 40 we show the central 200 MHz of the spectral amplitudes derived from Figures 36 and 37 after this kind of adjustment. The fact that both curves tend to reach rather high values at the high frequency edge is disturbing and again brings into question our pulse calibration of Section 6.

69
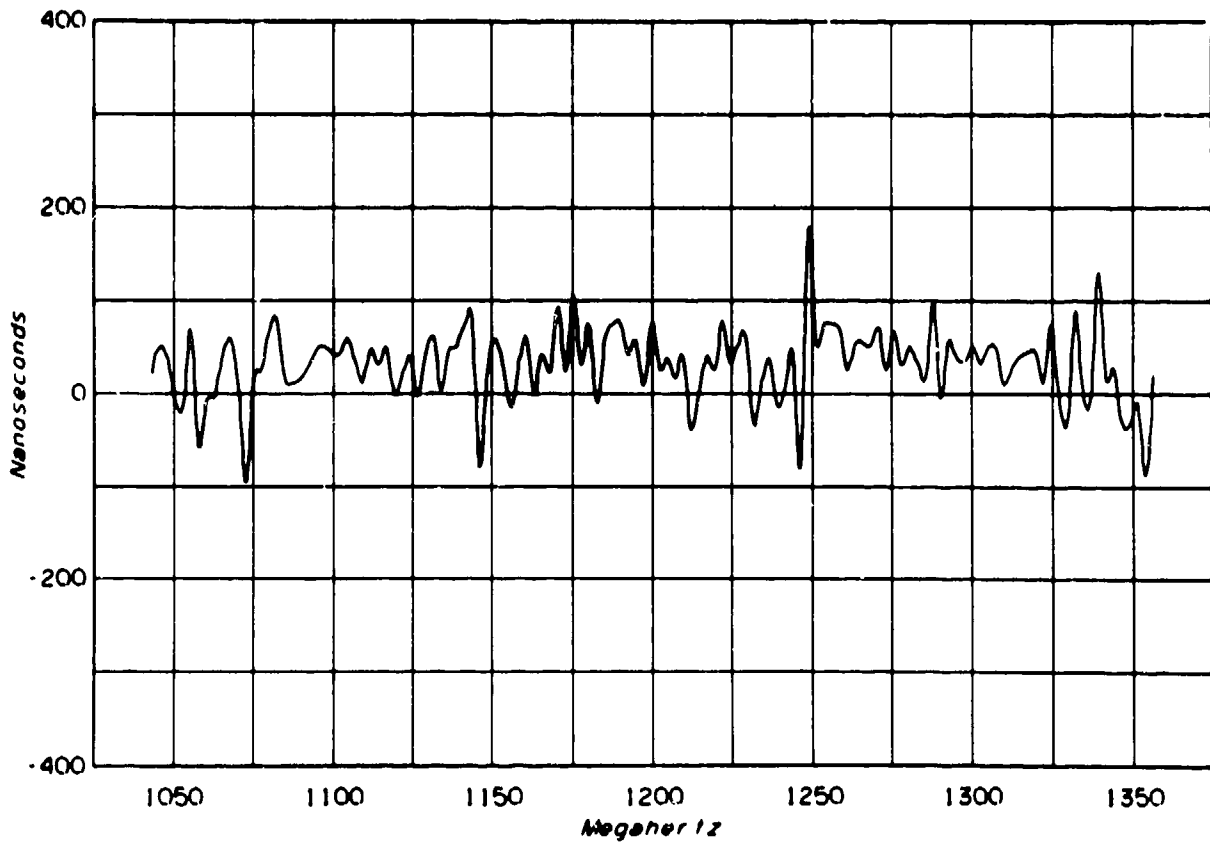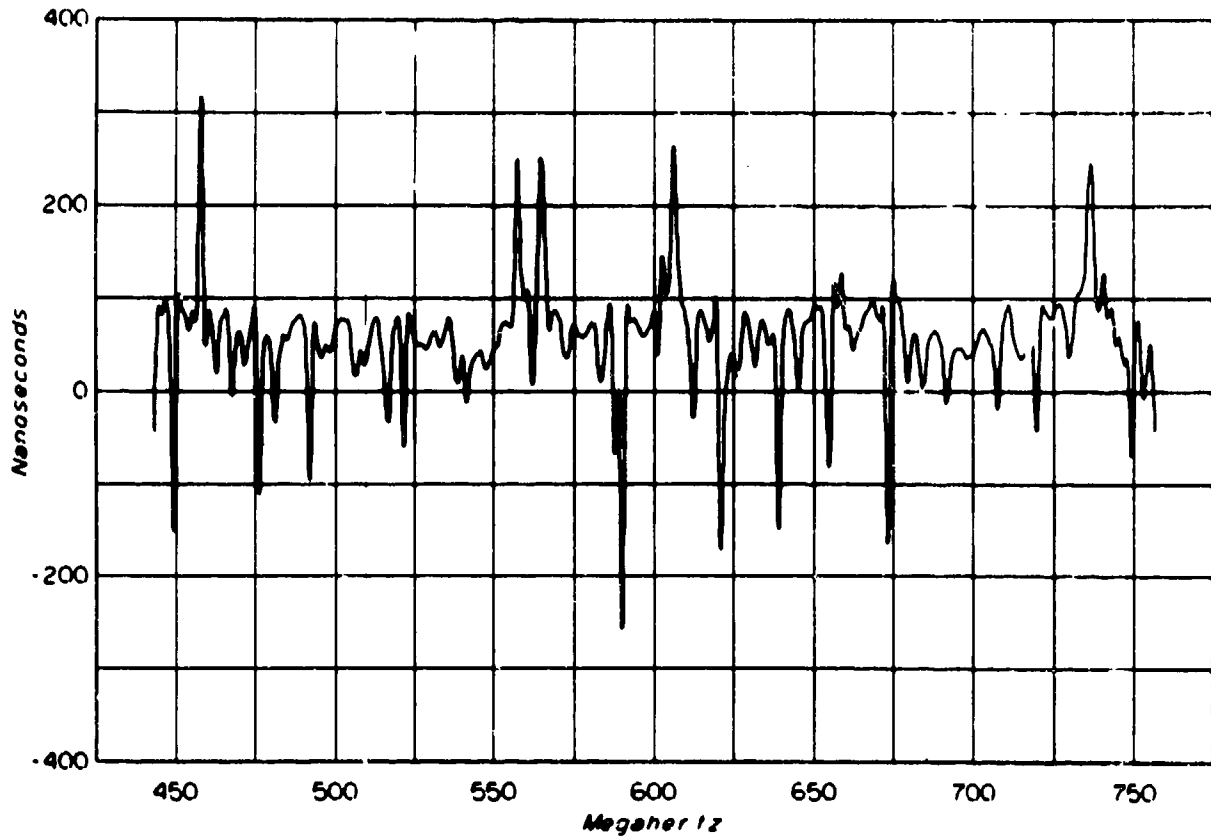
Figure 39. Group delay times; derivatives of the phase responses of
Figure 38.

70
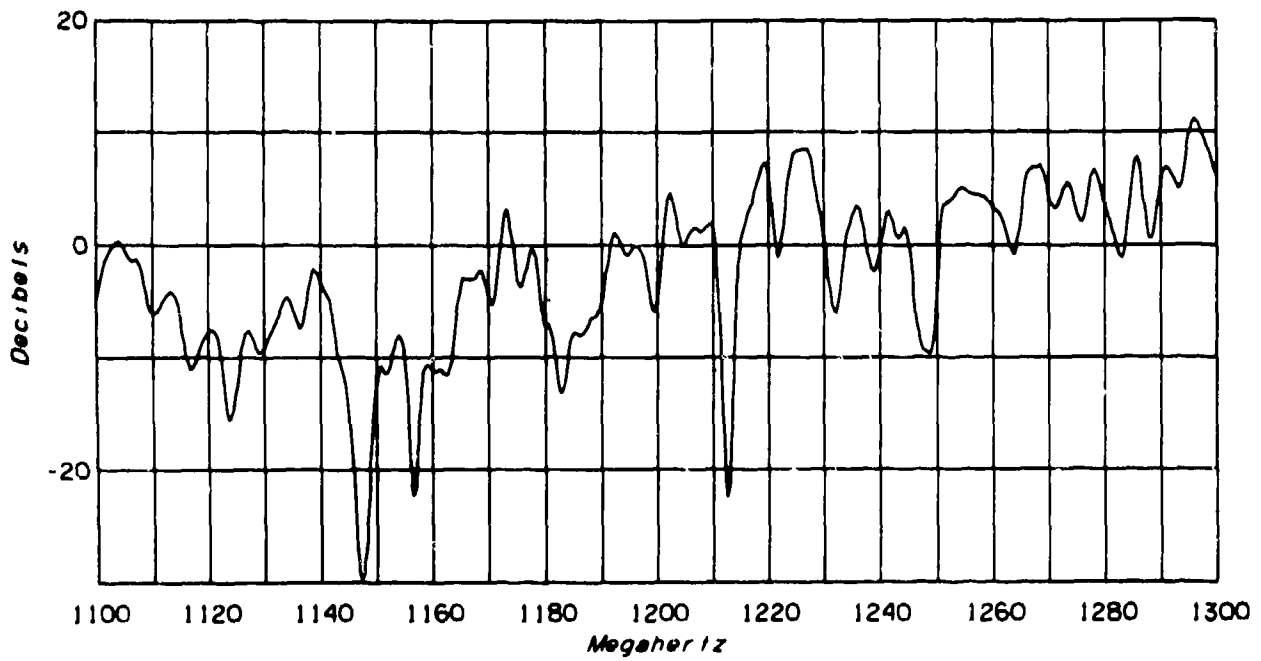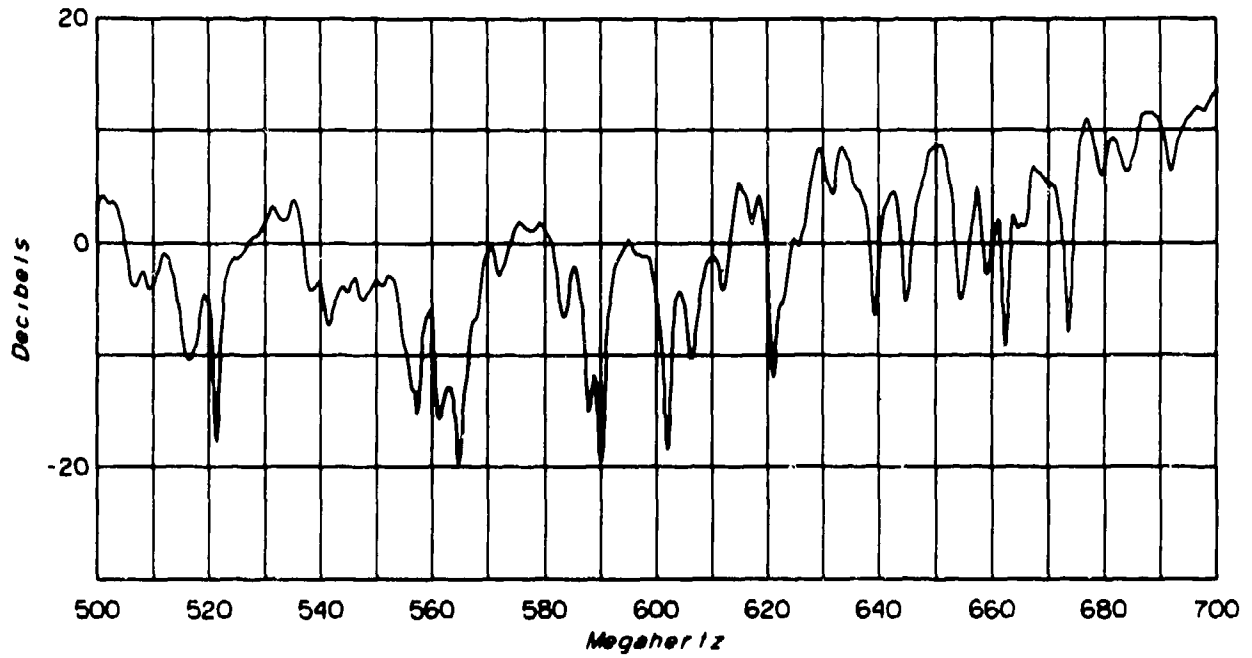
Figure 40. Spectra of the response functions of Figure 33 after division by the spectrum of the system-generated pulse.

Continuing, we might well ask whether it would be useful to evaluate the inverse Fourier transforms of the spectra of Figure 40. This should "deconvolute" the channel response from the original pulse and so produce a response function which is a more accurate representation of the actual channel response. To put this another way, this process should discover what linear combination of shifted copies of the original pulse will reproduce the measured response function and thus discover also the precise multipath components that have gone to make it up.

In Figure 41 we show our first attempt in this direction. This is the 600-MHz response of Figure 33 deconvoluted very straightforwardly using the entire spectra without alteration. Obviously, this is not satisfactory; the interesting standing wave pattern that takes over the tail of the response is undoubtedly due to noise components at the edges of the frequency band. To produce something more reasonable we have filtered out these components using raised-cosine filters whose nontrivial effects are over the final 50 MHz at each edge. The results for the 600-MHz response are portrayed in Figure 42. The companion 1200-MHz response is similarly portrayed in Figure 43. In both figures the upper graph is simply a copy of the corresponding response from Figure 33, put there to allow easy comparison. Both co- and quad- phases are given and the tails now tend satisfyingly to zero.

If we want to claim that these figures expose the distinct multipath compon- ents, then these components should correspond to the various amplitude peaks of these deconvolved responses. In the 600-MHz case, for example, one perceives first
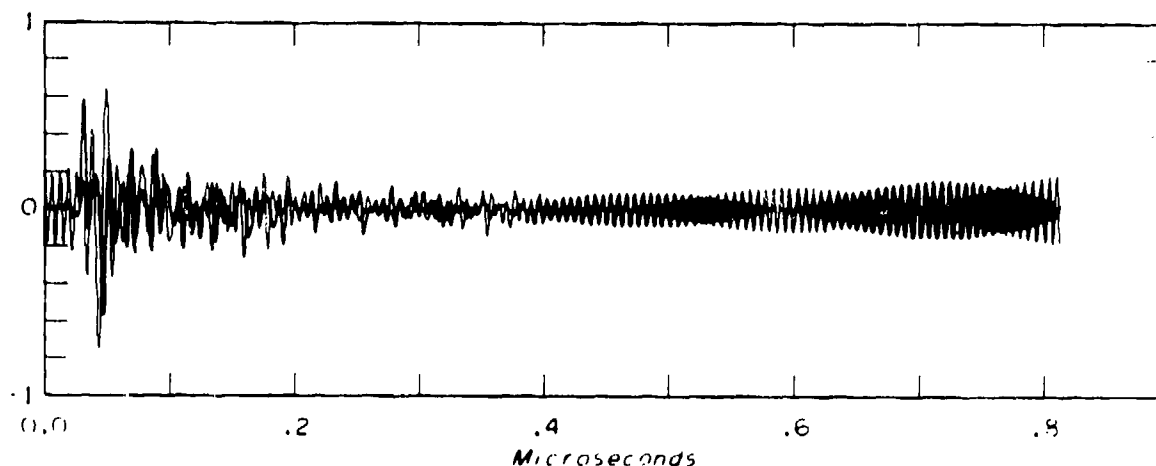
Figure 41. The 600-MHz response function of Figure 33 after the system-generated pulse has been "deconvoluted" from it. Noise components at the edges of the band have made this unacceptable.

72
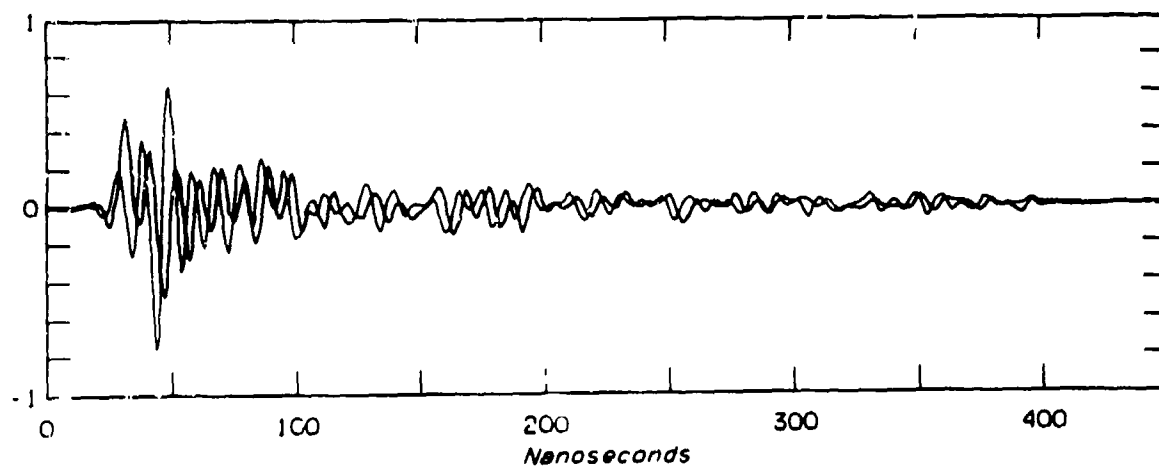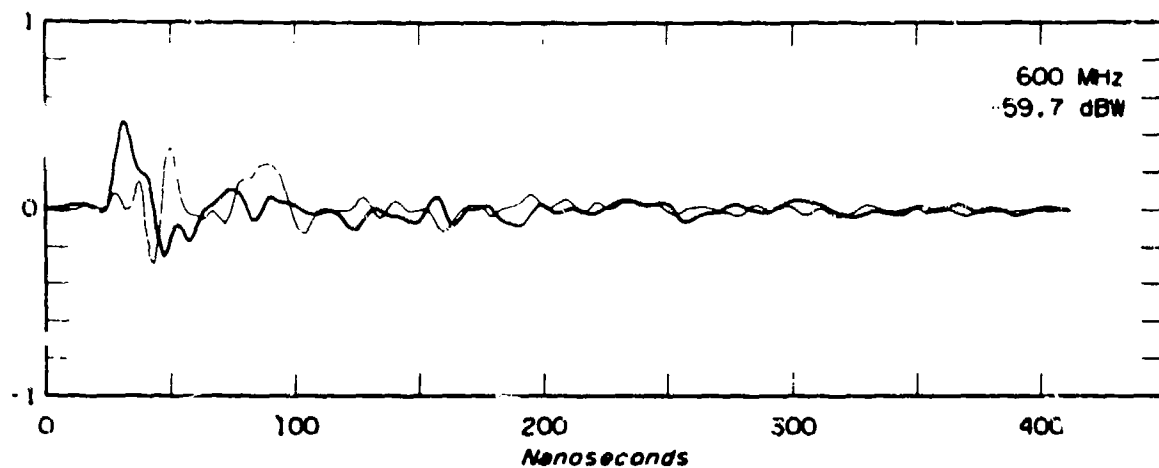
Figure 42.   The deconvoluted 600—MHz response function.   The upper graph
             is a copy from Figure 33 and has been included here to make
             comparison easy.

73
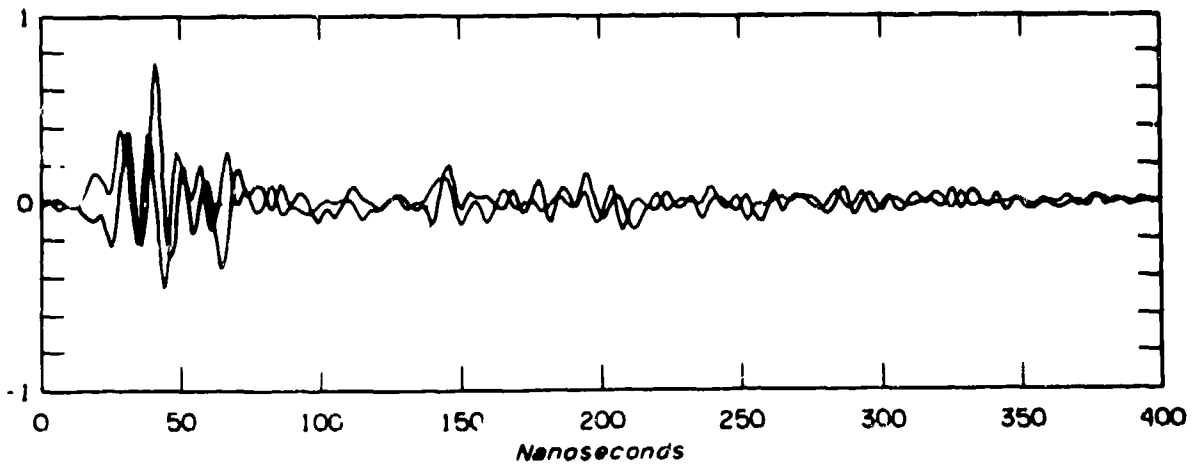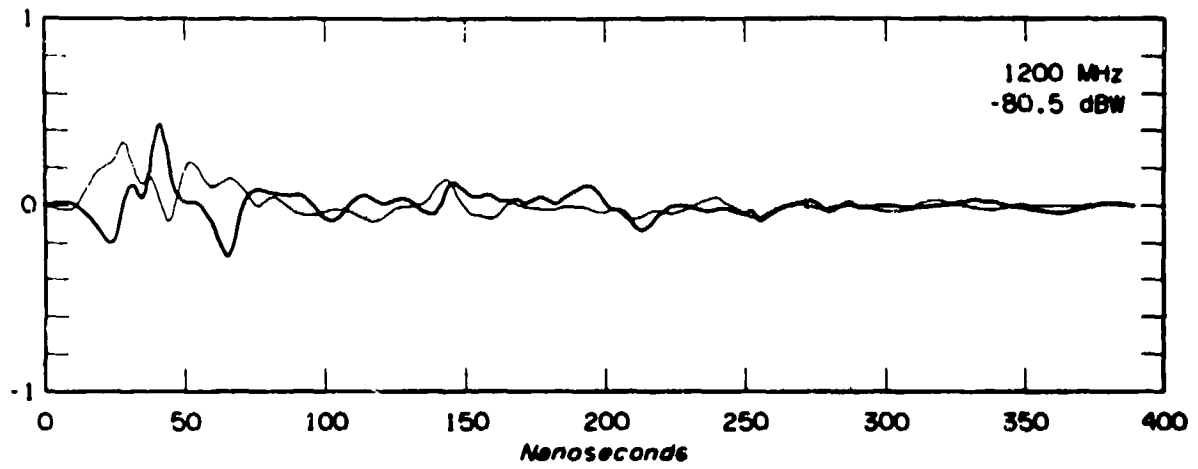
Figure 43.   The deconvoluted 1200—MHz response function of Figure 33.

a burst of perhaps three fairly large components followed by what seem like five components of medium size which in turn are followed by innumerable small components. But such an interpretation seems to us rather questionable. The oscillations in Figure 42, and also in Figure 43, seem too regular to have come from a forest environment; indeed, the appearance of these two figures looks suspiciously like a travelling wave pattern in which one quadrature component merely duplicates the other after a small time delay. This, it seems to us, might confirm the notion stated in Section 5 that it is probably wrong to look for discrete multipath components and that the proper model for study in this kind of path is one of a continuum of components. Thus, the travelling wave appearance might be due to the interaction of our deconvolution process with a narrowband representation of such a continuum. On the other hand, it might also be due simply to errors in our process--particularly to the fact we have already noted that in both spectra of Figure 40 the higher frequencies seem inordinately emphasized. We feel the technique used here and the results obtained from it deserve further study.

8. ANALYSIS OF TIME VARIABILITY

An examination of trains of impulse responses, as presented, for example, in Figures 24, 26, and 28, reveals the fact that the responses vary from frame to frame: sometimes only a little, sometimes quite a lot. Since in all these cases the terminals were fixed, we would suppose that these variations are caused either by the wind blowing in the trees or by the motion of atmospheric inhomogeneities. In any case, the propagation channels we observed appear to have been "time variant" and so to have exhibited a "doppler spread."

Given this fact an immediate question we must ask is whether we have recorded actual impulse responses or whether the channel changed as we measured it. In this regard note that at 10 frames per second we observe an entire frame in 100 ms. But since the response normally occupies only a small fraction of a frame, we observe the actual response in only about 12 ms. Thus we have indeed recorded true response functions provided only that the variations do not occur at a faster rate than about 40 Hz. At a slower frame rate of one per second, we require 120 ms to observe a single response function, and we are safe only if the channel varies at rates less than 4 Hz.

To describe the magnitude of the variability, we can examine the responses of a single run, and, for any delay time t, we can speak of the average of the responses and of the standard deviation from that average. The average will be again a complex valued function of t, but the standard deviation, being the square root of the

75

average of the square magnitudes of the deviations, will be a real valued function. For a time invariant channel the average will be identical to all the individual response functions, and the standard deviation will be zero. In Figure 44 we show the results of the process applied to the 600-MHz responses pictured in Figure 24. The results when applied to the companion 1200-MHz train are portrayed in Figure 45. In both cases the entire 100 frames of the run (occupying a time period of 60 s) were used. Note that the scale used for the standard deviation is considerably exaggerated so that the variability measure is not really so large as might seem at first glance. The two curves of averages should be compared with Figure 33.

For the response functions used in Figures 44 and 45, and also for those used in the other studies of this section, we have employed a consistent normalization. We have truncated all functions of a train at the same points, and we have multiplied all the functions by the same normalizing factor adjusted, however, for any changes in the measured AGC voltage.

Note that the 1200-MHz train has a standard deviation almost four times as great as that of the 600-MHz train. It would be interesting to know whether this is consistently so. The spikes that appear in the plots of standard deviation arise because of changes in the delay times of particular multipath components. Such spikes are positioned on the sloping edges of the corresponding pulse; they often appear in pairs, one spike on the leading edge and one on the trailing edge.

The next question of interest concerns how rapidly the responses change. Let $h(s,t)$ be the response function where t is the delay time and s the clock time; in terms of Figure 24, for example, t is the time running from left to right while s is the time running from top to bottom. What we have shown thus far, especially in Section 7, has been the response as a function of t for particular values of s. We can now turn this procedure around and show $h(s,t)$ as a function of s for particular values of t; we obtain "time slices" of the response function.

In the recorded measurements, the discretization of s is, of course, much coarser than that of t. Indeed, in the run that corresponds to Figures 24, 44, and 45, the successive responses were separated by a time interval of 0.6 s; and this is the fastest recording rate available to the system. It took 0.1 s to measure a single frame and some 0.5 s to assemble the data and write them on tape. One objective of our study must be to determine whether this rate is fast enough to capture the variations involved; we are restricted to rates of variation less than 0.8 Hz.

In Figures 46 and 47, we show such time slices for some five selected delay times each from the 600-MHz train and the 1200-MHz train. The o's for the co-phase components and the x's for the quadrature phase components all indicate actual data

76

Figure 44.   The averages and standard deviations versus delay time for the train of 600-MHz response functions in Figure 24.

RUN 008   79/10/11. 15.46.16.
TEST SITE 01   /FIRST TEST 001
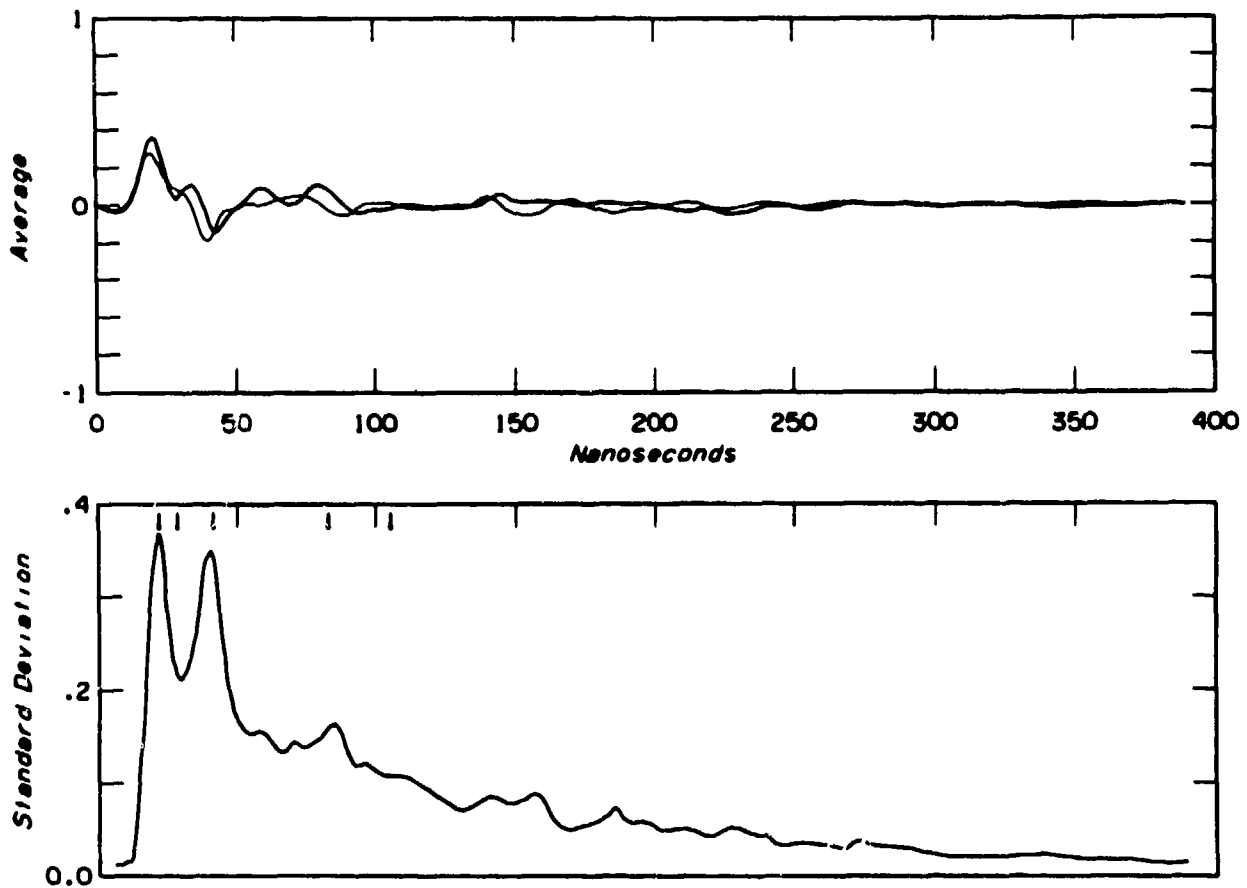
Figure 45.   The averages and standard deviations versus delay time for the
train of 1200-MHz response functions in Figure 24.

points. The selected delay times are displayed above each pair of curves; they are also indicated as small arrows in the corresponding curves of standard deviations in Figures 44 and 45. Note that we have tried to select a variety of kinds of delay times: some at the peaks of variability, some at local minima of variability.

From Figure 46 we would conclude that the 600-MHz train changes at a fairly slow rate and that we have indeed sampled rapidly enough to capture the variations. The 1200-MHz train in Figure 47, however, seems to tell a different story. The variations are not only larger in magnitude, but they are also considerably more rapid. There are, indeed, several periods of time in which the data seem clearly undersampled; on the other hand, there also remain many periods of time where the sampling appears adequate. As a whole, the picture seems borderline.

From plots such as these (preferably more refined), one could continue with a further analysis. One could test whether the time slices represent stationary Gaussian processes; and one could find autocorrelation functions, cross-correlation functions, and power spectra. Since it is presumably the wind in the treetops that is causing the observed variabilities, such a study should be carried out for a variety of wind conditions. In particular, the stationarity ought clearly to depend upon how constant are the wind speed and direction.

A second approach to the study of variability involves the spectral responses. For each clock time s, one forms the Fourier transform $H(s,\nu)$ of the corresponding response function, thus obtaining a time variant spectral response function. In Figures 36 and 37 we have plotted such functions versus ν for a fixed value of s. In Figures 48 and 49 we show "time slices" for fixed values of ν. The run involved is the same run as portrayed in Figures 46 and 47, and the density of measured points is also the same. For each figure we have chosen four arbitrary frequencies separated by about 20 MHz. The fifth curve at the top is the overall wideband received signal level; it is included for comparison purposes.

As before, the 1200 MHz curves show greater and faster variability than the 600 MHz curves. And as before, one could continue the analysis by testing for Gaussian properties and by evaluating auto- and cross-correlations and power spectra.

9. RECEIVED SIGNAL LEVELS AND PATH LOSS

The single most important characteristic of a propagation channel is undoubtedly the general overall power loss. But a question that immediately arises is that of describing just what one wants to mean by "overall" loss and how this might relate to other measurements made by other equipment, particularly by narrowband equipment.

Figure 46.   Variation of the 600-MHz response functions of Figure 24 for
              selected delay times. The delay times chosen correspond to
              the arrows in the lower graph of Figure 44.
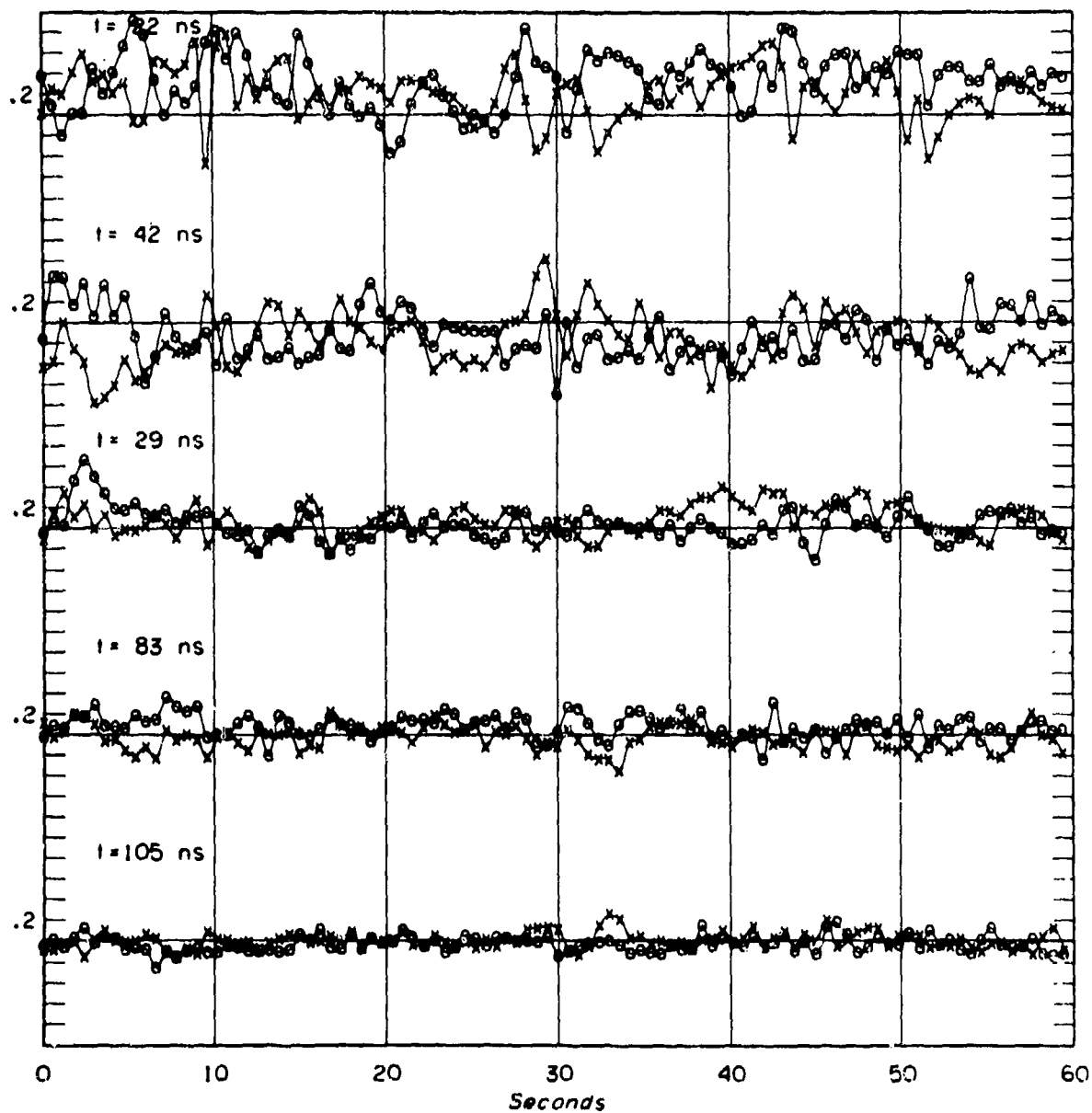
Figure 47.   Variation of the 1200-MHz response functions of Figure 24 for
             selected delay times. The delay times chosen correspond to
             the arrows in the lower graph of Figure 45.
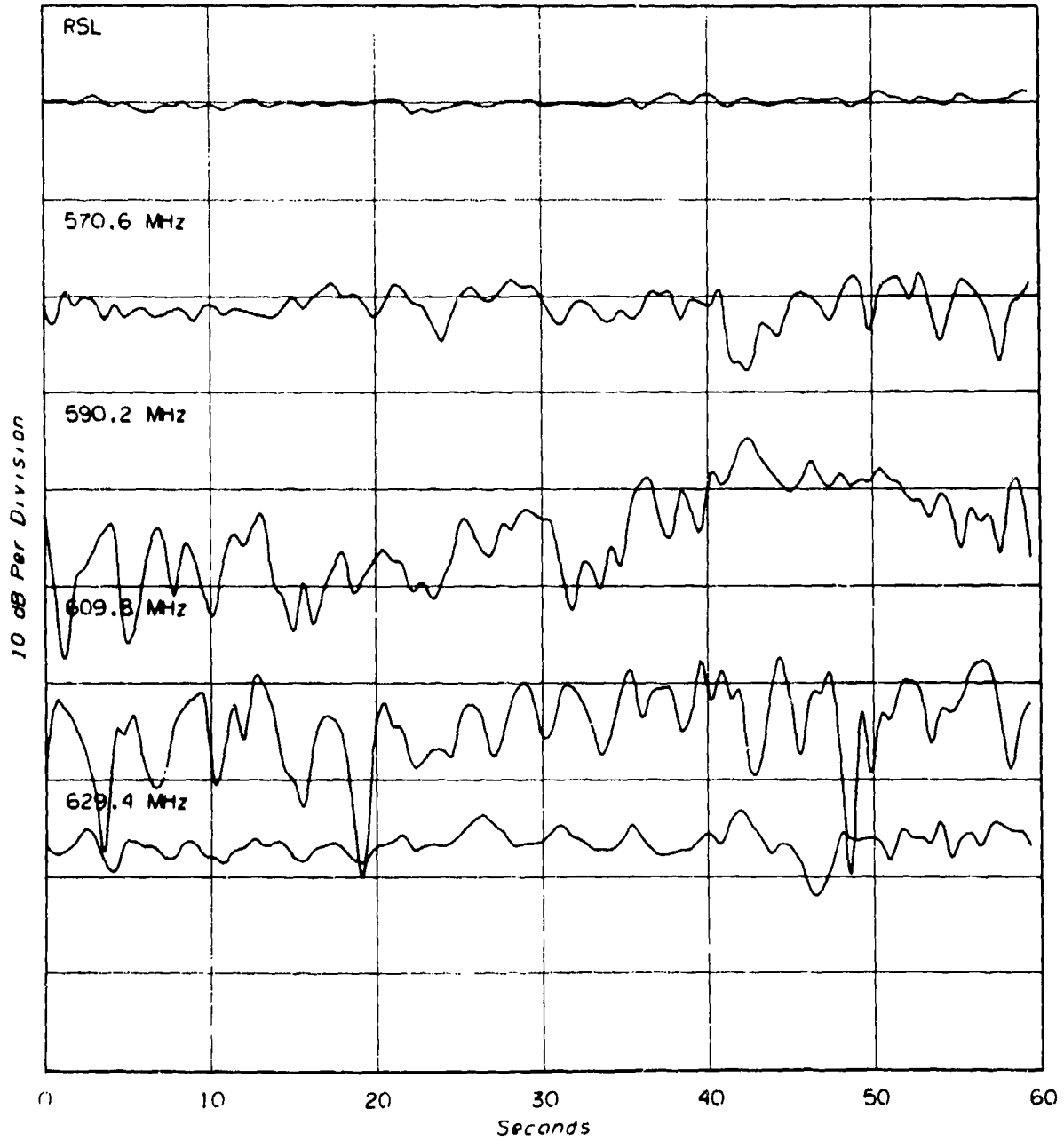
Figure 48. Variation of the 600-MHz response functions of Figure 24 for
            selected frequencies. The topmost curve is the wideband
            received signal level.

Figure 49.   Variation of the 1200-MHz response functions of Figure 24
for selected frequencies. The topmost curve is the wideband
received signal level.

The problem here arises from the fact that narrowband radio signals are highly variable in both time and space. This is particularly so in a multipath environment where complex standing wave patterns are set up. Even a slight change in the terminal positions or in the positions or allignments of scattering objects or in the carrier frequency is apt to lead to a very large change in the received signal level. The only reasonable approach in describing such a situation is to talk about the statistics of the fields and, in particular, to measure some central value of received signal levels. Such a central value would be a smoothed version of actual instantaneous values; it would be an "overall" received signal level.

There are similar considerations when one uses a radio propagation model. Most present-day models try to estimate values (or statistics) of these same overall losses. They are either of the theoretical type using greatly simplified geometrical constructs to model the environment or of the empirical type using smoothed versions of measured data. The idea, usually only implicit in the statement of the model, is that multipath environments are to be treated as a separate variability to be superimposed on the overall loss.

In addition, the use of diversity reception is a design solution to many of the deleterious effects of multipath. Once again, diversity provides a crude form of signal level averaging so that the overall loss becomes the important quantity. Indeed, when field strength measurements or received signal level measurements have been made to provide a data base for the construction of propagation models, they have very often imitated diversity systems of one kind or another. On fixed paths, for example, one will treat the received signal level as a time series, and one will record hourly medians, i.e., the median levels observed during successive hours. The process is very like a time diversity system. When measurements are made with one terminal mobile, one often reports on selected mobile runs of, perhaps, 30 m in length. Again, what one records is the median levels of such runs, and one has simulated a space diversity system. These two approaches are the ones that have been widely used in the past to measure "overall" power levels. To them, we could clearly add a simulated frequency diversity system, i.e., a wideband measurement. This would be the average or median power over some segment of the spectrum--in other words, exactly the received signal level measured by a wideband channel probe. In a fraction of a second we can find the analogue to an hour of stationary measurements or a 30-m mobile run. We pay for this convenience by requiring a large band of frequencies.

Figures 48 and 49 provide a case in point. Each of the time slices of the spectral responses can also be interpreted as what one would have observed if one were making a cw measurement at the indicated frequency. The wide variations would have been a nuisance, and one would have had to find an average or median value over some extended period of time. In contrast, the wideband received signal levels which are pictured at the top of each of the two figures show very little variability with time, and any one value will probably be adequate for most purposes. Of course, in principle there is probably some difference between time averages, spatial averages, and spectral averages and between averages and medians. We conjecture that these differences are slight and that making the distinction implies more precision in our measurements than the present state of the art allows. Thus, in what follows we shall assume that the wideband RSL is a very useful quantity and that it corresponds closely enough to what propagation models try to estimate and to what other field studies using other systems have tried to measure.

The runs of 12 October were largely directed toward a study of forest penetration and are amenable to a straightforward analysis. In particular, two of the runs involved vehicle-mounted antennas and paths that passed through one and two blocks, respectively, of solid forest in the Camp Forrest grid of streets. A third, three-block long, run was attempted, but no signal could be found.

Using the process described in Appendix B, we adjust the received signal level as measured by the AGC voltage to allow for the possible effects of interfering signals. Then taking into account the transmitter powers, the line losses, antenna gains, and free-space losses, we can convert these received signal levels to attenuations relative to free space. The results for the two runs with the two channels set at 600 and 1200 MHz are shown in Figure 50.

With only two points it is impossible to draw any firm conclusions. On each curve, however, the two points seem reasonably colinear with the origin, and the commonly made assertion that attenuation through a forest is directly proportional to distance seems satisfactorily confirmed. The average rate of attenuation for the two-block length (290 m) is 0.13 dB/m at 600 MHz and 0.19 dB/m at 1200 MHz. A test related to the development of JTIDS and carried out a few weeks later over almost the identical paths used here (the antenna heights were a little different) has been reported by Presnell (1980). The system was in the frequency hop mode and so had a bandwidth of 250 MHz with a center frequency of about 1100 MHz. Although measurements of received signal level used an entirely different technique, exactly the same attenuation rate of 0.19 dB/m was observed for the two-block long path.
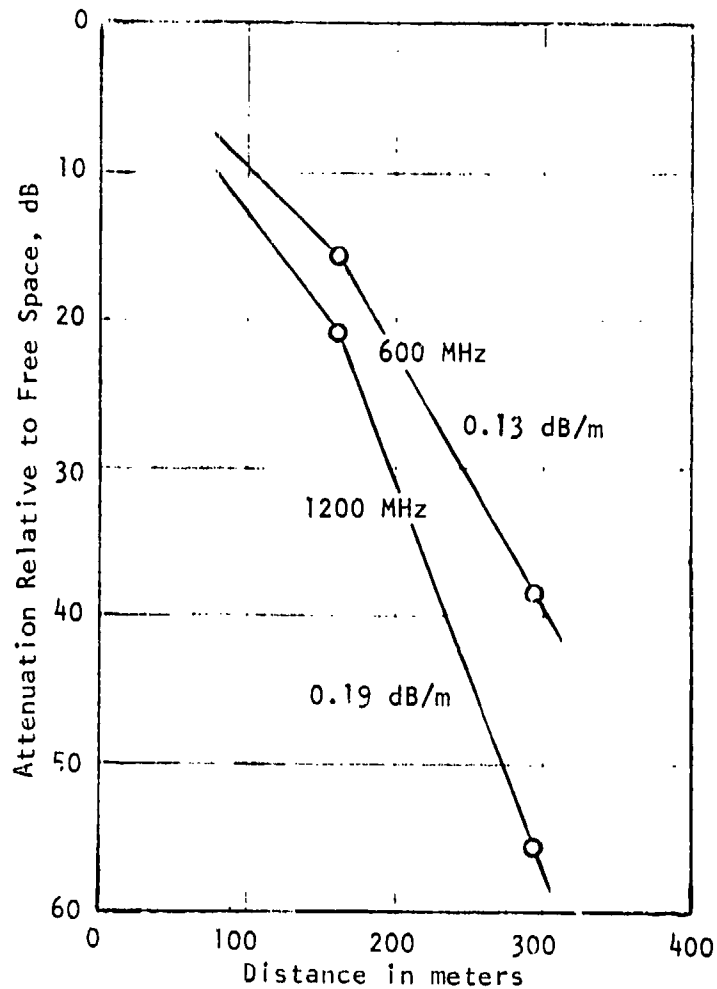
Figure 50. Attenuation relative to free space versus separation
distance when the two terminals are buried in the
forest.

Those values of attenuation rate are only half those reported by Saxton and Lane (1955) and by other sources (Rice, 1971). On the other hand, Frankel (1978), using a 10-MHz wide system at 1850 MHz, reported an average rate of 0.17 dB/m through fairly dense forests in California. That the three wideband systems report smaller rates of attenuation than had been observed before probably has nothing to do with the bandwidth. The single most important factor of a "dense" forest in determining what rates of attenuation it will produce is its moisture content; the forests of California are probably drier than those in Tennessee, and the autumn trees in Tennessee drier than the trees in England where Saxton and Lane made their measurements.

It is of interest to estimate what signal levels were present on the abortive three block run; extending the measured attenuation rates to the third block (440 m away), we find attenuations of 56.4 dB and 81.6 dB for the two frequencies, or received signal levels of -127.4 dBW and -153.7 dBW. Both are beyond the system sensitivity.

As part of the forest penetration study of 12 October, there was a second set of runs that form what might be called an "up and over" study in which the terminals were stationed at the same points as in the first study, but the receiving antenna was on a tower about 8 m above the forest top. In Figure 51 we have plotted the resulting attenuations relative to free space when the terminals were separated by one, two, and three blocks of forest. Two of the transmitter locations were revisited, giving us an estimation of the repeatability of the measurements, and at three blocks away the transmitter van was driven through one of the cross streets of Camp Forrest to a point where the trees and underbrush seemed to crowd in more closely.

The curves of Figure 51 are not inconsistent with consequences of the "slab model" (Tamir, 1967) of a forest. In that model one replaces the forest with a homogeneous lossy dielectric--a slab covering the ground. Presumably, a wave begins at the transmitter, struggles up through the lossy forest, is refracted at the
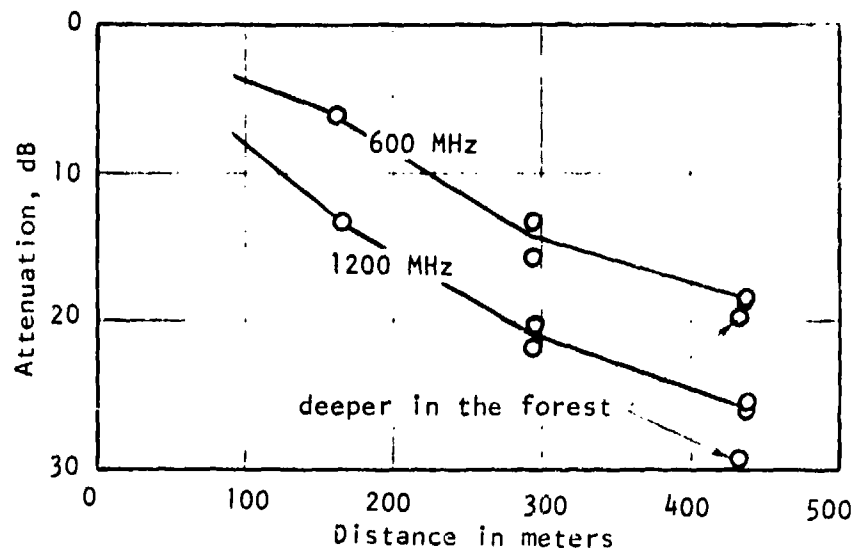
Figure 51. Attenuation relative to free space versus separation distance when one terminal is buried in the forest and the other is about 8 m above the forest top.

fo est top, and crosses to the receiver. Of course, such a model says absolutely
nothing about the multipath characteristics of the received signal; it is another of
those models that are concerned only with the overall loss.

There is also an "up-over-and-down" mode that is predicted by this slab model
when both terminals are within the forest. Using the path geometry associated with
the runs of Figure 50, we would estimate that this mode ought to become apparent
after 400 m or more. For longer distances the rate of attenuation should be much
reduced; but for most present-day equipment this is of no help, since at that dis-
tance the signal will already be too low to measure. Certainly, the sensitivity of
the channel probe system was insufficient to observe any such phenomenon.

10. CONCLUSIONS

From the oak, hickory, and pine forests of southern Tennessee we have acquired
valuable data concerning wideband transmission characteristics at UHF on paths in
forested environments. The combination of a pseudo-noise channel probe with a
digital data acquisition system has provided us with clean-cut representations of
the impulse response for a variety of propagation channels. And from these repre-
sentations we can perform a large number of analyses using the precision of digital
computers.

Of course, we cannot claim that our data even begin to provide a valid sta-
tistical sampling of any particular radio phenomenon. But we can say that we have
gained some preliminary insight into the magnitude of some of the important propa-
gation parameters. We have, for example, seen that our measurements of forest
penetration show the same order of magnitude for the rate of attenuation as have
previous cw measurements. For delay spreads we have seen that when one or both
terminals are buried in a fairly dense forest the entire impulse response is con-
tained within an interval of about 400 ns; and this seems to be relatively indepen-
dent of frequency or forest density. Presumably, multipath components with larger
delay times have been greatly attenuated by the trees. As expected, horizontally
polarized waves showed smaller delay spreads than did vertically polarized waves.
When, however, we talk of line-of-sight paths or of diffraction paths with both
terminals in the open, it would seem that longer delay spreads are possible. We
have already seen spreads of 0.6 μs and would suppose that 1 μs is easily attainable.
And we should not forget that in urban environments Turin et al. (1972) have
observed delay spreads of almost 7 μs.

As stated in Section 1, the primary purpose of this limited set of measurements
was to determine whether the approach was feasible, what special problems would

88

arise, and what solutions to these problems might be found. In this connection we offer the following suggestions for the design of any similar measurement program.

(1) The system sensitivity was gr   n   for many of our experiments but not for all. An in   desirable, particularly at the lower frequency.   r   transmitter power should be increased by about 10 dB.

(2) Interference in the IF passband   ser ou   and the bands in which we are interested are too rowded to ignore the problem. One of the best ways to fight this is with the correlation detector itself; for this introduces a very precise series of sharp passband filters into the system. Since it appears only after the IF amplifier, it might be wise to employ a second AGC circuit--this one in the baseband amplifier. Of course, such a circuit would require a second calibration sequence, which would be somewhat of a nuisance.

(3) In this measurement program the digital data acquisition system served merely as an external recorder in which many of the experiment parameters had to be introduced manually. It would be preferable to combine the channel probe and the acquisition system into one unit. Then control parameters could be directly available to the record; the system computer could even be used to enter these same control parameters. In particular, the sampling rate could be determined by the system as a simple function of frame rate.

(4) Calibration is an important, but tedious, process. Perhaps this could be automatically controlled by the system computer. In particular, calibration should always include a record of the effective pulse shape.

(5) In the present system we were able to make digital recordings at a rate no faster than one frame in 0.6 s. This is too slow to follow some of the time varying phenomena.

(6) Mobile runs have been included in our tests as a multiplexing scheme to obtain more useful data in a given period of time. However, unless the recordings can be made at a much faster rate, this may turn out to be a wrong approach. Perhaps a quasi-mobile scheme would be a satisfactory substitute. In this scheme the transmitting van would jump forward in small steps and would pause after each step for a few seconds.

89

(7) A limited amount of concurrent meteorological data would some-
times be advantageous. When it is a matter of short p   in the
presence of a forest, probably the most important parameter is
the wind speed. Also valuable would be a measure of the water
content of the trees.

With respect to the conduct of future experiments and to the analysis of the result-
ing data, we would offer the following suggestions and recommendations.

(8) In the case of propagation on short paths through a forest, one
should compile statistics for the two important quantities of
attenuation rate and delay spread. These should be treated as
functions of frequency, polarization, path length, and forest
type. The latter parameter is the most difficult to measure or
vary. We would simply suggest as many forest types as possible,
and we would leave open the question as to whether the parameter
is important. Following these two, easily defined, quantities,
one should study the internal structure of the response functions.
We feel it can be fairly simply modeled as a continuum of compon-
ents.

(9) If it appears that the up-over-and-down mode of propagation
through a forest might become useful for future radio systems (or
worrisome for interference problems), then it should certainly be
investigated.

(10) In the case where both terminals are in the open but are sur-
rounded by patches of forest, one suspects that delay spreads will
be considerably greater and much more variable. Useful statistics
will be difficult to compile. For urban propagation, Turin et al.
(1972) have suggested that the multipath components arrive in
bursts. Perhaps a similar concept applies here, too, with each
burst being a self-contained continuum of components.

(11) Finally, there is the case where one terminal is in the open and
the other inside a forest. This is probably an important situa-
tion that should be studied. Except for some selected paths
where one terminal was high above the forest, the present experi-
ment did not include such a case.

90

11. ACKNOWLEDGMENTS

12. REFERENCES

Bello, P. A., J. K. DeRosa, and C. J. Boardman (1973), Line-of-sight wideband propagation, Air Force Systems Command, Rome Air Development Center Report RADC-TR-73-167, May.

CCIR (1978), Propagation statistics required for broadcasting services using the frequency range 30 to 1000 MHz, Doc. XIVth Plenary $\underline{V}$, Report No. 239-4.

Frankel, M. S. (1978), L-band forest experiments, SRI International Packet Radio Temporary Note 254.

Hubbard, R. W. (1977), Measurements in microwave telecommunication systems using a pseudo-random noise (PN) probe, URSI Measurement in Telecommunications, Conference Record, Lannion, France, October.

Hubbard, R. W. (1979), Investigation of digital microwave communications in a strong meteorological ducting environment, NTIA Report-79-24, August.

Linfield, R. F., R. W. Hubbard, and L. E. Pratt (1976), Transmission channel characterization by impulse response measurements, OT Report 76-96, August.

Presnell, R. I. (1979), JTIDS ground-to-ground propagation test site survey--Arnold AFS, Contract MDA903-78-C-0126, SRI International, Menlo Park, California.

Presnell, R. I. (1980), JTIDS ground-to-ground propagation measurements, Contract MDA903-78-C-0126, SRI International, Menlo Park, California.

Rice, P. L. (1971), Some effects of buildings and vegetation on VHF/UHF propagation, IEEE EMC Conf. Proc., Tucson, Arizona.

Saxton, J. A., and J. A. Lane (1955), VHF and UHF reception--effects of trees and other obstacles, Wireless World 61, pp. 229-232.

Tamir, T. (1967), On radio propagation in forest environment, IEEE Trans., AP-15, pp. 806-817.

Turin, G. L., F. D. Clapp, T. L. Johnston, S. B. Fine, and D. Lavry (1972), A statistical model of urban multipath propagation, IEEE Trans., VT-21, pp. 1-9.

APPENDIX A.   SOME BACKGROUND THEORY OF THE PSEUDO-NOISE CHANNEL PROBE

In the following discussion we shall try to collect some of the general theory of communications that pertain especially to measurements made by a pseudo-noise probe. Although generalizations are obviously possible, we shall direct our development towards a scenario in which there is a radio transmitter and a receiver some distance away, and it is the propagation channel in whatever environment the terminals are placed that we want to measure. Of course, such a channel involves electromagnetic waves, and a full description would include the electric and magnetic fields as three dimensional vectors. But in what follows, the signals we speak of will be simply the voltages observed on the equipment side of the respective antennas. Further analysis must involve the antenna polarizations and how the antennas couple into the medium.

Sample numbers that we quote will usually pertain to the particular equipment used in the recent Tennessee experiment. We shall refer to it simply as "the ITS probe." Its principal characteristics are a clock rate (bit rate) of 150 MHz and a code length of 511.

In the terminology we use, the unit impulse is represented by the Dirac delta so that, for example, $\delta(t-t_o)$ is a unit impulse acting at time t_o. Signals will be represented by lower case letters and their Fourier transforms by the corresponding upper case letter. Thus, if $x(t)$ is a (perhaps complex valued) signal,

$$X(\nu) = \mathfrak{F}\{x\}(\nu) = \int x(t) \, e^{2\pi i\nu t} \, dt$$

and

$$x(t) = \mathfrak{F}^{-1}\{X\}(t) = \int X(\nu) \, e^{-2\pi i\nu t} \, d\nu \quad,$$

where the unmarked integrals here, as in similar expressions, are to be taken over the entire real line. If x is periodic with period T and frequency $\nu_1 = 1/T$, then

$$X(\nu) = \sum X_k \delta(\nu - k\nu_1)$$

$$x(t) = \sum X_k \, e^{-2\pi ik\nu_1 t} \quad,$$

where

$$X_k = \frac{1}{T} \int_o^T x(t) \, e^{2\pi ikt/T} \, dt, \quad k = \ldots -1, 0, 1, \ldots,$$

and where the unmarked summations are to be taken over all integers.

Note that the signs we have used in the exponentials do not follow the conventions normally used in communications theory. If the reader prefers, he should replace all occurrences of i with -j.

Finally, if x is a finite signal, we speak of its __total__ energy

$$||x||^2 = \int |x(t)|^2 \, dt = \int |X(\nu)|^2 \, d\nu \quad .$$

And if x is periodic with period T, we speak of its __average__ power

$$||x||_O^2 = \frac{1}{T} \int_O^T |x(t)|^2 \, dt = \sum |x_k|^2 \quad .$$

A.1. The Impulse Response

As mentioned above, the channel we want to measure consists of a transmitting antenna, the medium of propagation with all its clutter, and a receiving antenna. We assume this channel is at any rate a __linear__ channel and hence can be completely characterized by its __impulse response__ $h(t,\tau)$. This is the received signal at time t when the transmitted signal is a unit impulse acting at time t-τ. The value τ may be interpreted to be the time delay between transmission and reception. If, instead, we transmit any arbitrary signal x(t), the received signal y(t) may be expressed as

$$y(t) = \int h(t, \, t - t') \, x(t') \, dt' \tag{A.1}$$

$$= \int h(t, \, \tau) \, x(t - \tau) \, d\tau \quad .$$

It is this integral that allows us to say that h characterizes the channel.

If the input x and the output y have the same units, then it is clear from (A.1) that h must be measured in units of reciprocal time. Since the channel and the assumed input are both real, the response h must also be real--although, certainly, there is no reason that it cannot become negative. Because the channel is "causal," h must vanish for negative delay time τ. Indeed, if transmitter and receiver are separated by a distance r, the response cannot start until after τ > r/c, where c is the velocity of light.

Often, one supposes that h is composed of a sequence of impulses. First comes the primary impulse, the wave that passes directly from transmitter to receiver, and this is followed by a sequence of "multipath components," waves that have been scattered or reflected from objects in the environment. These latter components

94

arrive at larger and larger time delays because of the ever increasing distances over which the waves must travel; they are ever more attenuated because of the increasing inefficiencies in whatever scattering processes are involved. Although this picture is a good model to start from, one suspects that the scattering processes will serve as a kind of filter which will convert discrete impulses into pulses with a finite "spread." Note that the two antennas will also act as filters.

The duration of an impulse response--the time during which it is sensibly different from zero--is ordinarily some fraction of a microsecond. In unusual cases there may be a strong multipath component arriving from far off the direct path and hence delayed by a long time. There is then almost no limit to the measured duration.

If the physical environment where the channel operates is stationary, then one expects that the moment of transmission has no effect on reception, and that the impulse response is independent of the first variable t, depending only on the time delay τ. This is the important case of a time invariant linear channel. In such a case we may simplify our notation by suppressing the first variable and writing simply $h(\tau)$. Then (A.1) simplifies, becoming the straightforward convolution

$$y(t) = (h * x) (t) \hspace{4cm} (A.2)$$

$$= \int h(\tau) \, x(t - \tau) \, d\tau \quad .$$

Even when the channel is not time invariant, it usually varies only slowly. So slowly, indeed, that within any time interval on the order, say, of milliseconds, it has the appearance of being invariant. In particular, looking at (A.1) we would have to agree that over the interval of time delays τ, where h is sensibly nonzero, any variability with respect to the first variable is negligible. Thus it would seem to be nearly always true that one can replace (A.1) by (A.2) and still obtain an excellent approximation. If desired, one could still carry the first variable to denote not the instant of time but really an "epoch" of time within which the response is assumed to be invariant. One might say we have a "quasi-invariant" channel. In what follows we shall assume this is all true, and for simplicity we shall normally suppress mention of that first variable.

One obvious way to measure the impulse response is simply to transmit an impulse and then to record the received signal. In practice this is impossible, if only because we cannot generate the original impulse. Instead, we are restricted to some finite pulse $p(t)$ and to the received signal $y = h * p$. Now if p is a reasonable pulse--if it is smooth, zero for most of the time except for a small

95

interval about t=0 where it takes on positive values--then y is simply a "smoothed" version of h, a type of "running average," and hence an approximation to h. If the impulse response is composed of discrete multipath components as described above, then y is simply a sequence of copies of p with varying time delays and magnitudes. Of course, if the multipath components have very similar time delays, the pulse copies will overlap each other making resolution difficult or impossible.

Such a pulse is not only limited in time duration, it is also limited in bandwidth. For example, the ITS probe uses what is effectively a pulse with a time duration of about 13 ns and a bandwidth of about 300 MHz. For most purposes, it is necessary to deploy this bandwidth in some particular portion of the radio spectrum. This we can easily do by using the pulse p to modulate a carrier frequency. Then the signal we transmit takes on something like the form

$$p(t) \cos(2\pi\nu_o t - \theta) \quad ,$$

where ν_o is the carrier frequency and θ is an arbitrary initial phase. The frequency band now occupied is centered about ν_o and will, in practice, fall far short of the zero frequency. The ITS probe, again, uses carrier frequencies of 600 MHz and higher. If the carrier frequency is 600 MHz, then the band occupied extends from 450 to 750 MHz.

Under these new conditions the received signal becomes

$$y(t) = \int h(\tau) \; p(t - \tau) \; \cos(2\pi\nu_o(t - \tau) - \theta) \; d\tau \qquad (A.3)$$

$$= \hat{y}_c(t) \; \cos 2\pi\nu_o t + \hat{y}_q(t) \; \sin 2\pi\nu_o t \quad ,$$

where

$$\hat{y}_c(t) = \int h(\tau) \; \cos(2\pi\nu_o\tau + \theta) \; p(t - \tau) \; d\tau \qquad (A.4)$$

$$\hat{y}_q(t) = \int h(\tau) \; \sin(2\pi\nu_o\tau + \theta) \; p(t - \tau) \; d\tau$$

are called the co-phase and quadrature phase components, respectively. Note that the sinusoids introduced into these two integrals will perform a further smoothing process, and in the result only those components of h with frequencies near $\pm\nu_o$ will remain, and these will have been translated to base band--that is, to frequencies near zero.

The formulas (A.3) and (A.4) are easier to express and easier to visualize if we use complex numbers and replace the sinusoids with exponentials. In this new notation we say that the transmitted signal has the form

96

$$p(t) \; e^{-2\pi i \nu_o t + i\theta} \quad ,$$

and by this we really mean to say that the transmitted signal is the real part of this expression. The received signal then may be rewritten as (the real part of)

$$y(t) = \int h(\tau) \; p(t - \tau) \; e^{-2\pi i \nu_o (t - \tau) + i\theta} \; d\tau \tag{A.5}$$

$$= \hat{y}(t) \; e^{-2\pi i \nu_o t} \quad ,$$

where

$$\hat{y}(t) = \hat{y}_c(t) + i \; \hat{y}_q(t) \tag{A.6}$$

$$= \int h(\tau) \; e^{2\pi i \nu_o \tau + i\theta} \; p(t - \tau) \; d\tau \quad .$$

At this point in our argument we can abstract from the particular pulse $p(t)$. First, we introduce the notion of a _complex_ signal. This is a complex valued function $\hat{x}(t)$ of time. It is to be interpreted as a signal that modulates a carrier frequency so that the voltage actually present in a circuit has the form

$$x(t) = \text{Re}(\hat{x}(t) \; e^{-2\pi i \nu_o t}) \quad . \tag{A.7}$$

This is a convenient generalization that accomplishes many purposes. For example, note that phase modulation can now be easily represented as a complex signal in which $|\hat{x}(t)|$ is constant. Note, too, that in (A.6) the phase factor $e^{i\theta}$ can be absorbed into a now complex pulse $\hat{p}$.

Continuing, we define the _complex impulse response_

$$\hat{h}(t) = h(t) \; e^{2\pi i \nu_o t} \quad , \tag{A.8}$$

so that the real response h may be pictured as the carrier frequency ν_o modulated by $\hat{h}$. Then, if we transmit any arbitrary complex signal $\hat{x}(t)$ modulating the carrier frequency ν_o, it will follow from (A.2) that the received signal may be represented as the carrier frequency modulated by $\hat{y} = \hat{h} * \hat{x}$, the simple convolution. This is an important result that allows us to think of the modulating signals independent of the radio frequency carrier. Note that its derivation depends on the fact that the actual impulse response h is real. We should also note that the real utility of this result appears in the case where the "arbitrary" signal $\hat{x}$ is restricted to those that are band limited with bandwidths considerably less than the carrier frequency.

Let us now consider a process of importance to us. This is the straight multiplication of two radio frequency signals through a mixer of some kind. Let us suppose

$$\tilde{x}(t) = \hat{x}(t) \ e^{-2\pi i \nu_0 t}$$

$$\tilde{y}(t) = \hat{y}(t) \ e^{-2\pi i \nu_1 t}$$

so that $\hat{x}$ is a complex signal modulating the carrier frequency ν_0 and $\hat{y}$ modulates the, perhaps different, carrier frequency ν_1. To say we multiply the signals together is actually to say we multiply their real parts together. We have

$$\text{Re}(\tilde{x}) \ \text{Re}(\tilde{y}) = \tfrac{1}{2} \ \text{Re}(\tilde{x}\tilde{y}^* + \tilde{x}\tilde{y}) \ , \tag{A.9}$$

where we have here used the star (*) to denote the complex conjugate. It follows that this product can be separated into two familiar components. One is the complex signal $\tfrac{1}{2}\hat{x}\hat{y}^*$ modulating the difference frequency $\nu_0 - \nu_1$. The other is the signal $\tfrac{1}{2}\hat{x}\hat{y}$ modulating the sum frequency $\nu_0 + \nu_1$. If both $\hat{x}, \hat{y}$ are band-limited, these two components are easily separated by suitable filters.

If $\nu_0 = \nu_1$, it is then improper to say that the first component "modulates" a 0 frequency. The above equation still remains true, however, and we can say instead that the first component is "at base band" and equals $\tfrac{1}{2} \ \text{Re}(\hat{x}\hat{y}^*)$. What we now have is an example of "coherent detection" in which, if x is an incoming signal and y a locally generated signal, we have separated the modulation $\hat{x}$ from the carrier frequency by a process that is almost linear. Indeed, the process would be linear if it were not that we are restricted to obtaining only the real part of the product. This restriction has another disadvantage in that phase information contained in $\hat{x}$ is largely lost. Indeed, it is, in practice, very difficult to determine, and then to retain, a fixed phase relation between the two radio frequency signals x and y; and the resulting indeterminancy will be reproduced in the product $\hat{x}\hat{y}^*$.

To overcome these disadvantages, most coherent detectors employ a slight extension of the ideas given above. They split the incoming signal to feed two separate channels called the co-phase channel and the quadrature phase channel. In the co-phase channel the signal is multiplied by the locally generated signal just as before. In the quadrature phase channel, however, the locally generated signal is first given a phase lag of 90°, and only afterwards is the product produced. Since the phase lag corresponds to multiplying the locally generated $\hat{y}$ by i, the output of the two channels is the pair of base-band signals $\tfrac{1}{2} \ \text{Re}(\hat{x}\hat{y}^*)$

and $\frac{1}{2} \text{Re}(\hat{x}(i\hat{y})^*) = \frac{1}{2} \text{Im}(\hat{x}\hat{y}^*)$. Clearly, this pair can be conceptually combined to form an effective "complex base-band signal" equal to $\frac{1}{2}\hat{x}\hat{y}^*$. The result is now linear in the input signal $\hat{x}$ and all phase information has been retained. Further processing, however, must always take into account the fact that there are now two physical channels.

To conclude this section on the impulse response and complex signals, we must consider how these appear in the frequency domain. It is here that restrictions on bandwidth will become clearly of importance.

From (A.7) we find

$$X(\nu) = \frac{1}{2}(\hat{X}(\nu - \nu_o) + \hat{X}^*(-\nu - \nu_o)) \quad ,$$

so that X is separated into two components, one centered about the frequency ν_o, the other about $-\nu_o$. Of course, X satisfies the identity $X(-\nu) = X^*(\nu)$ as must any real signal. But furthermore, if $\hat{X}$ is limited to frequencies much less than ν_o, then these two components are very clearly separable. Indeed, we can then go in the opposite direction and write

$$\hat{X}(\nu) = 2X(\nu + \nu_o)$$

provided it is clearly understood that this formula is to be used only for values of ν near 0--to be precise, only for values of ν whose absolute values are (much) less than ν_o.

Turning to the impulse response, we see that if X is the transmitted signal, then

$$Y(\nu) = X(\nu) \, H(\nu)$$

is the received signal. In base-band modulation terms,

$$\hat{Y}(\nu) = \hat{X}(\nu) \, \hat{H}(\nu) \quad ,$$

where, from (A.8),

$$\hat{H}(\nu) = H(\nu + \nu_o) \quad .$$

These are simple formulas, but they carry with them some important implications. Since $\hat{X}(\nu)$ will be sensibly different from zero only for small values of ν, the same limitations will apply to $\hat{Y}$. Furthermore, the only values of $\hat{H}$ that we need, or that we can measure, will be for the same limited range of frequencies. This last formula for $\hat{H}$, therefore, is to be taken in the same sense as the formula for the Fourier transform of a complex modulation signal--it is to be used only for small values of ν. We have a "narrowband representation" of the impulse response, and the result is a true complex signal.

99

In the case of a time varying channel, we can write

$$H(t,\nu) = \int h(t,\tau) \; e^{2\pi i\nu\tau} \; d\tau$$

thus giving us a "time varying Fourier transform." This introduces no further com-
plication, provided that the variation with t is sufficiently slow.

Throughout this section we have carefully distinguished three different ways
of expressing the same signal; and we have written x, x̃, and x̂ for the real signal,
the "complexified" signal, and the complex modulation signal, respectively. In the
sections that follow we shall suppress these diacritical marks and depend only on
context to determine which representation we are using in any one instance.

A.2.   The Cross-correlation Detector

In the actual measurement of an impulse response, one does not transmit a
single pulse whose received signal is to be recorded; instead one transmits what is
effectively a periodic train of pulses. This not only provides us with a somewhat
continuous picture of how the response changes with time, but also allows us to do
some signal processing and so overcome problems of noise and interference.

The processing used by a pseudo-noise probe employs what is known as a cross-
correlation detector. This class of devices is excellent for measuring the shape
and size of periodic signals. In our discussion below we treat the configuration
employed by the ITS probe. Other configurations are treated, for example, by Lee
(1960, Ch. 12).

A sketchy block diagram of the probe receiver is given in Figure A.1. We
assume an input consisting of a periodic signal modulating a carrier frequency. It
is first brought down to our intermediate frequency and amplified. A second signal
is locally generated. It has the same period as the input signal and modulates the
same intermediate frequency. These two signals are then multiplied together in the
manner described in Section A.1, and finally the product is sent through a low-
pass filter. What we have now done is essentially to have integrated the product
of the input signal and the locally generated signal, thus providing a kind of
cross-correlation between them. From this is derived the name.

Although in concept the device is fairly simple, note that it is really a
coherent detector and so for practical implementation requires many additional com-
plications. It needs, for example, very close tolerances on the generation of the
intermediate frequency. And, as suggested in Section A.1, the signal flow must
split into co-phase and quadrature phase channels.
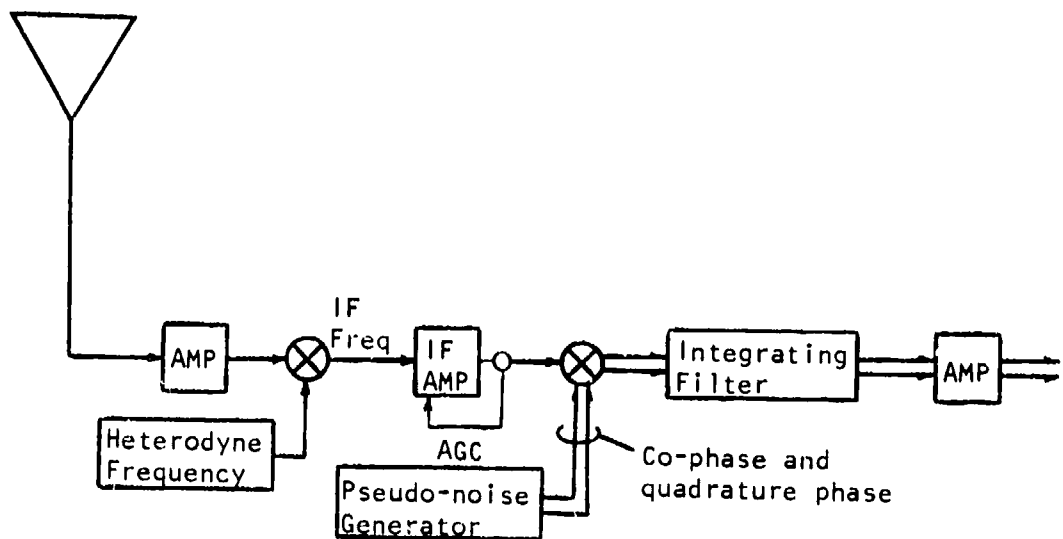
Figure A.1. A simplified block diagram of a pseudo-noise channel
            probe receiver.

We want now to analyze such a detector. We assume an input signal $x(t)$ which
modulates the intermediate frequency. The locally generated signal we shall denote
by $u(t)$. It, too, may be complex and it modulates the same intermediate frequency.
It is periodic with period T_r and, hence, a repetition rate $\nu_r = 1/T_r$. The signal
product then becomes (in the base band) $x(t) u^*(t)$, but, as we recall, only when we
generate both the co-phase and quadrature-phase channels. (We ignore the factor of
one-half that has appeared before, since it can be included in the calibration
analysis that will be eventually necessary.) Finally, we suppose that the low pass
filter has the (real) impulse response $f(t)$. This response vanishes for negative t
and decreases to zero very slowly for positive t. Note that, in reality, we require
two of these filters--one for each of the co-phase and quadrature-phase channels.
Our analysis here requires that these two filters have identical impulse responses.

The output of the detector can be written as

$$y = (xu^*)*f \quad . \tag{A.10}$$

We assume that u is dimensionless and that f has dimensions of reciprocal time;
then y will have the same dimensions (probably volts) as x. We assume further that
f has been normalized so that

$$\int f(t)\ dt = 1 \quad . \tag{A.11}$$

Since u is periodic we can separate the integral into successive intervals of
length T_r and rewrite (A.10) as

101

$$y(t) = \int x(t - \tau) \; u^*(t - \tau) \; f(\tau) \; d\tau$$

$$= \sum_{j=0}^{\infty} \int_{o}^{T_r} x(t - jT_r - \tau) \; u^*(t - \tau) \; f(jT_r + \tau) \; d\tau \quad . \qquad (A.12)$$

One important point to note here is that we will soon be assuming that f varies so slowly that within any interval of length T_r we may say it is almost constant. Thus it will be a good approximation for this last formula to say that in each of the integrals we may simply bring the value of f outside.

In the frequency domain we have

$$Y(\nu) = (X(\nu) * U^*(-\nu)) \; F(\nu)$$

$$= \sum X(\nu + k\nu_r) \; U_k^* \; F(\nu) \quad , \qquad (A.13)$$

where

$$U_k = \frac{1}{T_r} \int_{o}^{T_r} u(t) \; e^{2\pi ikt/T_r} \; dt \quad .$$

Note that U_k and F are dimensionless and that, from (A.11), $F(0) = 1$.

Thus far, we have left the input signal x of an indeterminate nature. This is so we can consider several kinds of signals, both intended and otherwise. First, let us suppose that x is the intended received signal v. Its important characteristic is that it is periodic with period T_r identical to that of the locally generated signal u. From (A.12) and (A.13) we have

$$y(t) = \sum_{j=0}^{\infty} \int_{o}^{T_r} v(t - \tau) \; u^*(t - \tau) \; f(j \; T_r + \tau) \; d\tau \quad , \qquad (A.14)$$

$$Y(\nu) = \sum_{j} \sum_{k} V_{j+k} \; U_k^* \; F(j\nu_r) \; \delta(\nu - j\nu_r) \quad . \qquad (A.15)$$

Clearly, y is also periodic with period T_r. It consists of a dc component, which is just the term in (A.15) corresponding to j=0, and a "ripple" at the frequency ν_r. But the ripple is dominated by the factor $F(\pm\nu_r)$, which will, assuming that the pass band is much less than ν_r, therefore say that the output from the detector is approximately a constant dc value,

$$y = \sum_{k} V_k \; U_k^*$$

$$= \frac{1}{T_r} \int_{o}^{T_r} v(t) \; u^*(t) \; dt \quad . \qquad (A.16)$$

102

This result may also be obtained from (A.14) simply by replacing the function f by its average value during each time interval of length T_r. Note that the final integral here looks very much like the "inner product" on a function space of square integrable functions. If, for any functions $x_1(t)$, $x_2(t)$ whose magnitude squared is integrable on the interval from 0 to T_r, we define

$$(x_1, x_2)_o = \frac{1}{T_r} \int_o^{T_r} x_1(t) \ x_2*(t) \ dt \quad ,$$

then the dc output from the cross-correlator is

$$y = (v, u)_o \quad .$$

Next, let us suppose the input signal x is a noise signal $n(t)$. We assume it is white Gaussian noise whose power spectral density w_N is constant, at least over any bandwidth we shall need to consider. Then the output $y(t)$ is also Gaussian, and, from (A.13), its power spectral density is given by

$$w_Y = w_N \sum |U_k|^2 \ |F(\nu)|^2$$

$$= w_N \ ||u||_o^2 \ |F(\nu)|^2 \quad . \tag{A.17}$$

Its total power is just the integral of this over all ν, and hence equals

$$W_Y = w_N \ ||u||_o^2 \ ||f||^2 \quad . \tag{A.18}$$

If the input signal x combines both the intended received signal v and the additive noise signal n, then, of course, the output consists of a dc component given by (A.16) and a noise signal whose power is given by (A.18). The signal-to-noise ratio is then

$$R_o = |(v, u)_o|^2/(w_N ||u||_o^2 \ ||f||^2) \quad . \tag{A.19}$$

Suppose we were able, somehow, to make the same "measurement" of the input signal using only a single cycle of length T_r. Then, in the presence of noise, the output signal would be

$$y_1 = (v, u)_o + (n, u)_o \quad .$$

As Helstrom (1968, Ch. 2), for example, shows, this is a random variable with mean $(v, u)_o$ and variance $w_N \ \nu_r \ ||u||_o^2$. The resulting signal-to-noise ratio is thus

$$R_1 = |(v, u)_o|^2/(w_N \, \nu_r ||u||_o^2) \quad .$$

Comparing this result with (A.19), we arrive at what might be called the "processing gain" of the cross-correlation detector:

$$R_o/R_1 = \nu_r/||f||^2 \quad . \tag{A.20}$$

To visualize these results better, let us suppose that the low-pass filter is a simple RC circuit. It has the impulse response

$$f(t) = \begin{cases} 0 & t < 0 \\ \dfrac{1}{T_1} \, e^{-t/T_1} & t > 0 \end{cases} , \tag{A.21}$$

where T_1 is the associated "time constant" equal to the "RC constant." We find

$$F(\nu) = \frac{1}{1 - 2\pi i \nu T_1} \quad , \tag{A.22}$$

$$||f||^2 = \frac{1}{2T_1} \quad . \tag{A.23}$$

In the case of a more general filter, we might, indeed, define an "effective time constant" by the formula

$$T_1 = \tfrac{1}{2}(\textstyle\int f(t) \, dt)^2/\int f^2(t) \, dt \quad .$$

In either case, we may use these results to simplify some of the above formulas. For example, the processing gain in (A.20) becomes simply $2\nu_r T_1$.

In the ITS probe, the repetition rate ν_r is approximately 300 kHz, and the time constant used is on the order of 50 µs. Thus the processing gain is approximately 30; i.e., about 15 dB.

The ripple of frequency ν_r, discussed in connection with (A.15), will look very much like an additional noise signal. Its principal component will, relative to the dc component, have an attenuation factor equal to

$$|F(\nu_r)|^2 + |F(-\nu_r)|^2 = 2|F(\nu_r)|^2 \quad .$$

For the ITS probe, and using (A.22), this amounts to an attenuation of about 62 dB.

Untill now, we have spoken of one single complex-valued "measurement," $(v,u)_o$, of the received signal. This, by itself, will not, of course, determine the function v, and we would need to consider a whole set, u_1, u_2, ..., of locally generated signals, each of which would determine a separate measurement. For this set, one thinks, perhaps, of a sequence of orthogonal signals, but simplest and most natural to use is a set of delayed copies of a single signal u. We call this "most natural," because, in practice, we cannot know exactly when v begins a period, and there will already be an ambiguity in the delay between v and u.

Following along with this notion, we would want to consider the set of locally generated signals u(t-s), using the delay time s as a parameter. For each value of s, we would proceed as before and find that the dc component leaving our detector has the value

$$y_o(s) = (v(t), u(t - s))_o$$

$$= \frac{1}{T_r} \int_o^{T_r} v(t) u^*(t - s) dt \quad . \tag{A.24}$$

Note that y_o is periodic in s with period T_r. Note, too, that this formula defines precisely what one would mean by the "cross-correlation function" between v and u.

A second way of formulating this last result is as a convolution integral. If we set

$$u'(t) = u^*(-t) \quad , \tag{A.25}$$

then (A.24) becomes

$$y_o = v * u' \quad . \tag{A.26}$$

But to interpret this formula properly, we must always remember that the independent variable here does not represent actual time but, instead, simply the parameter s.

There remains, now, the question of how to generate the delayed copies of u. We could, for example, consider a sequence s_1, s_2, ... of time delays, each corresponding delayed signal being obtained, perhaps, from a suitable port on a tap delay line. Or, we could use the same sequence in a "time division multiplex" scheme, where we introduce successive stepped delays into the locally generated signal and spend a short interval of time measuring the resulting cross-correlation at each step. Or, finally, we could, as is done in the ITS probe, allow the time delay to increase steadily and continuously. If the increase is slow enough, we can say that we have effectively obtained the whole continuum of time delays.

To say we have, in our locally generated signal, a time delay which is steadily increasing, is to say that we replace the function $u(t)$ with, say, $u_0(t) = u(t-\eta t)$. The time delay is then $s=\eta t$, where η, which might be called the "time scale factor," is presumably very small. This replacement is equivalent to a change in the repetition rate of the signal u. Thus, while we will still say that the received signal v has the repetition rate ν_r, we must now agree that the locally generated signal u_0 has the "slow" repetition rate $(1-\eta)\nu_r$, an alteration which can be straightforwardly implemented in our cross-correlation detector. The consequences can be analyzed in a fashion very similar to that used before. Thus, from (A.13) it will follow that the output, in the frequency domain, has the form

$$Y(\nu) = \sum_k V(\nu + k(1 - \eta)\,\nu_r)\,U_k{}^*\,F(\nu)$$

$$= \sum_j \sum_k V_{j+k}\,U_k{}^*\,F(j\nu_r + k\eta\nu_r)\,\delta(\nu - j\nu_r - k\eta\nu_r) \quad . \qquad (A.27)$$

We must now argue, as before, that, because $F(\nu)$ nearly vanishes for all but small values of ν, it is only the terms with $j=0$ that will add significantly to this sum. But now there is the possibility that $k \sim -j/\eta$, thus destroying the simplicity of this argument. We must therefore make the further assumption that η is so small that when $|k|$ is as large as $1/\eta$, either or both of the terms V_k, U_k have become negligibly small; in other words, we must impose a bandwidth limitation on v and u, and we must suppose that the product of η with this bandwidth is much less than $2\nu_r$.

With this additional assumption, we may proceed as before and say that a very good approximation to the output of the cross-correlation detector is given by

$$Y_0(\nu) = \sum_k V_k\,U_k{}^*\,F(k\eta\nu_r)\,\delta(\nu - k\eta\nu_r)$$

$$= \sum_k V_k\,U_k{}^*\,F(\nu)\,\delta(\nu - k\eta\nu_r) \quad . \qquad (A.28)$$

As expected this no longer represents a constant dc output. Instead, it represents a periodic function $y_0(t)$ with the frequency $\eta\nu_r$ and the period T_r/η. The formula may then be interpreted as the Fourier transform of a convolution,

$$y_0 = v_1 * u_1' * f \quad , \qquad (A.29)$$

of three functions, the first two of which are periodic with the frequency $\eta\nu_r$. The two new functions would be defined by

$$v_1(t) = \sum_k V_k\,e^{-2\pi i k\eta\nu_r t} \qquad (A.30)$$

$$= v(\eta t) \quad ,$$

$$u_1'(t) = u_1^*(-t) \quad ,$$

$$u_1(t) = u(\eta t) \quad .$$

If we artificially scale time back to represent the course of the original input signal, we would set $y_1(t) = y_o(t/\eta)$ and $f_1(t) = f(t/\eta)$, and obtain

$$y_1 = v * u' * f_1 \quad , \tag{A.31}$$

with the first two functions here periodic with period T_r. This, except, perhaps, for the appearance of the filter f_1, is a very satisfactory reproduction of (A.26) and, we recall, a continuously generated measurement of that function.

For the ITS probe, the frequency $\eta \nu_r$ can take on values from 1 to 10 Hz. Since ν_r is approximately 300 kHz, this means that η ranges from $3 \cdot 10^{-6}$ to $3 \cdot 10^{-5}$ and $1/\eta$ from 300,000 to 30,000. Also, U_k and V_k are vanishingly small when $|k|$ is somewhat greater than 500, and therefore the assumption that allowed us to go from (A.27) to (A.28) is certainly satisfied. On the other hand, if we wanted to claim that the final low-pass filter has no extra effect on the measured results-- as displayed, for example, in (A.28)--then we would need to require that F be flat out to $\pm k\eta \nu_r$, where k is, again, the range for which U_k or V_k differ significantly from zero. For the ITS probe this means that F should be flat out to 0.5 kHz or 5 kHz. If we assume that F has the form in (A.22) with T_1 equal to 50 μs, then F gives an attenuation at these limits of 0.1 dB in the first case and 5 dB in the second.

Because it is conceptually simpler, we shall usually use the notation of (A.26) where the independent variable is really just a parameter s representing a certain delay time. It will often be important, however, to replace the locally generated (and represented in reverse time) signal u' with the filtered signal $u'*f_1$.

It may, perhaps, be still unclear as to how (A.26) represents a measurement of the received signal v. In general, we seem to require some further post-processing to rid ourselves of the convolution with u'. Of course, if, as suggested by Lee (1960), we let u be a very sharp pulse, then it is clear that (A.26) is a direct measurement of v. On the other hand, for our present purposes, it is not really the received signal that we are interested in but rather the impulse response h of the transmission channel. Changing our notation slightly, let us suppose we transmit the periodic signal v. Then we receive the periodic signal $v*h$, and the output from the cross-correlation detector becomes, from (A.26),

$$y_o = h*(v * u') \quad . \tag{A.32}$$

Thus, it is the convolution $v*u'$ (or, if you will, $v*u'*f_2$) that we would like to represent a sharp pulse, so that the output becomes a faithful reproduction of the impulse response. One way to do this, of course, is to construct both the transmitted signal v and the locally generated signal u as sharp pulses; but an even better solution (and the one used in any pseudo-noise channel probe) is the one given in the next section.

A.3. Pseudo-Noise Codes

If $n(t)$ is a (real) signal of white Gaussian noise with power spectral density w, then

$$\lim_{T\to\infty} \frac{1}{T} \int_o^T n(t)\ n(t-s)\ dt = w\delta(s) \quad .$$

Thus, if we could use n as both the v and u of (A.32), we would be in a very nice position to measure the impulse response. We can do almost this very thing by utilizing the so-called pseudo-noise codes. This, of course, is what gives the pseudo-noise channel probe its name. In this section we provide a brief discussion of these codes. Further details can be found, for example, in Golomb (1967).

A shift register sequence is an infinite sequence

$$\ldots,\ v_{-1},\ v_o,\ v_1,\ \ldots$$

of +1's and -1's which can be generated in a fairly simple way. One begins with a shift register consisting of, say, m different consecutive bi-static stages each of which can be in either an "on" state or an "off" state. An m-tuple of these states is called a "machine state." To generate the sequence one proceeds in consecutive steps, each of which alters the machine state and determines the next value v_j. First, one combines the states of certain of the stages using the "exclusive or" operation (Boolean addition). Then one shifts all of the states one stage further on, loses the last, or mth, state, and sets the first state equal to the combination we first computed. The value of v then corresponds to the state of the first stage. In the correspondence we shall want to use, if the state is on, the value is +1; if off, it is -1.

Note that just before the jth step, the state of the kth stage corresponds, because of the action of the shift register, to the value of v_{j-k}. Thus the above process is equivalent to a recurrence relation of the form

108

$$v_j = -\Pi_{k \in K}(-v_{j-k}) \quad ,$$

where K is a certain non-empty subset of the integers 1, ..., m. Clearly it is the set K that defines the process. Together with an initial state (say, $v_{-m}, ..., v_{-1}$), it will define a particular shift register sequence.

One thing to note here is that if, at some step, all m stages are in the off state, then the "exclusive or" combination will remain in the off state, and at the next step, and therefore at all steps, all m stages are in the off state. The resulting sequence is therefore identically equal to -1. We call this machine state, with all stages off, the trivial machine state. During the course of a sequence, either it appears at all steps or it never appears.

Since there are only a finite number of possible machine states, they must repeat, and since a given machine state defines the entire sequence, a shift register sequence must always be periodic. Now, there are 2^m possible machine states. If we exclude the trivial state as being inappropriate, there remain $n = 2^m - 1$ possible states. A __maximal length__ shift register sequence is one in which all n states are attained and which therefore has period n. The basic theorem in the subject of these sequences is that for every $m \geq 1$ there do exist subsets K so that the shift register sequence defined by (A.32) is of maximal length. Lists of such subsets may be found in the textbooks devoted to the subject.

The simple statement that all n non-trivial machine states are attained lead to the following properties for maximal length shift register sequences:

(1) For any one period of the sequence, we have

$$\sum_{\ell+1}^{\ell+n} v_j = 1 \quad , \tag{A.33}$$

so that the average of the entire sequence is 1/n.

(2) We may speak of "runs" of +1's or -1's, where the one value is repeated over a series of steps, preceded and followed by the other value. Let us start at the beginning of any such run and consider the next n values. Then for any k, $1 \leq k \leq m-2$, there are exactly $(n+1)/2^{k+2}$ runs of +1's of length k and an equal number of runs of -1's of length k. There is also exactly one run of -1's of length m-1, and exactly one run of +1's of length m.

(3) For any one period of the sequence, we have what is essentially the auto-correlation function

$$\sum_{\ell+1}^{\ell+n} v_j \, v_{j-k} = \begin{cases} n & \text{if } k=0, \text{ or if } k \\ & \text{is any multiple of } n \quad . \\ -1 & \text{otherwise} \end{cases} \qquad (A.34)$$

For example, the first property follows from the fact that there are $(n+1)/2$ non-trivial states with $v_j=+1$ and $(n-1)/2$ non-trivial states with $v_j=-1$.

These three properties come as close as possible for such a periodic function to having the same expected values for a sequence generated by flipping a balanced coin. For this reason the maximal length shift register sequences are also called <u>pseudo-noise</u> <u>sequences</u> or <u>pseudo-noise</u> <u>codes</u>.

Let us choose a particular pseudo-noise code v_j, $j=\ldots, -1, 0, 1, \ldots$. Then we may define the function of time

$$v(t) = v_j \qquad \text{for } j - 1 < t < j \quad , \qquad (A.35)$$
$$j = \ldots -1, 0, 1, \ldots \quad .$$

It has period $n=2^m-1$ and the same properties, suitably restated, as those described above for the pseudo-noise code. In particular, if we define the auto-correlation function

$$r(s) = \frac{1}{n} \int_0^n v(t) \, v(t-s) \, dt \quad , \qquad (A.36)$$

then it will follow from (A.34) that for integer k,

$$r(k) = \begin{cases} 1 & \text{if } k \text{ is a multiple of } n \\ -1/n & \text{otherwise} \quad . \end{cases}$$

And it is not hard to see that, in general, $r(s)$ is a periodic train of triangular pulses with base width 2, base value $-1/n$, and peak value 1. More precisely, we have

$$r(s) = \frac{n+1}{n} p(s) - \frac{1}{n} \quad , \qquad (A.37)$$

where

$$p(s) = \begin{cases} 1 - |s| & \text{for } |s| < 1 \\ 0 & \text{for } 1 < |s| < n/2 \quad , \end{cases}$$

and may be defined elsewhere by periodicity.

Finally, we set

$$u(t) = v(\nu_c t) \quad , \qquad (A.38)$$

110

where ν_c is called the <u>clock frequency</u>. Then u has the <u>bit rate</u> ν_c and is periodic with period $T_r = n/\nu_c$ and repetition rate $\nu_r = \nu_c/n$. Setting $u'(t) = u(-t)$, we would also have

$$(u * u')(s) = \frac{1}{T_r} \int_0^{T_r} u(t) \, u(t-s) \, dt$$

$$= r(\nu_c s) = r_0(s), \text{ say,} \qquad (A.39)$$

which has a pulse width of $2/\nu_c$.

This, then, is the signal a pseudo-noise channel probe uses to replace both the v and u of (A.31). Note that, since the u of (A.38) attains only the values +1 and -1, when it is used to modulate a carrier frequency, the result amounts to bi-phase shift keying. Herein lies one of the advantages of the system. For since the signal amplitudes remain constant, problems related to peak power handling do not occur, either in the transmitter or in the receiver.

The ITS probe employs a nine-stage shift register and hence a code length n = $2^9 - 1 = 511$. The clock rate is set very accurately to 150 MHz, and thus the repetition rate is $\nu_r = 293.542$ kHz. The bit length is 6.67 ns, and the effective pulse length is twice that or 13.33 ns.

If the function u were truly a noise signal, then its Fourier transform would have a constant amplitude and a wildly random phase. In the actual case, since u is periodic, we have

$$U(\nu) = \sum U_k \, \delta(\nu - k\nu_r) \quad .$$

We may determine the amplitudes of U_k very simply from (A.39) and (A.37). We have, first,

$$|U_k|^2 = R_k \quad ,$$

whence, using the notation sinc x to represent the function (sin x)/x, we find

$$U_k = \begin{cases} \dfrac{1}{n} & k = 0 \qquad\qquad (A.40) \\[2ex] e^{i\theta_k} \dfrac{\sqrt{n+1}}{n} \text{ sinc } \dfrac{\pi k}{n} & k \neq 0 \quad , \end{cases}$$

where the θ_k are suitable phase values. The phase and value of U_0 may be simply computed from (A.33). The remaining phases do have some interesting properties, as Golomb (1967, Ch. 4) shows, but, in general, their values vary rapidly and

111

irregularly and depend on the specific one of the allowable maximal length shift register sequences.

To summarize, if we let both the v and u of (A.32) equal the pseudo-noise code u of (A.38), then the output from the cross-correlation detector becomes

$$y_o = h * r_o$$

where r_o represents about as sharp a pulse as one could expect. It is, however, superimposed on a constant "bias" whose magnitude is $1/(n+1)$ times the peak height of the pulse. For most purposes this bias is too small to be of any importance. For some, however, it should probably be taken into account. For example, the value of U_o as given in (A.40) is considerably smaller than values of the adjacent Fourier components. For the ITS probe with n=511 the reduction is 27 dB. Since U_o represents the dc component, this reduction arises because of the bias. A Fourier transform of y_o will show a striking notch at the zero frequency.

Since U_k vanishes at k=±n and is reasonably small for all larger values of $|k|$, it seems proper to call the interval $|k| < n$ the occupied band. This means that the function u occupies the band $|v| < v_c$ and hence has the bandwidth $2v_c$. For the ITS probe this bandwidth is 300 MHz.

Of course, we cannot suppose that any practical equipment will generate the perfect rectangular pulses required in (A.35). Indeed, the designer of such equipment will deliberately introduce extra band-pass filters, not only to reduce noise and interference, but also to separate multiplication components as described in Section A.1. At both the transmitter and receiver there will be a sequence of intended and unintended filters which modify the generated code signals. If f_2 is the effective impulse response of the train of filters at the transmitter and f_3 that at the receiver, then the effective pulse of the channel probe becomes

$$r_1 = r_o * f_4$$

where

$$f_4 = f_1 * f_2 * f_3' \quad ,$$

a formulation that includes the effects of the time-expanded filter f_1 of (A.31). If the combined filter f_4 is suitably broadband, then its effect on r_o is small, and r_1 remains a satisfactorily sharp pulse. The exact effect of f_4 and the real shape of the pulse r_1 can probably be determined only through measurement. Note, in addition, that, since much of the filtering action comes in the modulation and demodulation stages and in the IF and rf stages, the filter f_4 is not necessarily real.

112

Nor is it even "physically realizable" since the inclusion of f_3' implies a reversed time component.

A.4. References

Lee, Y. W. (1960), Statistical Theory of Communication (John Wiley & Sons, New York).

Golomb, S. W. (1967), Shift Register Sequences (Holden-Day, San Francisco).

Helscom, C. W. (1968), Statistical Theory of Signal Detection (Pergamon Press, Oxford).

APPENDIX B.   DETAILS CONCERNING THE MEASUREMENT OF IMPULSE RESPONSES

In this appendix we continue the arguments of Appendix A emphasizing, however, the recorded impulse response and its analysis, and assuming nearly always that it is the ITS channel probe that is being employed. We begin with a list of terminology, notations, and, where meaningful, values associated with the Tennessee measurements.

Code length; $n_p = 2^9 - 1 = 511$.

Clock rate; $\nu_c = 1/T_c = 150$ MHz, very accurately. This is also called the "bit rate." Note that the length of a single bit is $T_c = 6.67$ ns and that the length of the simulated pulse is $2\ T_c = 13.33$ ns.

Repetition rate; $\nu_r = 1/T_r = \nu_c/n_p = 293.542$ kHz; $T_r = 3.407$ μs. This is the rate at which the pseudo-noise code, and hence also the simulated pulse, is repeated. The value T_r is also the maximum delay that is observable before aliasing between successive responses occurs.

Center frequency; ν_o. In Tennessee this took on the three values of 600, 1200, and 1800 MHz, all in the UHF band. Note that ν_o/ν_c is the number of rf cycles in each bit and took on the values of 4, 8, and 12.

Frame rate; $\nu_f = 1/T_f$. This is the rate at which complete impulse responses were measured by the channel probe. The pseudo-noise code in the receiver had the "slow" repetition rate $\nu_r - \nu_f$. The value of ν_f was variable and could equal 1, 2, 5, or 10 Hz. Most often it was 1 Hz, but the body of this report stresses those runs in which it was 10 Hz.

Delay time, recording time. Time can be treated from two very different points of view--that of the actual impulse response and that of the process of measuring it. When it becomes necessary to distinguish the two points of view, we shall use the terms above. Note that delay time is normally measured in microseconds (or nanoseconds) while recording time is measured in seconds (or milliseconds).

Time scale factor; $\eta = \nu_f/\nu_r$. This can be thought of as the ratio between delay time and recording time; it is the factor by which recording time must be scaled to obtain the corresponding delay time. It has the values $3.41 \cdot 10^{-6}$ and $3.41 \cdot 10^{-5}$ when ν_f is 1 and 10 Hz, respectively.

Time constant of the final filter; T_1. This important parameter had a value approximately equal to 50 μs.

Sampling rate; $\nu_s = 1/T_s$. This is the rate at which the response functions were digitized for subsequent recording. Its value was variable, but most often equal

114

to the maximum (full out) rate of 10.671 kHz. Thus T_s usually had a value slightly less than 100 μs. These values, of course, are scaled in recording time. To scale them in delay time, we would multiply by the time scale factor η. Thus, for v_f equal to 1 and 10 Hz, we find ηT_s equal to about 0.32 and 3.2 ns, respectively. A related parameter is the number, $N_c = T_c / \eta T_s$, of samples in each clock interval (bit). In the above cases it takes on values of approximately 20 and 2. Note that the Nyquist criterion says that to achieve an adequate sampling rate we must have at least two samples per bit, so that in the latter case we have just barely sufficient samples.

B.1 Power

We can assume that we transmit a signal $\sqrt{w_o}\, v$, where v is our pseudo-noise code and w_o is the equivalent isotropically radiated power (EIRP). We are being deliberately vague here about the particular characteristic of the signal to be measured and about the units in which to measure it. We should probably be talking about electric field intensity although the formula above seems to refer to voltage across a 1 ohm line. In any case, we assume v is dimensionless and attains the values ±1.

At the receiver the available signal has become $\sqrt{w_o}\, h*v$ where h is the impulse response of the propagation channel. After cross-correlation and filtering, we have the final detected signal

$$y = \sqrt{w_o}\ h*v*u'*f_4 = \sqrt{w_o}\ h*p$$

where p is now the simulated pulse or, more accurately, the simulated stream of pulses.

For many purposes it is most convenient to treat p as though it were a single, unrepeated pulse. Doing that here, the total energy in the received pulse is

$$||y||^2 = w_o\ ||h*p||^2 = w||p||^2 \tag{B.1}$$

where w is a normalized power. If the channel disappears (as when the system is calibrated) so that h(t) becomes δ(t), then w becomes simply w_o. Passing to the frequency domain, we have

$$||y||^2 = ||Y||^2 = w_o||HP||^2 = w||P||^2 \quad ,$$

or

115

$$w = w_o \int |H(\nu)|^2 \ |P(\nu)|^2 d\nu / \int |P(\nu)|^2 d\nu \quad , \tag{B.2}$$

so that w is seen to be a <u>weighted</u> <u>average</u> of the spectral power $w_o |H(\nu)|^2$. Less precisely, it is the average power in the measured band. The weighting is given by $|P(\nu)|^2$, a function that also defines what we mean by the term "measured band." Thus, the power w is an important characteristic of the received signal and will serve very well to define a "locally averaged received signal level"--one that tends to be free of the local variability due to multipath. We note here that if p were a perfect triangular pulse we would have $||p||^2 = (2/3) \ T_c$.

The measurement of "received signal level" is, of course, done largely by measuring the AGC voltage on the IF amplifier. Unfortunately, this does not quite correspond to a measurement of the power w. The signal reaches the IF amplifier before there has been any cross-correlation. We may suppose it takes the approximate form $\sqrt{w_o} \ h*v$, although there will also have been some initial filtering action. The average power, which is what the AGC voltage would measure, is then

$$||\sqrt{w_o} \ h*v||_o^2 = w_o \sum |H(k\nu_r)|^2 \ |V_k|^2 \quad .$$

Assuming that the filters have little effect so that $|V_k|^2 = |P_k|$ and approximating the sum with an integral, we may define a second normalized power

$$w' = w_o \int |H(\nu)|^2 \ |P(\nu)| \ d\nu / \int |P(\nu)| d\nu$$

and say that it is this that the AGC voltage measures. This is a second weighted average of the spectral power; the difference being that here the weight function is $|P(\nu)|$ and not its square. But both weights clearly demarcate the same band of frequencies, and if H is not strikingly different at the edges of that band from what it is at the center, then the two weighted averages ought to be very nearly equal. In this report we assume that this is the case and that the AGC voltage may be assumed to measure a close approximation to the first normalized power w. We note here only that the question is probably worth further study, with some emphasis placed on the effects of interference.

Interference from other radio systems operating within the channel—probe band causes some rather unexpected effects. First, as we describe in more detail in the following section, such interference will most likely be decorrelated by the detector and unobservable in the final output. On the other hand, the energy from interfering signals will be included along with the desired signal as part of the energy in the IF amplifier. Since it is the total energy that the AGC voltage

116

measures, the principal damage caused by interference is to reduce the gain of the IF amplifier and to adulterate the measure of received signal level. The latter problem, however, can be remedied. Since it is really the energy in the impulse response that we want to measure, it seems very natural to measure the apparent energy in the detector output and then to divide by the system gain. Now, the system gain is essentially defined by the AGC voltage; and therefore if we compute the apparent energy in the resonse using a formula analogous to (B.1) in which the integral of the square amplitude is compared to that in a full-scale normal response, we will obtain a correction to apply to the received signal level as implied by the calibrated AGC voltage. Interference, then, will usually reduce the IF amplifier gain and produce a weakened detector output; but this effect can be measured and, aside from practical limitations arising from a reduced precision, it should present no limitations to the final computations.

Note that in the absence of limitations this same scheme can be used to extend considerably the receiver sensitivity. If the signal level drops below the noise power in the IF bandwidth, the AGC voltage will drop to its lowest level and the IF amplifier will perform at maximum gain. The cross-correlation detector, however, will eliminate much of the noise and will still generate an acceptable output signal. Again, by comparing the apparent output energy with that in a full-scale normal response, we may recover most of what appears otherwise to be lost information. We would suppose that such an extension could carry us at least 20 dB beyond the normal limits.

B.2 Noise and Interference

In the presence of additive noise, the received signal can be represented by

$$\sqrt{w_c} \; h*v+n$$

so that the detected signal has mean $\sqrt{w_o} \; h*p$ and, as we see from (A.18) and (A.23), a variance (or noise power)

$$\sigma_N^2 = w_N/2T_1 \; , \tag{B.3}$$

where w_N is the power spectral density of the noise and T_1 is the time constant of the final filter. If the noise is thermal noise at 300 K and if $T_1 = 50$ µs, then

$$w_N = kT = 4.14 \cdot 10^{-21} \; W/Hz$$

$$\sigma_N^2 = 4.14 \cdot 10^{-17} \; W \; ,$$

117

the latter of which reduces to -164 dBW.

On the other hand, we may assume that the IF channel has a noise bandwidth of about 300 MHz. In such a band thermal noise is

$$kTB = 1.24 \cdot 10^{-12} \text{ W}$$

$$\text{or } -119 \text{ dBW} \quad .$$

This is the noise power seen by the IF amplifier. Indeed, it does seem to correspond to the limits of IF amplification in the ITS equipment.

Now let us consider a worst case where the IF amplifier is at full gain, and let us suppose that -119 dBW corresponds to full scale. After detection the noise will be down some 45 dB and so the observed standard deviation will be

$$\sigma_N = 0.006 \text{ of full scale} \quad .$$

The noise should be just barely discernable in the plots we have drawn.

We may go a step further and ask about the appearance of a noise signal after detection. From (A.17) we see that white Gaussian noise in the IF channel becomes, after detection, a colored noise with the power spectral density

$$w_Y(\nu) = w_N |F(\nu)|^2 \quad .$$

This coloring, however, is not very significant. One of our requirements for the filter F was that it be flat to about $\pm n_p \eta \nu_r$, which is just exactly the bandwidth of the probe ($\nu_c = n_p \nu_r$) reduced to recording time. Thus the power spectral density of the output noise should be flat to the limits of the probe.

In another way of looking at the question, we might note that the recording of noise is quite different from the recording of a response function and that the appearance of output noise is more highly dependent on the sampling rate. Recalling that the power spectral density is the Fourier transform of the covariance function $R_N(\tau)$ of the noise and assuming that $F(\nu)$ has the form given in (A.22), we find

$$R_N(\tau) = w_N \Im^{-1}\{|F|^2\} \tag{B.4}$$

$$= \frac{w_N}{2T_1} e^{-|\tau|/T_1} \quad .$$

The correlation function is

$$R_N(\tau)/R_N(0) = e^{-|\tau|/T_1} \quad ,$$

and hence the correlation between two successive samples is

$$\rho = e^{-T_s/T_1} \quad . \tag{B.5}$$

If $T_1 = 50$ μs and $T_s = 100$ μs (the fastest rate used in the ITS program), then

$$\rho = e^{-2} = 0.14 \quad .$$

Note that the function e^{-t/T_1} also describes how a recorded value of a response function depends on previous values because of the action of the final low-pass filter.

It is useful to explore the results when we assume from the beginning that the noise is colored. From (A.13) we find that if w_N is a function of frequency, then

$$w_Y(\nu) = \sum w_N(\nu + \nu_o + k\nu_r) \, |U_k|^2 \, |F(\nu)|^2 \quad . \tag{B.6}$$

It follows that about every 300 kHz we pick up a narrow band of noise with a kind of comb filter, the effective noise bandwidth of each tooth of the comb being $1/2T_1 =$ 10 kHz. If the undetected noise is colored only because of band pass filters in the IF stage, then the above result is the same as the previous result provided only that w_N is constant over the range where the U_k are sensibly large.

A second reason to discuss colored noise is that it may be used to model interference from other radio systems. In this case we imagine that w_N differs from zero only in a sequence of narrow bands. If such a band falls within one of the teeth of the comb filter described above, then the corresponding interference will be apparent in the detected output; otherwise, the interfering signal is "decorrelated" and has no effect on the output. Note also that even if an interfering signal does occupy one of the comb filter teeth it will probably occupy only a single one of those teeth. In that case the single U_k that enters into the computations serves as an additional attenuator. From (A.40) we see that even for small k this additional attenuation will be on the order of 27 dB.

Finally, let us compute the exact shape of the detected output when the probe is subject to cw interference. Let us suppose the interference has the frequency ν_1 so that at base band we may assume it takes the form

$$x(t) = e^{-2\pi i (\nu_1 - \nu_o) t} \quad .$$

From (A.13) the detected output in the frequency domain is

$$Y(\nu) = \sum \delta(\nu-\nu_1+\nu_0+k\nu_r) \; U_k^* \; F(\nu)$$

$$= \delta(\nu-\nu_1+\nu_0+k_1\nu_r) \; U_{k1}^* \; F(\nu)$$

where k_1 is the closest integer to $(\nu_1-\nu_0)/\nu_r$. In the time domain this becomes

$$y(t) = e^{-2\pi i(\nu_1-\nu_0-k_1\nu_r)t} \; U_{k1}^* \; F(\nu_1-\nu_0-k_1\nu_r) \quad . \tag{B.7}$$

Thus, y is negligibly small unless $(\nu_1-\nu_0)/\nu_r$ is very close to an integer value and unless ν_1 is within the probe pass band where the U_k have sensibly large values. If these two conditions are met, y is a complex sinusoid with the shifted frequency $\nu_1-\nu_0-k_1\nu_r$.

B.3   The Pulse Bias

As indicated in Section A.3, the pulse generated by a pseudo-random sequence is not really a simple triangular pulse because it is superimposed on top of a small constant function which we have called the "bias." In functional notation we might write for the actual generated pulse

$$r_0(t) = p_0(t) - \alpha_0$$

where p_0 is a true triangular pulse with zero base and α_0 represents the bias. If we assume that p_0 attains the value 1 at its apex, then $\alpha_0 = 1/(n_p+1) = 1/512$ (for the ITS probe).

The pulse the system sees is a filtered version of r_0. In this regard let us first note that the convolution of a constant function α with the impulse response f of, say, a filter is

$$\alpha * f = \int f(s) \; \alpha ds = \alpha \int f(t) \; dt \quad ,$$

which is again a constant function. Then, applying the system filter f_4 to r_0, we obtain

$$r(t) = p(t) - \alpha$$

where

$$p = p_0 * f_4$$

and

$$\alpha = \alpha_0 * f_4 = \alpha_0 \int f_4(t) \; dt \quad .$$

Thus the actual received signal is

$$y = h * r = h * p - \alpha \int h(t) \, dt \quad . \qquad (B.8)$$

Now, α is a small number and for most purposes there would seem to be little difference between the above formula and the simpler expression $h * p$. The trouble, however, is that while $h * p$ has a finite (small) delay spread such is not the case with the constant. Thus, although locally small, when there is any extended treatment of the recorded response function—when, for example, an integration is performed over a long interval—then this constant is very definitely in evidence.

One solution to the problem is simply to avoid such extended treatments—to always restrict one's study to the interval of time where $h * p$ is sensibly different from zero. This approach requires the ability to locate that interval—to "delimit" the response function; and often that is not an easy task. It is, however, the approach we have taken in the present report.

A second solution might be to try to eliminate the constant through some manipulation of the recorded response. For example, if we simply integrate (B.8) over some interval $(0,T)$, we obtain

$$\int_0^T y(t) \, dt = \int_0^T \int h(s) p(t-s) \, ds \, dt - \alpha T \int h(t) \, dt \quad .$$

Now if the interval $(0,T)$ contains within it the entire range where $h * p$ differs from 0, then the finite integral on the right-hand side can be replaced by an infinite integral, and we find

$$\int_0^T y(t) \, dt = [\int p(t) \, dt - \alpha T] \int h(t) \, dt$$

from which we may determine $\int h(t) \, dt$, and hence the constant term in (B.8). Furthermore, we might note that

$$\int p(t) \, dt = \int p_1(t) \, dt \int f_4(t) \, dt$$

$$= T_c \int f_4(t) \, dt$$

whence

$$\alpha \int h(t) \, dt = \frac{\alpha}{\int p(t) \, dt - \alpha T} \int_o^T y(t) \, dt$$

$$= \frac{\alpha_o}{T_c - \alpha_o T} \int_o^T y(t) \, dt \qquad (B.9)$$

which is easily calculable.

B.4 The Discrete Fourier Transform

Given a finite sequence x_j, $j=0 \ldots n-1$, of complex numbers, the discrete Fourier transform (DFT) is defined by

$$X_k = \sum_o^{n-1} x_j \, e^{2\pi i j k/n}, \quad k = 0 \ldots n - 1 \quad ,$$

thus giving a second finite sequence of complex numbers. The transformation has a convenient inverse given by

$$x_j = \frac{1}{n} \sum_o^{n-1} X_k \, e^{-2\pi i j k/n} \quad .$$

Note that the first summation is actually defined for all integer values of k while the second is defined for all values of j. In both cases one obtains the _periodic_ _extension_ of the two sequences with $X_{k+n} = X_k$ and $x_{j+n} = x_j$.

The reason for introducing the DFT is, of course, to enable us to compute spectral response functions. Suppose we are considering a narrowband representation h(t) of an impulse response function, for which we have a sequence h_j of samples separated by the time interval δt. The spectral response is given by

$$H(\nu) = \int h(t) \, e^{-2\pi i \nu_o t} \, e^{2\pi i \nu t} \, dt$$

which we compute using the quadrature formula

$$H(\nu) = \sum_o^{n-1} h(j\delta t) \, e^{2\pi i (\nu - \nu_o) j \delta t} \, \delta t \quad .$$

As suggested in Section C.1, this quadrature is not only a convenient one, it is much more accurate than might appear. It can be converted to a DFT if we set $\nu = \nu_o + k\delta\nu$ where

$$\delta\nu = 1/(n\delta t) \qquad (B.10)$$

for then we have

122

$$H_k = H(\nu_o + k\delta\nu) = \delta t \sum_o^{n-1} h_j \, e^{2\pi i j k/n} \quad . \tag{B.11}$$

Normally, we would suppose $k=-(n/2), \ldots, 0, \ldots, (n/2)$. The inverse is then straight-forward:

$$h_j = \delta\nu \sum_o^{n-1} H_k e^{-2\pi i j k/n} \quad . \tag{B.12}$$

The three numbers n, δt, and $\delta\nu$ (subject to $n\delta t\delta\nu=1$) are "design parameters" of the process. They must be chosen with due regard to the actual appearance of the functions $h(t)$ and $H(\nu)$. As we have said, the h_j form a sequence of samples of the function $h(t)$; in exactly the same way, the H_k form a sequence of samples of the function $H(\nu)$. We must make certain that there are sufficiently many samples in each case.

But the response is both band limited and time limited; so, reading the sampling theorem in two directions, we have the following two statements:

(1) If the bandwidth of $H(\nu)$ is B, we should sample fast enough so that $\delta t \leq 1/B$.

. (2) If the time length of $h(t)$ is T, we should sample the spectrum with enough resolution so that $\delta\nu \leq 1/T$.

In both cases we should be able to obtain intermediate values of $h(t)$ or $H(\nu)$ using interpolation with the function $\sin x/x$.

For the ITS probe, we have $B=2\nu_c=300$ MHz, and therefore we require $\delta t \leq 3.33$ ns. To put this in terms of recording time, we note that $\delta t=\eta T_s=\eta/\nu_s$, whence we require $\nu_s \geq 2n_p\nu_f$. The sampling rate should be faster than 1022 times the frame rate.

On the other side, we must certainly assume that we have recorded for a long enough time to include the entire response function--in other words that $n\delta t \geq T$. It follows that automatically we have $\delta\nu \leq 1/T$. Note, too, that the total bandwidth we purport to have represented equals $n\delta\nu$. If this is sufficiently wide--i.e., if $n\delta\nu \geq B$--then we automatically have $\delta t \leq 1/B$.

APPENDIX C.   SOME PARTICULAR ALGORITHMS FOR THE ANALYSIS OF
IMPULSE RESPONSES

In this appendix we shall describe in a fairly explicit manner some of the
algorithms we have used to obtain results in the body of this report.

C.1   Quadratures and Interpolation

We use a very simple quadrature formula, writing, for example,

$$\int_0^T f(t)\, dt = \delta t \sum_{j=1}^n f(j\delta t)\ ,$$

where $T = n\delta t$. Although simple, there are two conditions under which this formula is
much more accurate than one might first think: (1) the function f vanishes at and
near the endpoints or (2) the function f is periodic with period T. Note that the
quadratures in which we are interested here will always fall into one of these two
classes. The impulse response, being, as we suppose, time limited, will belong to
the first class since our integrals will be over the entire duration of the func-
tion and, usually, a little bit more. When we speak of spectral properties we use
the DFT and thus find we are treating, perhaps artificially extended, periodic
functions.

The reason the quadrature above is so much more accurate under either of these
conditions is that it may then be classified as a "trapezoidal rule with end cor-
rections" in which the end corrections vanish. Even in the simplest case this
means that our formula is a little better than Simpson's rule, but if we also know
that the integrand is band limited, then it becomes a high order rule indeed.

If we want to interpolate from a sampled sequence of a band limited impulse
response (or a time limited spectral response), then the usual rule is to use the
interpolating function sinc $x = \sin x / x$. In other words, if $f_j = f(j\delta t)$, $j = \ldots -1,\ 0,\ 1,$
..., are the sampled values, then for any t we should be able to write

$$f(t) = \sum f_j\ \text{sinc}(t/\delta t - j)\pi\ .$$

But this is an inconvenient formula and inconvenient for at least two reasons:
(1) it is an infinite summation and (2) each summand requires a nontrivial computa-
tion. We prefer a much simpler approximate interpolation.

First, we should note that the above formula is, in a way, a Lagrangian inter-
polation in which the order has passed to infinity. This, together with a wish for
a local interpolation rule, has inspired the following forumulation.

We suppose we have given us not only the sampled values f_j, but also the first order derivatives f_j'. Then to interpolate in the interval from $j\delta t$ to $(j+1)\delta t$, we use the four values f_j, f_{j+1}, f_j', and f_{j+1}'. These four values provide sufficient information to define uniquely a cubic polynomial having the same values and derivatives, and it is the value of this polynomial at the interpolating point that provides our interpolated value. This is then a local interpolation rule which is sometimes called an Hermition interpolation.

To be explicit, we define the four cubic polynomials

$$p_o(x) = (1-x)^2 (1+2x) = 1 - 3x^2+2x^3 \qquad (C.1)$$

$$p_1(x) = x^2(3-2x) = 3x^2-2x^3$$

$$q_o(x) = (1-x)^2 x = x - 2x^2 + x^3$$

$$q_1(x) = -x^2(1-x) = -x^2 + x^3 \quad ,$$

and then setting

$$x = t/\delta t - j \qquad (C.2)$$

we have

$$\hat{f}(t) = f_j \, p_o(x) + f_{j+1} \, p_1(x) \qquad (C.3)$$
$$+ \delta t \, f_j' \, q_o(x) + \delta t \, f_{j+1}' \, q_1(x) \quad .$$

At the outset, of course, we do not have the derivatives, and they must be found by a separate technique. Here we use the derivative of a symmetric Lagrangian interpolation formula hoping in this way to imitate the sinc x function. As a rather drastic compromise towards program efficiency and convenience, we have used a five-point Langrangian formula and so derive the simple result

$$f_j' = (1/12 \, \delta t)(f_{j-2}-8f_{j-1}+8f_{j+1}-f_{j+2}) \quad . \qquad (C.4)$$

Edge effects for the first and last two elements of a finite sequence should also be considered, but we shall not propose details here.

C.2 Delimiting an Impulse Response

To delimit (truncate or time-clip) an impulse response is to find where it begins and where it ends. We are speaking here of _outer_ limits which contain almost all of the response function. This is a difficult task since there are likely to be small "precursors" that precede what appears to be the main body of the response and innumerable small components that tail off at the end. These very often become indistinguishable from what is more correctly described as noise. The following algorithm is designed to separate the response from the noise. It is probably too costly to use in the field and not robust enough to handle all cases.

We suppose we are given a sequence h_j, $j=1...N_s$, of samples from a complex response function. We first form the sequence

$$P_j = |h_j|^2, \quad j = 1...N_s \quad , \tag{C.5}$$

of square amplitudes, and we shall use only this sequence in what follows.

Let

$$P_x = p_{kx} = \max p_j \quad . \tag{C.6}$$

If $P_x < X_1$ (where $X_1=0.005$ of full scale), we consider the signal to be "too noisy." We call this "error condition number 1" and we do not continue.

Otherwise, we try to estimate the noise level. Set $q_1 = A_1 P_x$ (where $A_1=0.05$), and let

$$P_1 = avg[p_j | p_j \leq q_1] \quad , \tag{C.7}$$

so that P_1 is the average of all those p_j which do not exceed q_1. It is a first estimate of the noise level. If the number of p_j that make up this average is less than $X_2 N_s$ (where $X_2=0.02$), we call this "error condition number 2" and we do not continue. If $P_1 \geq X_3 P_x$ (where $X_3=0.1$), we call this "error condition number 3" and again we do not continue.

Otherwise, set $q_2 = A_2 P_1$ (where $A_2=5$) and let

$$P_n = avg[p_j | p_j \leq q_2] \quad . \tag{C.8}$$

If $P_n \geq X_4 P_x$ (where $X_4=0.1$), we call this "error condition number 4" and we do not continue. Otherwise P_n is our final estimate of the noise level. Note that all four error conditions are designed to protect us from trying to deal with responses that are too noisy. We are essentially requiring that the response maximum be at least 10 dB above the noise.

Next we determine time intervals which locate intervals of signal and intervals of noise. We set $q_3 = A_3 P_n$ (where $A_3 = 3$) and define a sequence of 0's and 1's

$$K_j = \begin{cases} 1 & \text{if } p_j < q_3 \\ 0 & \text{otherwise} \end{cases} \quad , \quad (C.9)$$

for $j = 1, \ldots, N_s$. For completeness we may also suppose $K_j = 1$ for all $j \leq 0$ and all $j > N_s$. Thus we have a doubly infinite sequence which consists of alternating "strings," first of 1's and then of 0's. We speak of "noise strings" and "signal strings." Ideally there will be one signal string flanked on either side by infinitely long noise strings, but in the actual case the signal may become momentarily small as when it passes through zero and there may be large noise "spikes" to be allowed for.

Recall that N_c is the number of samples in each clock interval. We use this value as a scale factor to help determine what a "short interval" is. Note that N_c is not necessarily an integer.

Set $n_1 = \{A_4 N_c\}$ (where $A_4 = 0.7$ and where the braces indicate the nearest integer), and then in the K_j convert every signal string whose length does not exceed n_1 to a noise string. This should eliminate noise spikes.

Now note that $j = k_x$ should definitely be a member of a signal string. With this in mind, set $n_2 = \{A_5 N_c\}$ and $n_3 = \{A_6 N_c\}$ (where $A_5 = 1$ and $A_6 = 3$). Then convert all noise strings to signal strings which are to the left of k_x and whose lengths do not exceed n_2 and also which are to the right of k_x and whose lengths do not exceed n_3.

We should now have a central signal string containing the element at $j = k_x$. We let k_o be the first element of that central string and k_f' the last. Then we set

$$k_o = k_o' + \{N_c\} \quad , \quad (C.10)$$

$$k_f = k_f' \quad ,$$

$$k_1 = k_o - n_3 \quad ,$$

$$k_2 = k_f + n_3 \quad .$$

These numbers are our final output. The value k_o represents the "onset"--the peak of the first component of the response function. The value k_f is the "final" point where the response sinks into the noise. The values k_1 and k_2 are outer limits designed to provide "working space" for further computations. Note that we may have $k_1 \leq 0$ or $k_2 > N_s$. Note also that we have ignored all "signal strings" other

than the central one. This is done deliberately under the assumption that they represent unknown, extraneous effects.

The constants $X_1, \ldots, X_4$ and $A_1, \ldots, A_6$ are judgmental in nature. The values we have indicated are our own present choice, but may be subject to change.

C.3 The Discrete Fourier Transform

As suggested in Section B.4 we obtain spectral responses by using the DFT. For computational purposes, however, we should reformulate the process to make it a _fast_ Fourier transform (FFT).

Now, although there are many forms the FFT takes, for our purposes the fastest and most convenient form occurs when the number n of samples is equal to a power of two--in other words when n takes on the form 2^m for some positive integer m.

Of course, we cannot suppose that the number of recorded samples (or the number of samples we wish to use from a delimited response) is fortuitously a power of two. We must force it into such a structure.

What we have therefore done is to find the smallest integer m so that $2^m \geq n$ and then artificially extended the response function to fill out the larger time interval. Since the response function should have fallen to zero at both its end points, we have simply extended the function with further zeroes.

Unfortunately for the above argument there is the problem of noise and of the "bias" described in Section B.3. The response function will not be exactly zero at its two end points. Then if we simply fill in the remaining part of the interval with zeroes, we shall have small, but sudden, jumps in the extended response function. Since sudden jumps are apt to introduce relatively large amounts of energy near the limits of the spectral response, the introduction of spurious jumps, even if they are small, does not seem desirable.

Therefore, we have chosen to use slight alterations to the extension described above in which the transition from the recorded response function to the t-axis is made smoothly. In most cases we have simply faired in the function using the cubic interpolation of Section C.1. In other cases we have used linear interpolation from the end of the response function to the beginning of the implicitly defined repetition of the function in the following period.

Note that when we increase the number n of samples by extending the response function, we do not change the value of δt. This in turn implies that $\delta \nu$ is decreased but that the total recorded bandwidth $n\delta\nu = 1/\delta t$ is unchanged.

APPENDIX D. THE DIGITAL DATA ACQUISITION SYSTEM

D.1. Introduction

The need has existed for many years for a standard method of recording and documenting measurements of propagation data. With the development of LSI circuitry and small computer systems, it has become not only feasible but cost effective to use computer-controlled measurement systems in field environments.

When the measured data are digitized and recorded on magnetic tape in a standard format, they become easily accessible on various computer systems to researchers that need to utilize propagation information. The system developed here can be upgraded to record data in a standard format so that a wide range of users can access the data and analyze them to extract the specific information for their needs.

The analog techniques used in the past have been slow and costly. Originally the use of strip chart recordings required a huge amount of hand labor to scale the results and analyze the data. In fact, many of these data are currently archived and will probably never be reduced or analyzed. Another drawback of the analog method was the necessity of keeping detailed notes of the experiment so that others could verify the procedures used and reduce the data to engineering terms. The use of the magnetic analog tape recordings was an improvement; however, they are limited in dynamic range and also make it very costly to reduce and analyze the recorded data.

It is believed that the digital methods developed here will alleviate the problems associated with the analog recording schemes and at the same time provide many other advantages such as nearly real-time results in the field and automatic experiment control.

At the start of the planning stage for the Tennessee measurements, it was recognized that an efficient means of digitizing and recording the channel probe data was required. Initially it was planned to make minimal modification of an earlier data acquisition system and then to determine later the requirements for a system to be used in a large measurement program.

Several assumptions were made both about the data to be collected and the operation of the data acquisition system. These assumptions were:

(1) The data to be digitized were analog signals lasting between 0.1 and 1 s.

(2) A trigger was available to initiate the digitizing.

(3) The analog signals were separated into two channels of two components each (called here the x and y or co- and quadrature-phase components).

(4) The operators of the system were to be technical personnel with no particular training in automatic data processing.

(5) The height of the receiving antenna would be recorded automatically.

(6) The date and time of day would be stored with each data record.

D.2. System Structure

After starting the development, it became evident that a more complex set of software was necessary to digitize the data at higher speeds and to provide a range of recording parameters. The interfacing of a distance (height) meter into the system would require additional hardware.

The system that was used was built around an INTEL 80/30 single-board computer. Included in the system were analog-to-digital converters, hardware math capability, digital calendar clock, and a high-speed digital magnetic tape recorder. A block diagram of the system is shown in Figure D.1. In order to achieve the maximum digitization rate (10000 samples per second per channel), a separate converter was used for each channel. A fifth, slower converter was also used in order to digitize the received signal level (RSL) of each receiver after each frame. The communication with the operator was through a 300-baud computer terminal (a TI 723) using a standard ASCII keyboard and thermal printer.

The software was designed to be interactive with the operator and to prompt the operator for the proper responses. A sample of the operator's question and answer input is shown in Figure D.2. The software was also designed to record automatically all of the setup information (equipment settings, site configurations, etc.) on the first record of each digital tape file so that the measured data would be documented on the tape. At the beginning of each frame of data the date and time were recorded, and when the receiving antenna was being lowered, the system would record the antenna height as measured by a distance meter.

Most of the software for the Digital Data Acquisition System is written in FORTRAN with programs designed to allow easy communication with the user through formatted I/O capabilities. The software is designed to be friendly to the user, asking for input data values with English questions, checking responses for legal options, and printing a complete summary of all input data entered. A simple editing capability allows the user to change any of the input data values, either

130
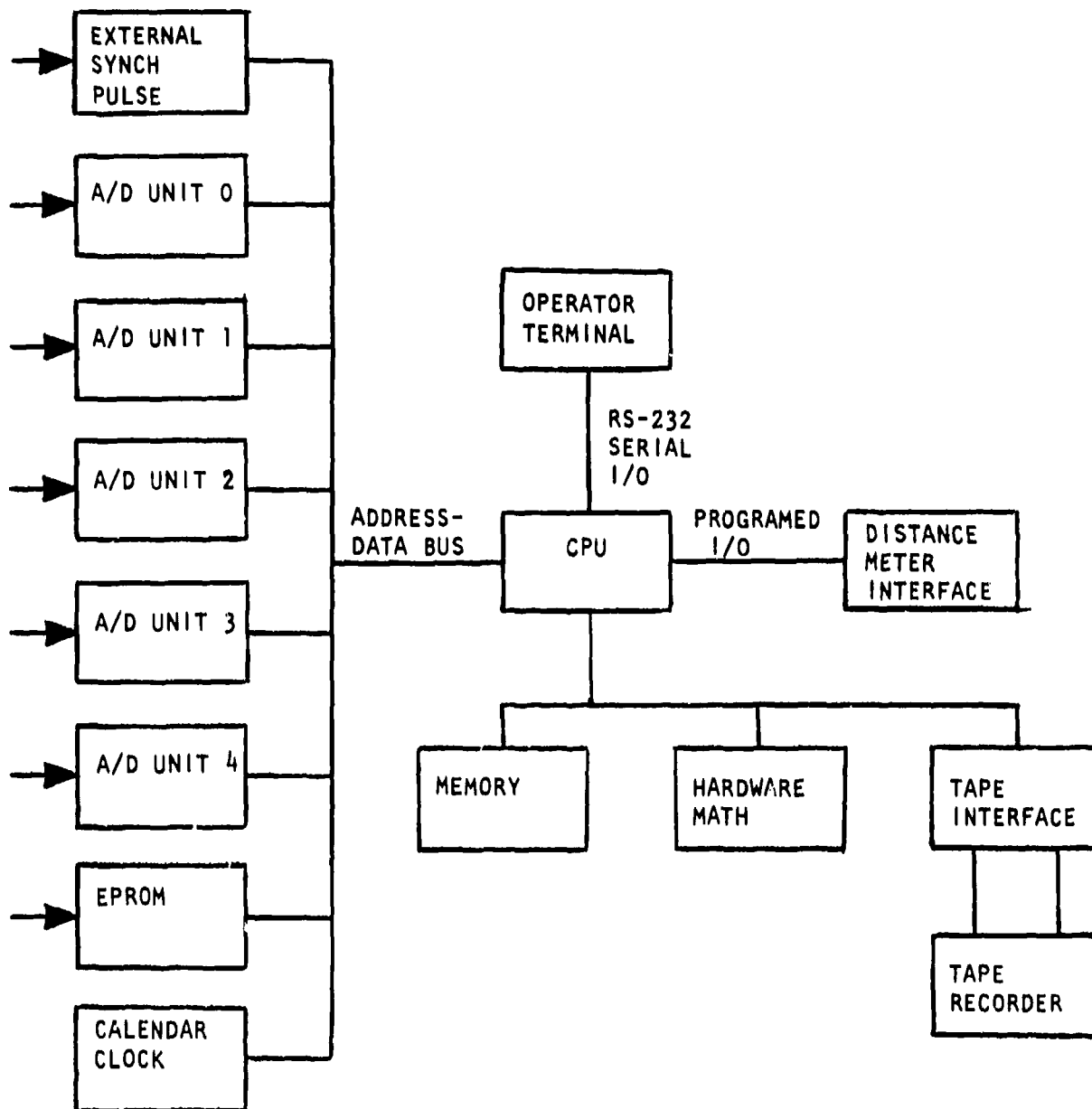
Figure D.1. A block diagram of the Digital Data Acquisition System hardware.

```
DATE:    8/27/79
TIME:    16:20:36
DO YOU WANT TO RESET THE CLOCK (Y/N)?    ?N

1)    ENTER LOCATION (<=20 CHRS):  ?BOULDER
2)    ENTER PATH ID (<=20 CHRS):  ?TEST
3)    ENTER FREQUENCY (MHZ) FOR RECEIVER 1:   ?400.0
4)    ENTER FREQUENCY (MHZ) FOR RECEIVER 2:   ?800
5)    ENTER NUMBER OF FRAMES OF DATA TO BE RECORDED (10-4500):   ?100
6)    ENTER FRAME RATE (1,2,5,10/SEC):   ?10
7)    ENTER SAMPLE RATE (10-10000/SEC):   ?10000
8)    ENTER NUMBER OF SAMPLES/FRAME (10-1000):   ?1000
9)    ENTER NUMBER OF FRAMES TO SKIP BETWEEN SAMPLE SETS (1-100):   ?0
10)   ENTER COMMENTS (1 LINE):  ?TEST
DO YOU WISH TO CHANGE ANY ANSWERS (Y/N)?   ?Y
ENTER QUESTION NO. OR CR WHEN DONE:   ?3
3)    ENTER FREQUENCY (MHZ) FOR RECEIVER 1:   ?600
3)    ENTER FREQUENCY (MHZ) FOR RECEIVER 2:   ?1200
ENTER QUESTION NO. OR CR WHEN DONE:   ?


WBPMS HEADER INPUT DATA SUMMARY:

DATE:    8/27/79
TIME:    16:24:18

1)    LOCATION:  BOULDER
2)    PATH ID:   TEST
3)    FREQUENCY (MHZ) FOR RECEIVER 1:   600.
      FREQUENCY (MHZ) FOR RECEIVER 2:   1200.
4)    NUMBER OF FRAMES OF DATA TO AVERAGE:      10
5)    NUMBER OF FRAMES OF DATA TO BE RECORDED:      100
6)    FRAME RATE:      1
7)    SAMPLE RATE:     1000
8)    NUMBER OF SAMPLES/FRAME:    1000
9)    NUMBER OF FRAMES TO SKIP BETWEEN SAMPLE SETS:      0
10)   COMMENTS:  TEST
```

Figure D.2.   Sample question/answer input.

initially or between measurement sessions. All input data is recorded on 9-track magnetic tape for later use in processing the measurement data. The measurements themselves are read from A-D converters by assembly language routines, written to maximize the sample rate. The measured values are then written to a tape as 16 bit integers. To convert RSL integers to input signal level, it is necessary to have calibrated each channel with a known source. The software allows the user to enter calibration values for four receiver/channel combinations on two A-D ports. The actual signal level is entered by the user, and the software inputs the corresponding integer from the A-D converter. These calibration data are written to the tape to be used in processing the data. The system also uses these data to print statistics for the measured data. The tape format is described in Figure D.3, and the record structures are given in Table D.1.

D.3. Operational Experience

The system was operated in the field for about 3 weeks. There were no hardware or software failures during that time. However, the operator of the system was an Army engineer very familiar with computer systems, and consequently the system was not tested using nontechnical operators. However, the Army engineer was able to provide some excellent suggestions for the design of a new system that would provide a great deal more flexibility in operation. These are detailed in Section D.4.

Due to the press for a wide variety of different measurements of the propagation channel, the test procedures in these field tests suffered a considerable number of ad hoc and sudden changes. This was not the operating climate for which the digital data acquisition system had been planned. While the recording system continued to request documentation, the measurement parameters (such as antenna polarization, path length, etc.) were changing faster than the operator could respond. The field "fix" was then to document the data with three sets of notes: one on the digital tape as originally planned, one set written on paper, and one set verbally on analog tape. Another expedient used in the field was physically to place EOT markers in the middle of the digital tape! These field practices have resulted in a good deal of additional labor in recovering the data from the digital tapes. For a fixed measurement program with nontechnical operators the system design would, we feel, have been quite appropriate and would not have required such field fixes.

133
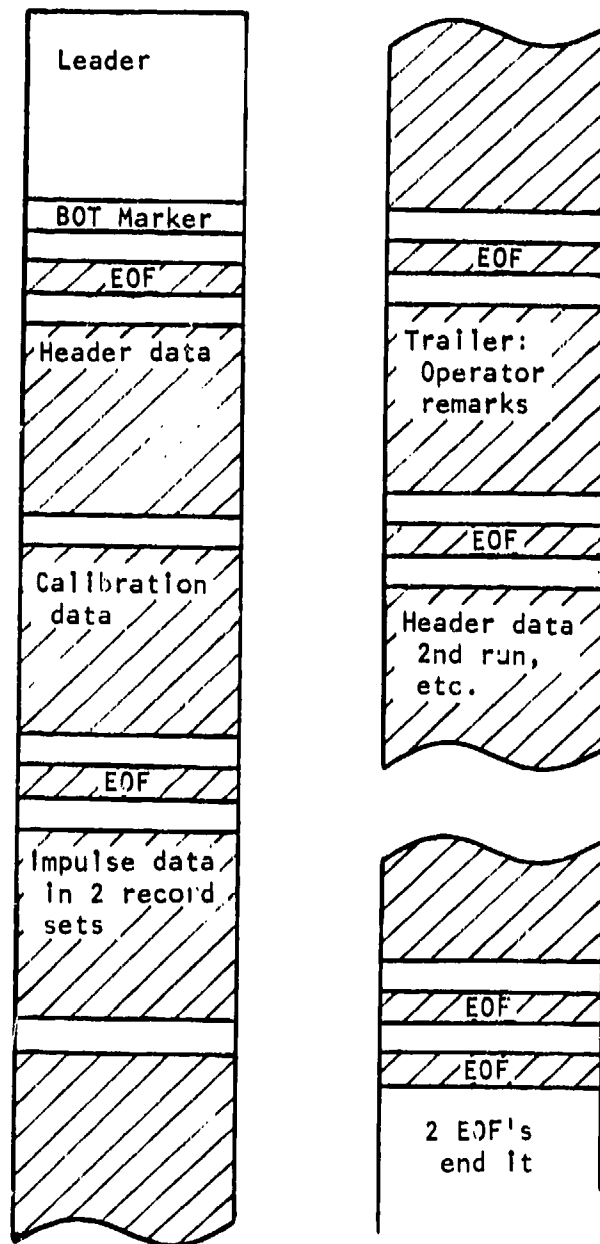
Figure D.3. Digital tape organization.

Table D.1. Record Format

	Header Record	
Byte	Format	Content
0	A20	location
20	A20	identification
40	A10	frequency 1
50	A10	frequency 2
60	A10	NAVG - number of frames to average
70	A10	NFR - number of frames to record
80	A10	FR - frame rate
90	A10	SR - sample rate
100	A10	NS - number of samples
110	A10	NSK - number of frames to skip
120	A60	comments
180	F4	frequency 1
184	F4	frequency 2
188	I1	NAVG - number of frames to average
189	I4	NFR - number of frames to record
193	I2	FR - frame rate
195	I2	SR - sample rate
197	I2	NS - number of samples
199	I4	NSK - number of frames to skip
203	3I1	year/month/day
206	3I1	hour/minute/second
209	---	

	Calibration Record	
0	I2	A-D, R1, level 1
2	I2	A-D, R2, level 1
4	I2	A-D, R3, level 1
6	I2	A-D, R1, level 2
8	I2	A-D, R2, level 2
10	I2	A-D, R3, level 2
12	I2	A-D, R1, level 3
.	.	.
.	.	.
.	.	.
.	.	.
298	I2	A-D, R3, level 50
300	F4	value, R1, level 1
304	F4	value, R2, level 1
308	F4	value, R3, level 1
312	F4	value, R1, level 2
.	.	.
.	.	.
.	.	.
.	.	.

135

Calibration Record (continued)		
Byte	Format	Content
896	F4	value, R3, level 50
900	I2	NLV1, no. levels, R1
902	I2	NLV2, no. levels, R2
904	I2	NLV3, no. levels, R3
906	end of record	

Data Record - Two Physical Records		
Byte	Format	Content
0	I2	R1, x, sample 1
2	I2	R1, y, sample 1
4	I2	R2, x, sample 1
6	I2	R2, y, sample 1
8	I2	R1, x, sample 2
.	.	.
.	.	.
.	.	.
.	.	.
8N-2	I2	R2, y, sample N
8N	I2	AGC, R1
8N+2	I2	AGC, R2
.	.	.
.	.	.
.	.	.
.	.	.
8004	3I1	year/month/day
8007	3I1	hour/minute/second
8010	14BCD	distance meter
8024	end of record	
.	.	.
.	.	.
.	.	.
8192	end of file	

Trailer Record		
Byte	Format	Content
0	A1	yes or no/Y,N
1	10A80	comments - may be empty
801	end of record	

136

D.4. Recommendations for a Next-Generation System

The Digital Data Acquisition System as described above and as implemented for the Tennessee measurement program was meant to be an experimental system in which ideas and techniques were to be tested and shortcomings discovered. As a result of the operational experience obtained in Tennessee, the following recommendations are provided:

Some of the channel probe parameters, such as the receiver frequencies and the frame rate, had to be transferred manually to the computer system. This should be changed. The computer system needs to be coupled directly into the channel probe so that either the operator controls the test setup with the computer system or so that all parameters are delivered to the system and automatically recorded.

Additional nonvolatile memory should be installed to allow larger programs, faster data storage, and continuity of test setups even when power failures occur. Bubble memory devices would be one solution.

Digitization of the data should be handled by a separate processor. An upgrade of the A-D boards used is now available that does have a separate processor. This allows faster digitization and would free memory and time for the main processor.

From the point of view of the operator, the mandatory sequence of questions and answers has a definite advantage when the operator is unskilled or simply unfamiliar with the system. It has the disadvantage of being rather inflexible. If the operator is familiar with adp equipment and can be given training for this particular system, then it would perhaps be better to restructure the system for greater flexibility. The following is a suggestion for such a restructured system.

Generally speaking, in the suggested system the operator initiates one of several commands in response to a computer initiated prompt character. There is an executive level from which one passes to one of several directive levels from which, in turn, one may pass to one of several procedures. Different prompt characters are used in the executive and directive levels.

General rules applicable at any level are: All commands are terminated with $\langle CR \rangle$. Only enough of the command to make it uniquely identifiable need be typed. There should be some method for backspacing over errors. At any level and at any time (even during a processing period) a typed Q (quit) will release the processor from a command and send the system back to the executive level; a typed K will kill the program and send the system to the monitor.

137

DIRECTIVES	MEANING OR ACTION
CALIBRATE	will go to calibration routine.
HEADER	will go to header routine.
RECORD	will begin taking data.
TAPE	allows manipulation of magnetic tape.
TYPE	will type statistics.

DIRECTIVE: CALIBRATE

COMMAND	MEANING OR ACTION
TAPE	will read calibration into processor from magnetic tape.
MANUAL	will prompt operator through calibration routine.
SPOT CHECK	will allow operator to spot check calibration data.
REC. I, NN00	will recalibrate only RECEIVER I at frequency NN00.

DIRECTIVE: HEADER

COMMAND	MEANING OR ACTION
EXAMINE	prints the entire header.
CHANGE - ALL - #NN	 prints prompting for header. prints question #NN and a dash; then input new value, $\langle CR \rangle$.

DIRECTIVE: TYPE, NN

COMMAND	MEANING OR ACTION
ALL	types out all frames of run NN.
II TO END	will type out frames II to end or record.
II TO JJ	will type out frames II to JJ.

DIRECTIVE: RECORD

COMMAND	MEANING OR ACTION
G (GO)	begin taking data.
S (SUSPEND)	cease takir.y data; to resume, G is pressed.
Q	end run prematurely, go back to executive level.
COMMENTS	will insert comments (up to 10 lines) to the end of the current run. COMMENTS can be invoked while taking data.
RATE	prints: sa. >le rate, frame rate, number of frames recorded, number of frames skipped, samples per frame; after each variable a dash is printed; to change that variable, enter new value; to continue through subroutine, hit CR .

DIRECTIVE: TAPE

COMMAND	MEANING OR ACTION
NEW	allows mounting of new tape.
NEW & REWRITE CAL	rewrites calibration to beginning of new tape after executing the above routine.
SKIP END	skips forward to double EOF.
SKIP FWD NN	skips NN files forward.
SKIP BACK NN	skips NN files backward.
REWIND	rewinds magnetic tape to beginning.

APPENDIX E.   SUMMARY OF RECORDED DATA

In the following pages we provide a summary of the digitally recorded data now available to us. Generally speaking, the data were recorded in a sequence of <u>runs</u> each of which corresponded to a particular arrangement of the experimental parameters. In Table E.1, the sequence number of each run is given in the first column. The time of day at which the run began is given in column two. Except for the first two days, the time indicated is Central Daylight Time; the early days used Standard Time.

In column three is a brief indication of the path location using the notation and the place names of Section 3. The next column gives the frequencies of the two receiving channels. Then come two columns that describe the frames of the run; these are the basic entities measured, each of them corresponding to a single measured impulse response. In column five are given two values: the frame rate ν_f and then the sampling rate ν_s. Both of these quantities are defined in Appendix B. The number of frames recorded for the entire run is given in column six. In columns seven, eight, and nine are given the distance between the two terminals, the height of the transmitting antenna above ground, and the height of the receiving antenna above ground. Finally, the last column provides miscellaneous comments. Unless otherwise indicated in these comments, the two antennas were motionless during the run and were vertically polarized.

Table E.1. Summary of Recorded Data

Tape #1 11 Oct, Camp Forrest--Test Runs

Run	Time	Location	f_1, f_2 (GHz)	fr/smpl rate	No. Frames	Dist (m)	h_T (m)	h_R (m)	Comments
001	1402	Calibration	-,1.2	10/10671	10				Freq in doubt
002	1413	Calibration	-,1.2	10/10671	10				Freq in doubt
003	1440	Calibration	-,1.2	10/10671	10				Freq in doubt
004	1502	- to S1	.6,1.2	10/10671	10		1.8	23.2	
005	1514	26&B to S1	.6,1.2	10/10671	10	535	1.8	23.2	
006	1519	23&B to S1	.6,1.2	10/10671	10	965	1.8	23.2	
007	1530	29&B to S1	.6,1.2	10/10671	10	162	1.8	23.2	
008	1546	29&B to S1	.6,1.2	10/10671	100	162	1.8	23.2	
009	1617	- to S1	.6,1.2	1/10671	303		1.8	23.2	Tx moving
010	1635			1/10671	2				Run aborted
011	1640	29 to S1	.6,1.2	1/10671	191	146	1.8	23.2	Tx moving
012	1649	29 to S1	.6,1.2	1/10671	233	146	1.8	23.2	Tx moving
013	1710	29 to S1	.6,1.8	1/10671	197	146	1.8	4.9	Tx moving
014	1718	29 to S1	.6,1.2	1/10671	190	146	1.8	4.9	Tx moving
015	1727			1/10671	2				Run aborted

141

Table E.1.   Summary of Recorded Data
(continued)

Run	Time	Location	f_1,f_2 (GHz)	fr/smpl rate	No. Frames	Dist (m)	h_T (m)	h_R (m)	Comments
Tape #2 12 Oct, Camp Forrest--Path Loss Study									
001	1307	29&B to S1	.6,1.2	1/10671	67	162	1.8	21.0	
002	1338	29&B to S1	.6,1.2	1/10671	10	162	1.8	4.9	
003	1347	28&B to S1	.6,1.2	1/10671	10	294	1.8	21.0	
004	1356	28&B to S1	.6,1.2	1/10671	10	294	1.8	4.9	
005	1408	30&B to S1	.6,1.2	1/10671	10	70	1.8	21.0	
006	1420	28&B to S1	.6,1.2	1/10671	10	294	1.8	21.0	
007	1428	27&B to S1	.6,1.2	1/10671	10	438	1.8	21.0	
008	1437	27 to S1	.6,1.2	1/10671	10	432	1.8	21.0	
009	1446	27 to S1	.6,1.2	1/10671	10	432	1.8	4.9	
010	1457	27&B to S1	.6,1.2	1/10671	10	438	1.8	21.0	
011	1520	B to 30&B	.6,1.2	1/10671	1015	~1000	1.8	4.9	Tx moving

Table E.1. Summary of Recorded Data
(continued)

Run	Time	Location	f_1,f_2 (GHz)	fr/smpl rate	No. Frames	Dist (m)	h_T (m)	h_R (m)	Comments
		Tape #3 16 Oct, Camp Forrest--Polarization Studies							
001	0922	Calibration	-,1.2	1/10671	3				Freq in doubt
002	0956	25&A to 26&B	.6,1.8	1/10671	1000	~139	1.8	4.9	Tx, Rx moving, polarization varied
003	1021	25&A to 26&B	.6,1.8	1/10671	747	~139	1.8	4.9	Tx, Rx moving, polarization varied
004	1035	25&A to B	.6,1.8	1/10671	1000	~139	1.8	4.9	Tx, Rx moving, polarization varied
005	1114			1/10671	0				Run aborted
		Tape #4 16 Oct, Continuation							
001	1119	15 to 14	.6,1.8	1/10671	1000	~146	1.8	4.9	Tx, Rx moving, polarization varied
002	1150	15 to 14	.6,1.8	1/10671	1000	~146	1.8	4.9	Tx, Rx moving, polarization varied
003	1208	15 to 14	.6,1.8	1/10671	81	~146	1.8	4.9	Tx, Rx moving, polarization varied
		Tape #5 16 Oct, Continuation							
001	1412	17 to 18	.6,1.8	1/10671	1000	~146	1.8	4.9	Tx, Rx moving, polarization varied
002	1444	17 to 18	.6,1.8	1/10671	1000	~146	1.8	4.9	Tx, Rx moving, polarization varied
003	1509	17 to 18	.6,1.8	1/10671	1000	~146	1.8	4.9	Tx, Rx moving, polarization varied
004	1530	17 to 18	.6,1.2	1/10671	917	~146	1.8	4.9	Tx, Rx moving, polarization varied
005	1602	27&B to S1	.6,1.2	1/10671	661	441	1.8	4.9	Tx moving, polarization varied

143

Table E.1. Summary of Recorded Data
(continued)

Run	Time	Location	f_1, f_2 (GHz)	fr/smpl rate	No. Frames	Dist (m)	h_T (m)	h_R (m)	Comments
Tape #6 17 Oct, Camp Forrest--High Antennas									
001	1211	T1 to S1	.6,1.8	1/10671	526	1176	20.6	~28	Tx LPA Ant Rx limited height gain
Tape #7 17 Oct, Continuation									
001	1443	T1 to S1	.6,1.8	1/10671	1321	1176		~28	Tx LPA Ant
Tape #8 17 Oct, Continuation									
001	1529	T1 to S1	.6,1.8	1/10671	420	1176	16.5	~28	Tx LPA Ant
002	1552	T1 to S1	.6,1.8	1/10671	137	1176	8.2	~28	Tx LPA Ant
003	1606	T1 to S1	.6,1.2	1/10671	695	1176	8.2	~28	Tx LPA Ant

144

Table E.1. Summary of Recorded Data
(continued)

Run	Time	Location	f_1, f_2 (GHz)	fr/smpl rate	No. Frames	Dist (m)	h_T (m)	h_R (m)	Comments
Tape #9 18 Oct, AEDC--Long Term Run									
001	1548	T2 to S6	.3,1.2	1/10671	3492	197	20.6	4.9	Sample every 12 s Tx LPA Ant, polarization varied
Tape #10 19 Oct, Continuation									
001	0105	T2 to S6	.6,1.2	1/10671	11	197	20.6	4.9	
002	0114	T2 to S6		1/10671	3499	197	20.6	4.9	Sample every 12 s Freq's, polarization varied
003	1010			1/10671	1				Run aborted
004	1020	T2 to S6	1.2,1.8	1/10671	557	197	20.6	4.9	Sample every 12 s Polarization varied
Tape #11 19 Oct, Camp Forrest--Studies of Forest Types									
001	1418	6 to 5	.6,1.8	1/10671	500		1.8	4.9	Tx, Rx moving
002	1445	6 to 5	.6,1.8	1/10671	1000		1.8	4.9	Tx, Rx moving, polarization varied
003	1508	6 to 5	.6,1.8	10/8775	815		1.8	4.9	Tx, Rx moving, polarization varied
004	1555			10/8775	0				Run aborted; end of tape
005	1610	3 to 4	.6,1.8	1/8775	208		1.8	4.9	Polarization varied

Table E.1. Summary of Recorded Data
(continued)

Run	Time	Location	f_1,f_2 (GHz)	fr/smpl rate	No. Frames	Dist (m)	h_T (m)	h_R (m)	Comments
		Tape #12 20 Oct, Normandy Lake							
001	1050	Calibration		1/10671	2				
002	1145	D to A	.6,1.8	1/10671	100	1939	1.8	4.9	
003	1153	D to A	.6,1.8	1/10671	368	1939	1.8	4.9	
004	1201	D to A	.6,1.2	1/10671	500	1939	1.8	4.9	
005	1211	D to A	1.2,1.8	1/10671	480	1939	1.8	4.9	
006	1222	D to A	1.2,1.8	1/10671	360	1939	1.8	4.9	H pol
007	1231	D to A	.6,1.2	1/10671	420	1939	1.8	4.9	H pol
C08	1243	D to A	.6,1.8	1/10671	420	1939	1.8	4.9	H pol
009	1310			1/10671	3				Run aborted
010	1313	C to A	.6,1.2	1/10671	323	1706	1.8	4.9	
011	1323	C to A	.6,1.8	1/3334	300	1706	1.8	4.9	
012	1329			1/3334	1				Run aborted
013	1330	C to A	1.2,1.8	1/3334	300	1706	1.8	4.9	
014	1349	B to A	.6,1.2	1/3334	300	1474	1.8	4.9	
015	1356	B to A	.6,1.8	1/3334	300	1474	1.8	4.9	

Table E.1. Summary of Recorded Data
(continued)

Run	Time	Location	f_1,f_2 (GHz)	fr/smpl rate	No. Frames	Dist (m)	h_T (m)	h_R (m)	Comments
Tape #13 20 Oct, Normandy Lake									
001	1409	B to A	1.2,1.8	1/3334	300	1474	1.8	4.9	
002	1429	B to F	.6,1.2	1/3334	300	2088	1.8	4.9	
003	1446	B to F	.6,1.8	1/3334	300	2088	1.8	4.9	
004	1453	B to F	1.2,1.8	1/3334	300	2088	1.8	4.9	
005	1513	B to F	1.2,1.8	1/3334	243	2088	1.8	4.9	H pol
006	1518	B to F	.6,1.2	1/3334	300	2088	1.8	4.9	H pol
007	1532	B to F	.6,1.2	1/3334	300	2088	1.8	4.9	
008	1540	C to F	.6,1.8	1/3334	300	2266	1.8	4.9	
009	1547	C to F	1.2,1.8	1/3334	300	2266	1.8	4.9	
010	1555	C to F	.6,1.2	1/3334	300	2266	1.8	4.9	H pol
011	1606	D to F	.6,1.2	1/3334	300	2465	1.8	4.9	
012	1615	D to F	.6,1.8	1/3334	300	2465	1.8	4.9	
013	1622	D to F	1.2,1.8	1/3334	300	2465	1.8	4.9	
014	1632	D' to F	.6,1.8	1/3334	300	2470	1.8	4.9	
015	1640			1/3334	4				Run aborted
016	1644	D' to F	.6,1.2	1/3334	115	2470	1.8	4.9	H pol

147

Table E.1. Summary of Recorded Data
(continued)

Run	Time	Location	f_1,f_2 (GHz)	fr/smpl rate	No. Frames	Dist (m)	h_T (m)	h_R (m)	Comments
		Tape #14 21 Oct, Across Normandy Lake and Negro Hill							
001	0953	Calibration		1/500	1				
002	1029	D' to F	.6,1.2	1/10671	300	2470	1.8	4.9	
003	1038	D' to F	.6,1.8	1/10671	300	2470	1.8	4.9	
004	1048	D' to F	.6,1.8	1/10671	300	2470	1.8	4.9	H pol
005	1056	D' to F/K	.6,1.8	1/10671	300	~2700	1.8	4.9	H pol, Rx moving
006	1111	D' to K	.6,1.2	1/10671	300	2895	1.8	4.9	H pol
007	1118	D' to K	1.2,1.8	1/10671	300	2895	1.8	4.9	
008	1127	D' to K	.6,1.2	1/10671	300	2895	1.8	4.9	
009	1134	D' to K	.6,1.8	1/10671	300	2895	1.8	4.9	
010	1143	D' to K	1.2,1.8	1/10671	300	2895	1.8	4.9	
011	1154	D' to K/G	.6,1.8	1/10671	300	~3100	1.8	4.9	Rx moving
012	1226	D' to G	.6,1.2	1/1007	10	3415	1.8	4.9	H pol. This run begins a sampling study.
013	1229	D' to G	.6,1.2	1/1007	10	3415	1.8	4.9	H pol
014	1233	D' to G	.6,1.2	1/2014	10	3415	1.8	4.9	H pol
015	1236	D' to G	.6,1.2	1/4025	10	3415	1.8	4.9	H pol

Table E.1. Summary of Recorded Data
(continued)

Tape #14 (continued) 21 Oct, Normandy Lake--Sampling Study

Run	Time	Location	f_1, f_2 (GHz)	fr/smpl rate	No. Frames	Dist (m)	h_T (m)	h_R (m)	Comments
016	1239	D' to G	.6,1.2	5/4025	10	3415	1.8	4.9	H pol
017	1242	D' to G	.6,1.2	5/10671	10	3415	1.8	4.9	H pol
018	1244	D' to G	.6,1.2	10/10671	10	3415	1.8	4.9	H pol
019	1249	D' to G	.6,1.2	1/1007	10	3415	1.8	4.9	
020	1254	D' to G	.6,1.2	1/1007	10	3415	1.8	4.9	
021	1256	D' to G	.6,1.2	1/2014	10	3415	1.8	4.9	
022	1259	D' to G	.6,1.2	1/4025	10	3415	1.8	4.9	
023	1301	D' to G	.6,1.2	5/4025	10	3415	1.8	4.9	
024	1305	D' to G	.6,1.2	5/10671	10	3415	1.8	4.9	
025	1307	D' to G	.6,1.2	10/10671	10	3415	1.8	4.9	
026	1308			10/10671	1				Run aborted
027	1420			10/10671	1				Run aborted

149

Table E.1. Summary of Recorded Data
(continued)

Run	Time	Location	f_1,f_2 (GHz)	fr/smpl rate	No. Frames	Dist (m)	h_T (m)	h_R (m)	Comments
		Tape #15 21 Oct, Normandy Lake							
001	1508	E to A	.6,1.2	1/3334	300	1590	1.8	4.9	
002	1531	E to A	.6,1.8	1/3334	300	1590	2.4	4.9	Tx LPA Ant
003	1538	E to A	1.2,1.8	1/3334	300	1590	2.4	4.9	Tx LPA Ant
004	1546	E to A	.6,1.2	1/3334	300	1590	2.4	4.9	Tx LPA Ant, H pol
005	1553	E to A	.6,1.8	1/3334	300	1590	2.4	4.9	Tx LPA Ant, H pol
006	1559	E to A	1.2,1.8	1/3334	300	1590	2.4	4.9	Tx LPA Ant, H pol
007	1629	E to F	.6,1.2	1/3334	300	1125	2.4	4.9	Tx LPA Ant
008	1636	E to F	.6,1.2	1/3334	300	1125	2.4	4.9	Tx LPA Ant, H pol
009	1649			1/3334	2				Run aborted
010	1706	E to G	.6,1.2	10/8775	300	1345	2.4	4.9	Tx LPA Ant, sampling averages attempted

Table E.1. Summary of Recorded Data
(continued)

Run	Time	Location	f_1, f_2 (GHz)	fr/smpl rate	No. Frames	Dist (m)	h_T (m)	h_R (m)	Comments
		Tape #16 23 Oct, Normandy Lake--Long Path							
001	1053	L to B	.6,1.2	1/3334	300	5020	2.4	4.9	Tx LPA Ant
002	1141			1/3334	11				Run aborted
003	1142	L to B	.6,1.2	1/3334	300	5020	2.4	4.9	Tx LPA Ant, H pol
004	1156	L to B	.6,1.2	1/3334	300	5020	2.4	4.9	Tx LPA Ant, H pol
005	1204	L to B	.6,1.2	1/3334	300	5020	2.4	4.9	Tx LPA Ant
006	1227	L to B	.6,1.2	1/3334	300	5020	1.8	4.9	Tx moving
007	1450	Calibration		1/3334	7				
008	1610	Meadow Hill	.6,1.2	1/3334	300		1.8	4.9	Tx moving
009	1616	Meadow Hill	.6,1.2	1/3334	300		1.8	4.9	Tx moving

151

Table E.1. Summary of Recorded Data
(continued)

Run	Time	Location	f_1, f_2 (GHz)	fr/smpl rate	No. Frames	Dist (m)	h_T (m)	h_R (m)	Comments
Tape #17 24 Oct, AEDC--Across Sparse Trees									
001	0939	AEDC Park	.6,1.2	1/3334	300	640	1.8	4.9	
002	1007		1.2,1.8	1/3334	300	640	1.8	4.9	
003	1018		.6,1.2	1/3334	300	640	1.8	4.9	H pol
004	1028		1.2,1.8	1/3334	300	640	1.8	4.9	H pol
005	1102		.6,1.2	1/3334	300	310	1.8	4.9	
006	1110		1.2,1.8	1/3334	300	310	1.8	4.9	
007	1119		.6,1.2	1/3334	300	310	1.8	4.9	H pol
008	1126			1/3334	2				Run aborted
009	1128		1.2,1.8	1/3334	300	310	1.8	4.9	H pol
010	1135		1.2,1.8	1/3334	227		1.8	4.9	Tx moving, H pol
011	1146		1.2,1.8	1/3334	41		1.8	4.9	Tx moving

Table E.1. Summary of Recorded Data
(continued)

Run	Time	Location	f_1,f_2 (GHz)	fr/smpl rate	No. Frames	Dist (m)	h_T (m)	h_R (m)	Comments
Tape #18 25 Oct, Camp Forrest Fire Tower--Height Gain Study									
001	0943	20&A to T1	.6,1.2	1/3334	180	283	1.8	19.8	
002	1025	20&A to T1	1.2,1.8	1/3334	180	283	1.8	19.8	
003	1031	20&A to T1	.6,1.2	1/3334	180	283	1.8	19.8	H pol
004	1036	20&A to T1	1.2,1.8	1/3334	180	283	1.8	19.8	H pol
005	1041	20&A to T1	.6,1.2	1/3334	180	283	1.8	17.1	
006	1100			1/3334	1				Run aborted
007	1102	20&A to T1	1.2,1.8	1/3334	180	283	1.8	17.1	
008	1107	20&A to T1	.6,1.2	1/3334	180	283	1.8	17.1	H pol
009	1112	20&A to T1	1.2,1.8	1/3334	180	283	1.8	17.1	H pol
010	1117	20&A to T1	.6,1.2	1/3334	180	283	1.8	13.6	
011	1132	20&A to T1	1.2,1.8	1/3334	180	283	1.8	13.6	
012	1137	20&A to T1	.6,1.2	1/3334	180	283	1.8	13.6	Cross polarized
013	1142	20&A to T1	1.2,1.8	1/3334	180	283	1.8	13.6	Cross polarized
014	1148	20&A to T1	1.2,1.8	1/3334	180	283	1.8	13.6	H pol
015	1153	20&A to T1	.6,1.2	1/3334	180	283	1.8	13.6	H pol
016	1157	20&A to T1	.6,1.2	1/3334	180	283	1.8	9.6	

153

Table E.1. Summary of Recorded Data
(continued)

| Run	Time	Location	f_1,f_2 (GHz)	fr/smpl rate	No. Frames	Dist (m)	h_T (m)	h_R (m)	Comments
		Tape #18 (continued) 25 Oct, Camp Forrest--Height Gain Study							
017	1219	20&A to T1	1.2,1.8	1/3334	180	283	1.8	9.6	
018	1224	20&A to T1	.6,1.2	1/3334	180	283	1.8	9.6	H pol
019	1229	20&A to T1	1.2,1.8	1/3334	180	283	1.8	9.6	H pol
020	1234	20&A to T1	.6,1.2	1/3334	180	283	1.8	6.4	
021	1246	20&A to T1	1.2,1.8	1/3334	180	283	1.8	6.4	
022	1251	20&A to T1	.6,1.2	1/3334	180	283	1.8	6.4	H pol
023	1256	20&A to T1	1.2,1.8	1/3334	180	283	1.8	6.4	H pol
		Tape #19 25 Oct, Continuation							
001	1307	20&A to T1	.6,1.2	1/3334	180	283	1.8	4.6	
002	1315	20&A to T1	1.2,1.8	1/3334	180	283	1.8	4.6	
003	1319	20&A to T1	.6,1.2	1/3334	180	283	1.8	4.6	H pol
004	1324	20&A to T1	1.2,1.8	1/3334	180	283	1.8	4.6	H pol
005	1334	20&A to T1	.6,1.2	1/3334	180	283	1.8	1.5	
006	1339	20&A to T1	1.2,1.8	1/3334	180	283	1.8	1.5	
007	1345	20&A to T1	.6,1.2	1/3334	180	283	1.8	1.5	H pol
008	1351	20&A to T1	1.2,1.8	1/3334	180	283	1.8	1.5	H pol

154

APPENDIX F. ANTENNA PATTERN MEASUREMENTS

The test antenna was a 13 cm, 90° cone mounted above a 1.2 m (4 ft) square ground plane. The antenna (with ground plane) was mounted on the roof of a Chevy Suburban about 10 cm above the vehicle roof and was tested at three frequencies and two orientations. For one series of tests the ground plane was vertical, and horizontally polarized radiation was used as the vehicle was rotated on a turntable. For the other series of tests, the ground plane was horizontal, and vertically polarized radiation was used as the vehicle was rotated. For each test the feed point of the test antenna was located on the axis of rotation, and the transmitting antenna was at the same height above ground as the test antenna (2.6 m for vertical ground plane tests and 2.0 m for horizontal ground plane tests). During those tests which used horizontally polarized waves (ground plane of test antenna in the vertical plane), a 1.2-m by 4.9-m section of rf absorber was placed midway between the antennas to reduce ground reflections. Measurements with and without the absorber show about a 3 dB difference in maximum gain.

The measurements used the substitution method illustrated in Figure F.1. First the cables leading to the two antennas are connected to each other through an atten-uator whose loss is set equal to the calculated free space loss less the transmitting antenna gain. Then the received signal level is observed and a reference level sig-nal generator is adjusted to provide an identical signal level which can be identi-fied as a 0 dBi gain. Finally, the attenuator is removed and the cables connected to their respective antennas for gain and pattern measurements.

In addition, the VSWR was measured over the frequency range of 400 MHz to 2 GHz. It is 2:1 or better over this range and typically is better than 1.5:1.

Copies of the measured gain and pattern data are presented in Figures F.2 through F.9. For measurements with the ground plane in its vertical position, the 0-180 axis of the plot corresponds to the ground plane. The cone axis, then, corre-sponds to the 90-270 axis of the plot, and data in the 180-270-0 portion of the plot describe the forward-direction performance of the antenna. For all data the 0-axis of the plot corresponds to the front of the vehicle. Antenna gain can be read directly from the plots. The gain interval is 5 dB per division and the outer circle (maximum value) is 10 dBi on all plots.
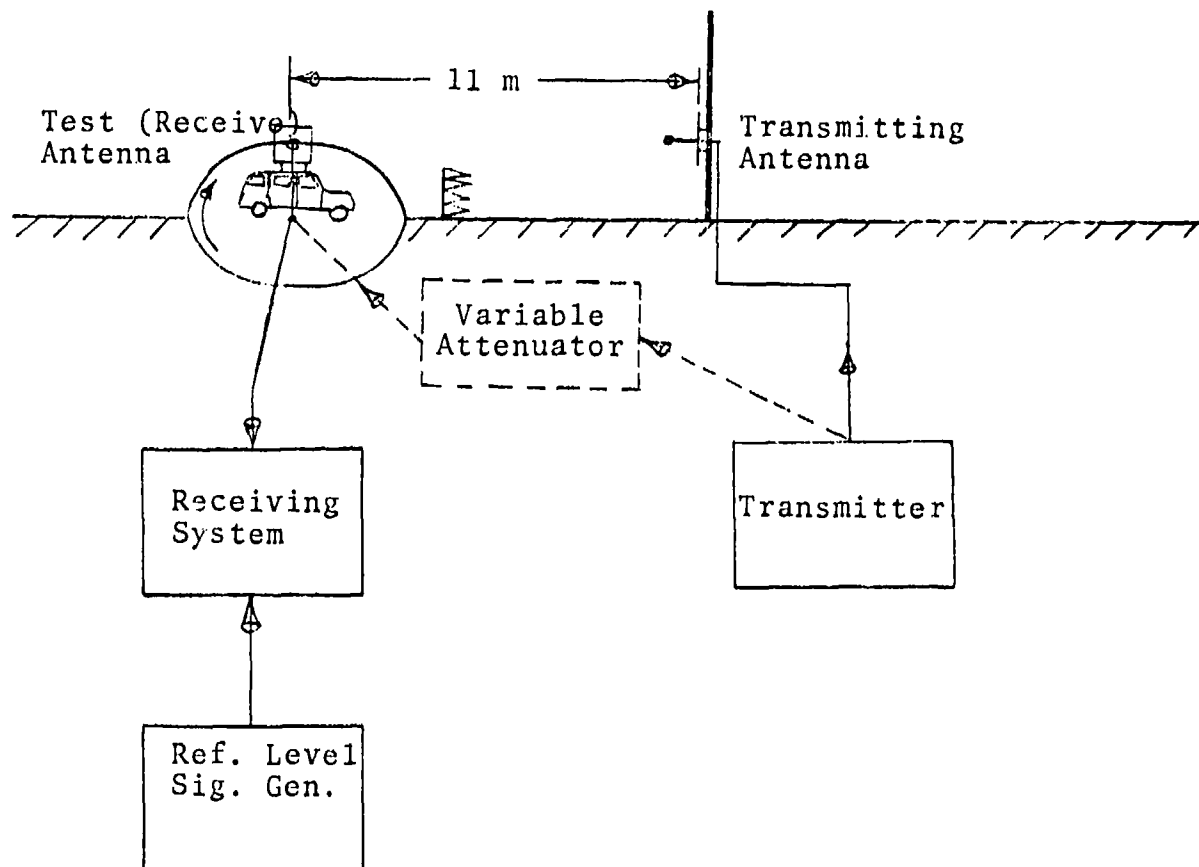
Test antenna:

   Conical monopole machined from solid aluminum stock.

Transmitting antennas:

   Reflector-backed $\lambda/2$ dipoles which are $\lambda/4$ away from reflector. Gain assumed to be 7 dBi.

Test frequencies:

   600, 1200, 1800 MHz

Figure F.1. Block diagram of the test setup.
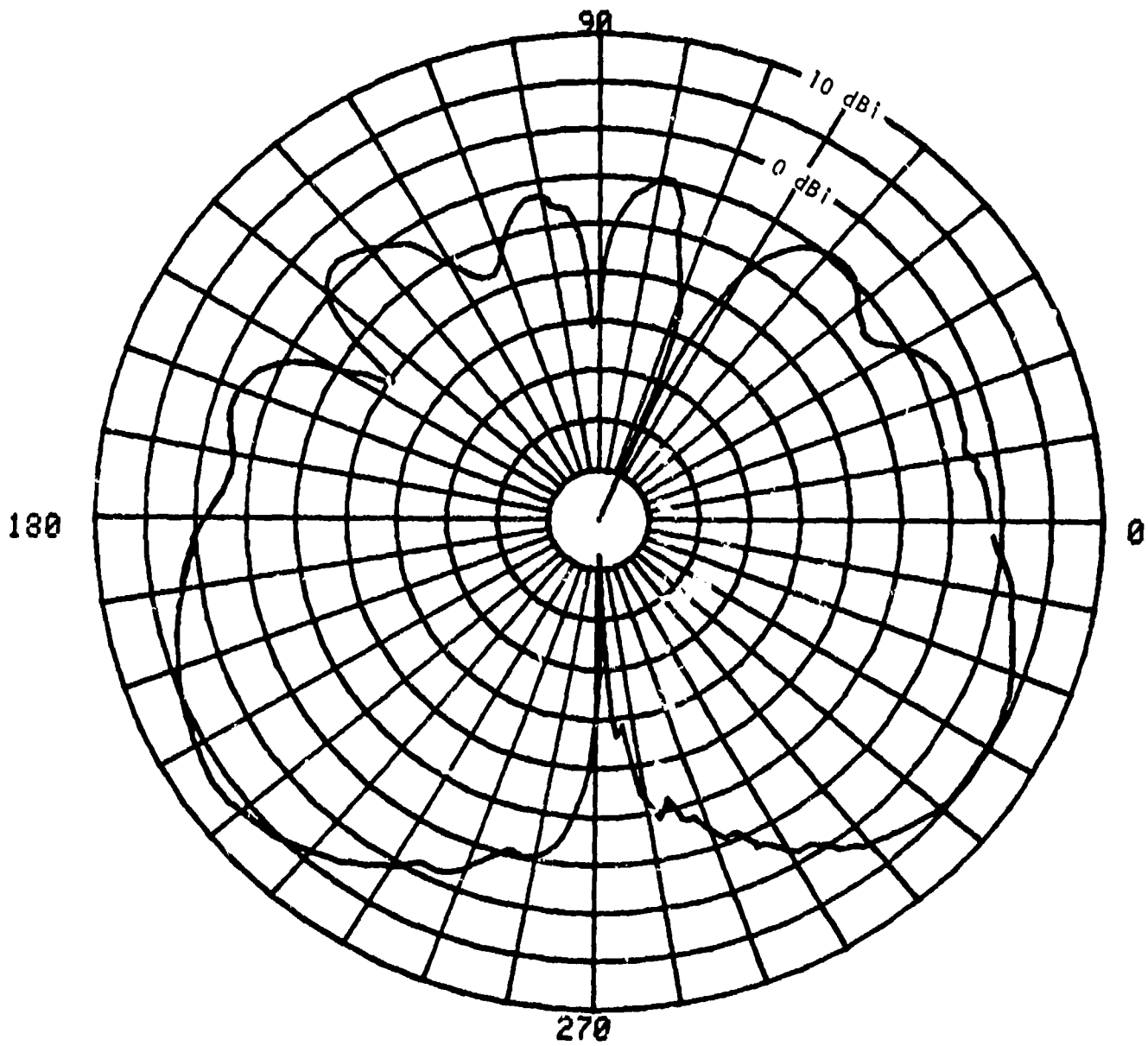
Figure F.2.   Conical monopole pattern with ground plane vertical, 600 MHz.
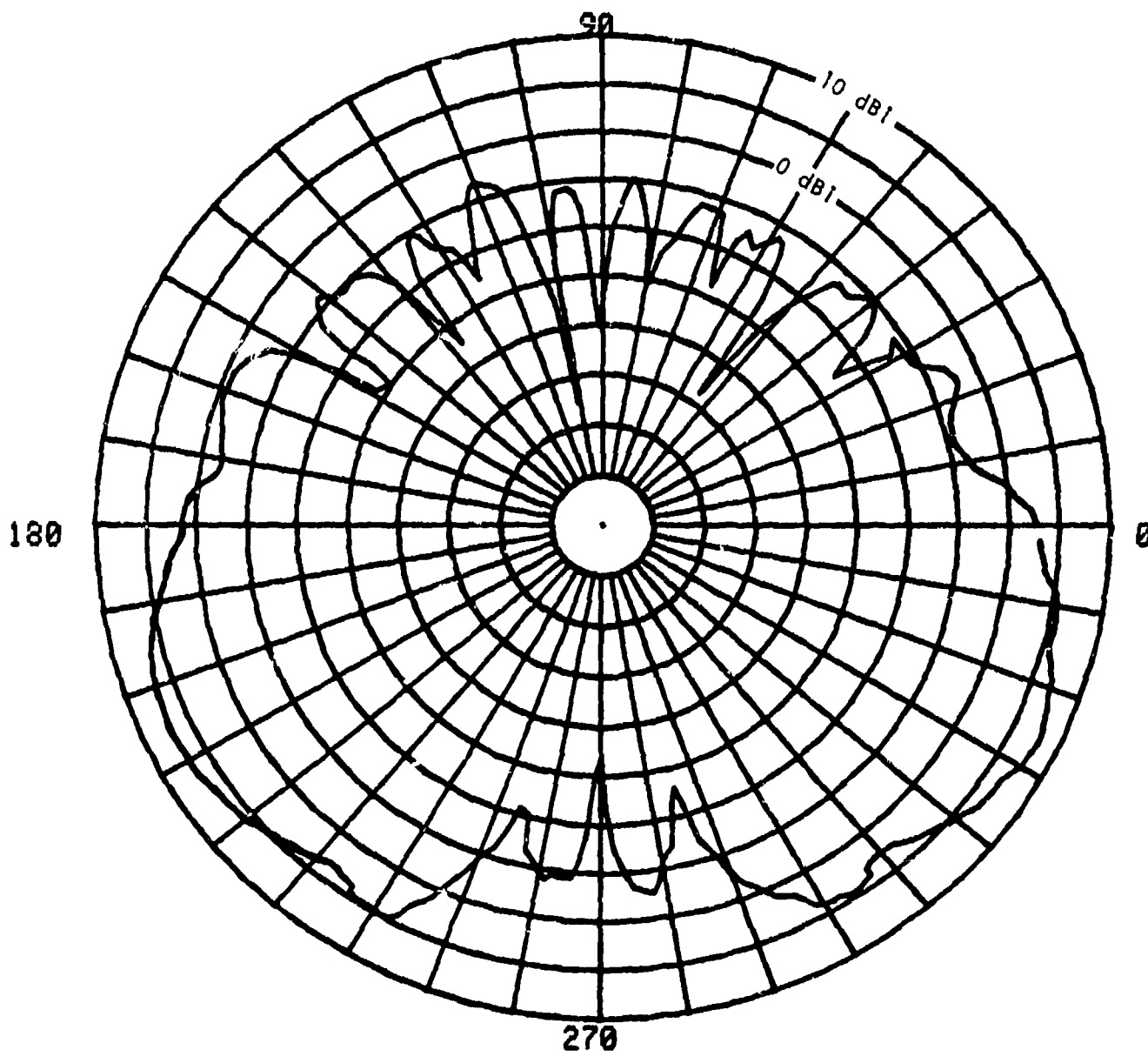
Figure F.3. Conical monopole pattern with ground plane vertical, 1200 MHz.
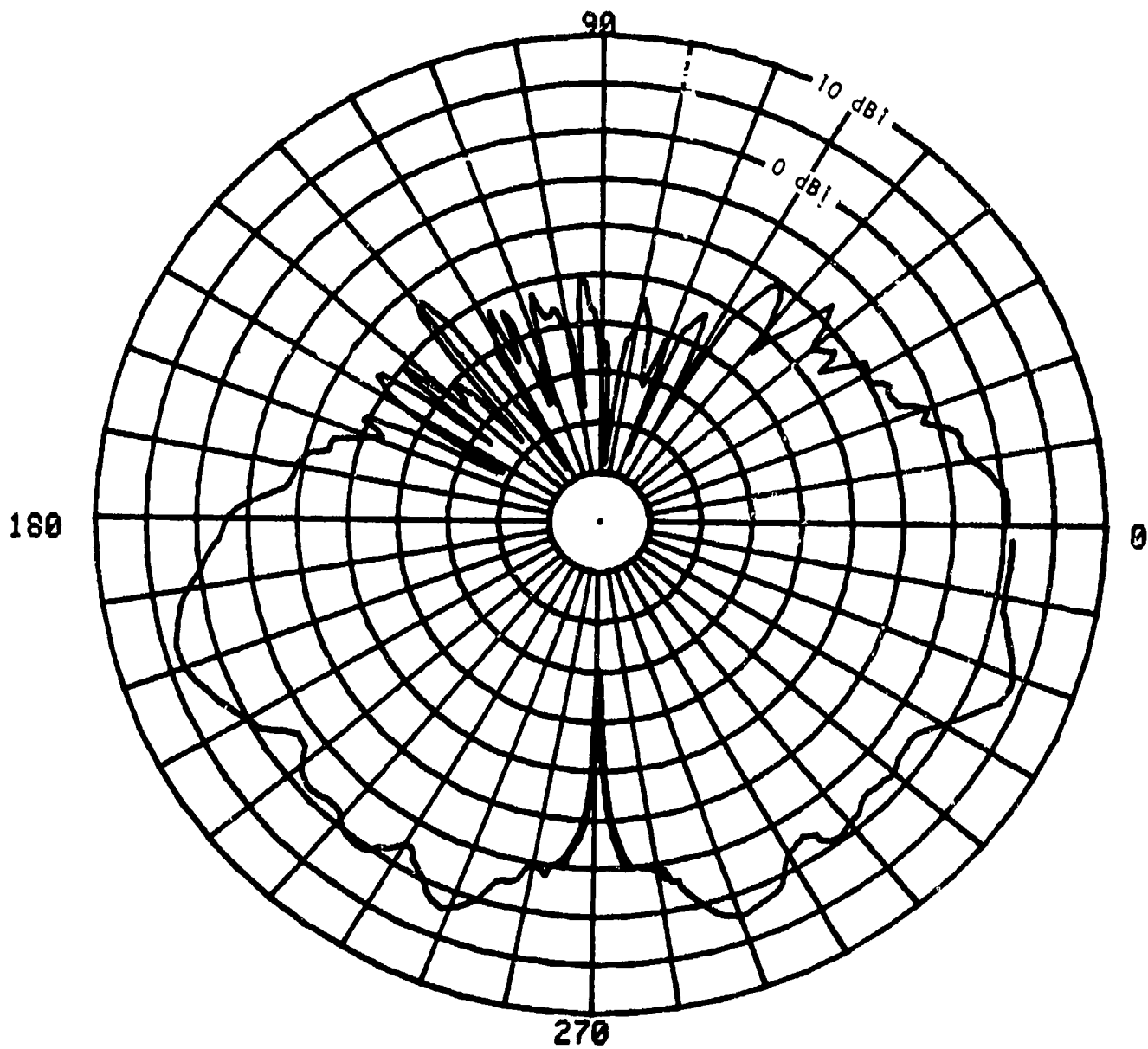
Figure F.4.   Conical monopole pattern with ground plane vertical, 1800 MHz.
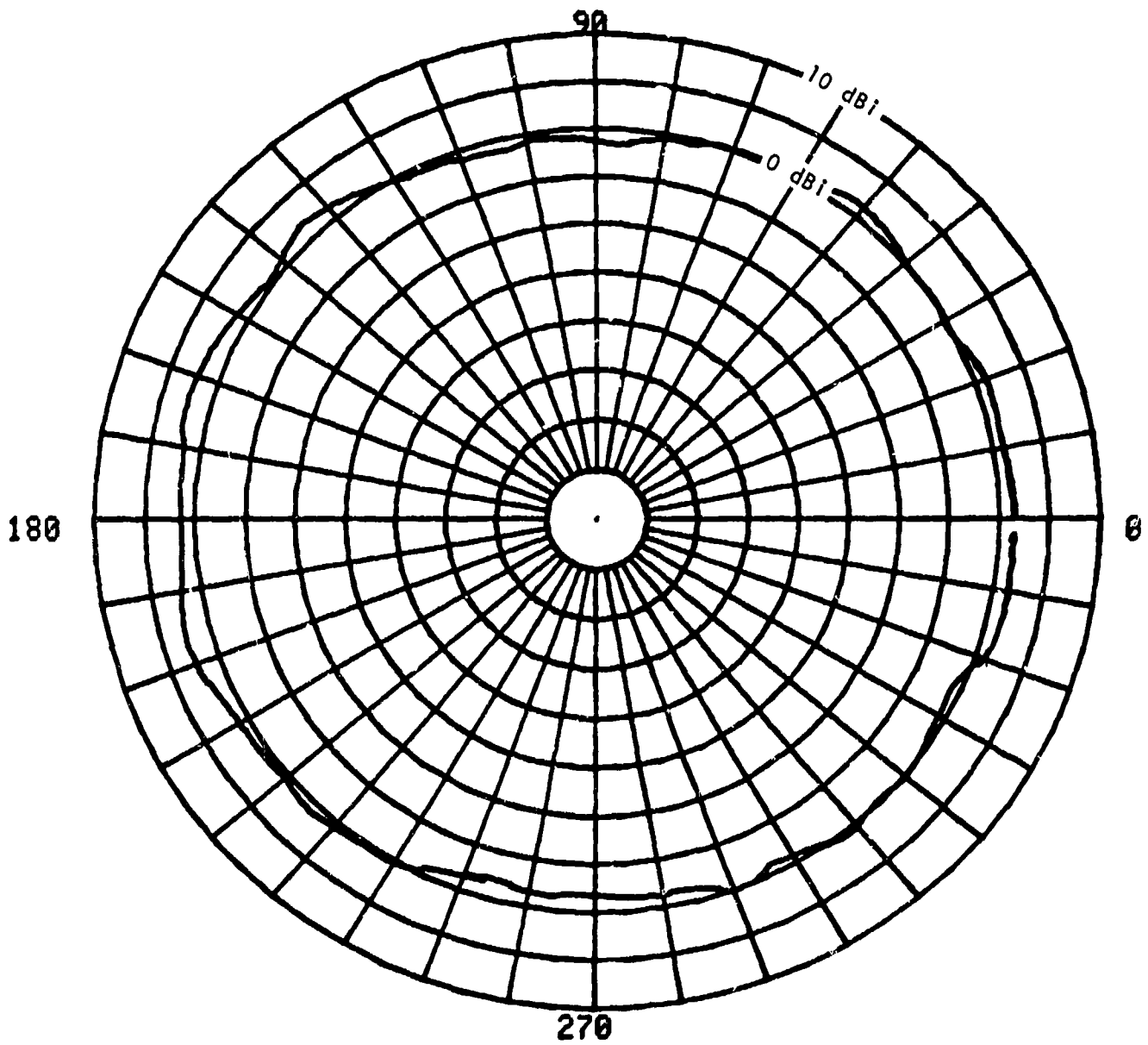
Figure F.5.   Conical monopole pattern with ground plane horizontal,
600 MHz.
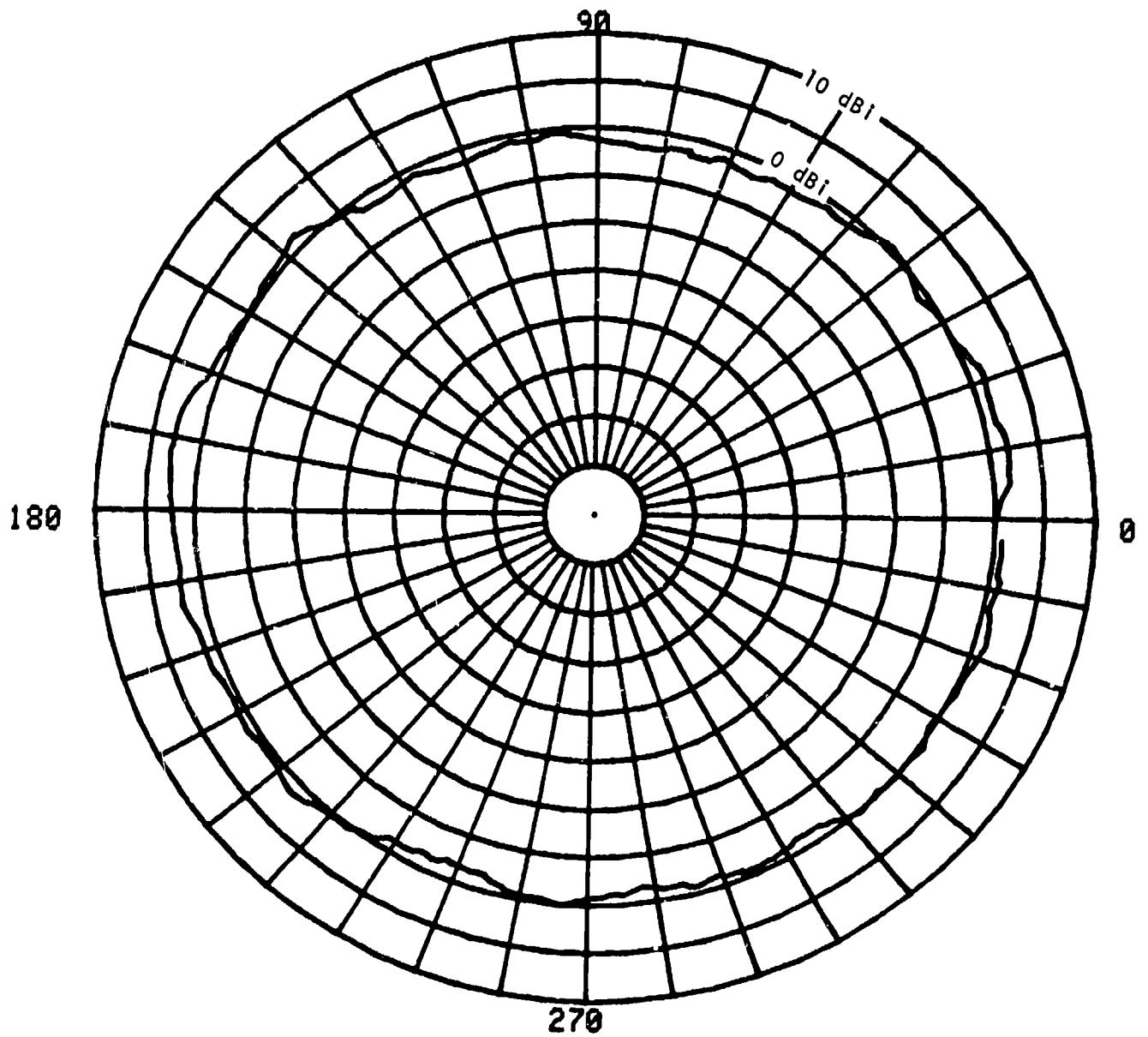
Figure F.6.   Conical monopole pattern with ground plane horizontal, 1200 MHz.
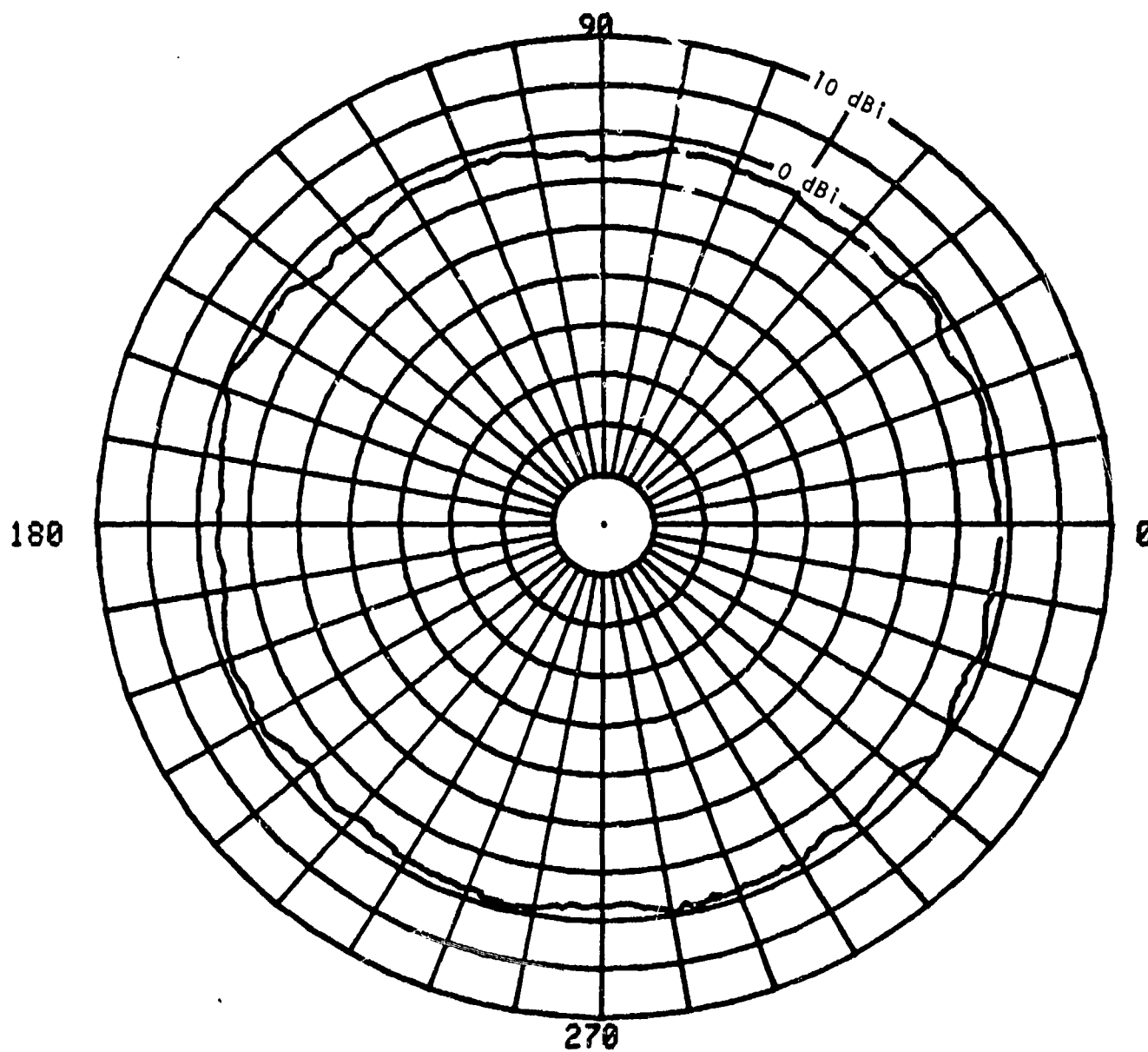
Figure F.7. Conical monopole pattern with ground plane horizontal, 1800 MHz.